

## THE HYDROGENATION OF CARBON DIOXIDE IN PARTS-PER-MILLION LEVELS

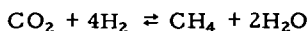
S. S. Randhava and A. Rehmat

Institute of Gas Technology  
Chicago, Illinois 60616

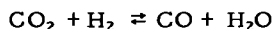
### INTRODUCTION

In recent years the development of the fuel cell, a device that converts chemical energy directly into electrical energy, particularly the low-temperature, acid fuel cell that uses reformed natural gas, made it necessary to design a process that can produce a reformat gas suitable for fuel cell application.

The process is well established, but the kinetics of some of the reactions that take place during the process are not very well known. One of the reactions that could take place during the process is



However, CO may be formed by the side reaction



Early investigations of the reaction between carbon dioxide and hydrogen were either primarily qualitative in nature or attempts to determine the equilibrium of the reaction; consequently, no data suitable for kinetic analysis were presented.

The first attempt to obtain rate data for this system was made by Nicolai, d'Hont and Jungers.<sup>1</sup> They studied the kinetics of carbon dioxide hydrogenation on a nickel catalyst at low pressures (0.10-1.0 atm) and temperatures of 180°-300°C. Binder and White<sup>2</sup> made an extensive study of this system for the first time. The rate of the reaction was correlated by a mechanism which assumes that the major resistance to the overall process is offered by the reaction of an adsorbed carbon dioxide molecule with at least two adsorbed hydrogen molecules; thus, the surface reaction appeared to be rate-controlling. This study was extended by Dew, White and Slipevich,<sup>3</sup> who studied the effect of total pressure and postulated a mechanism which assumes that the reaction takes place between four adsorbed molecules of hydrogen and an adsorbed molecule of carbon dioxide on the catalyst's surface.

In a search for a source of synthetic hydrocarbons, Fischer and Pichler<sup>4</sup> studied the reaction between carbon dioxide and hydrogen, and carbon monoxide and hydrogen over a ruthenium catalyst. Only high-molecular-weight hydrocarbons were obtained at 100 atmospheres; methane at one atmosphere. Pichler also reported that ruthenium could not be improved by promoters or carriers. For this reason and because of its high cost, this catalyst was not tried by other investigators for the hydrogenation of carbon dioxide or carbon monoxide until a later date.

In its search for better catalysts, the Bureau of Mines<sup>5,6</sup> found that ruthenium can be used on alumina in concentrations of 0.5%, at a cost no greater than commercially successful catalysts made from platinum. Ruthenium can also compete with nickel, considering the small quantities required (0.5% Ru vs. 48% Ni), and when compared to commercial nickel hydrogenation catalysts and the complexity of nickel pretreatment.

The purpose of this investigation was to obtain data over a range of temperatures, compositions, and space velocities, using a gas mixture containing carbon dioxide

(ppm) in hydrogen. Using a ruthenium catalyst impregnated on an alumina support for data at atmospheric pressure would yield an expression for the kinetics of the hydrogenation of carbon dioxide.

## EXPERIMENTAL

The basic description of the experimental apparatus has been presented elsewhere.<sup>7</sup> The reactor was fabricated from a 22-in.-long, stainless steel, Type-304 tube, having a 1/2-in. ID and a 1-in. OD. The thickness of the wall ensured longitudinal isothermality. A multipoint thermocouple was placed inside the bed, with three thermocouples observing temperatures at intervals of 1/4 in. A perforated screen, functioning as a catalyst support, was welded to the thermocouple rod 1 in. from the tip. A premixed mixture of carbon dioxide and hydrogen was passed through a pressure regulator and control valve to a calibrated rotameter. Then the gases entered the top of the reactor and flowed downward through the catalyst bed.

The catalyst used in this investigation was furnished by Englehard Industries, Inc., and consisted of 0.5% ruthenium impregnated on 1/8 x 1/8-in. cylindrical alumina pellets. Catalyst pellets (2 cc) dispersed in an equal volume of alumina pellets were used for every run. The catalyst was activated prior to a run sequence by passing H<sub>2</sub> over it at 450°C for approximately 2 hours. Because of the dispersed nature of the catalyst and the low gas concentrations, the reactor behavior was isothermal, with the temperature variance in three thermocouples never exceeding 1°C, even under conditions of maximum conversion. Steady-state conversions were achieved within 30 minutes for all variations of temperature and gas flow rate.

The product gases, after leaving the reactor, flowed through a condenser and were continuously monitored until a steady state was achieved. Two nondispersive, infrared analyzers (MSA Lira Model 300) were used to determine the concentrations of carbon monoxide and methane. The infrared analyzers were calibrated to read in the ranges of 0-100, 0-500, and 0-3500 ppm of CO and CH<sub>4</sub> and were never permitted to drift beyond 5 ppm on the 0-3500 ppm scale. The units were calibrated at the beginning of each run sequence (constant temperature with varying space velocities) with hydrogen used as the zero calibration gas. Five different gas mixtures were used to check the calibration scale of each of the Liras. The calibration gases were mixed and analyzed by The Matheson Co. and were accurate to within 2 ppm. All of the premixed and analyzed gases containing 1150, 2060, and 3580 ppm carbon dioxide in hydrogen were also supplied by The Matheson Co.

## RESULTS

In this investigation, the runs are grouped into three different sets, each having a different feed composition: 1150, 2060, and 3580 ppm CO<sub>2</sub> in H<sub>2</sub>. For each set five runs were made with varied flow rates and at constant temperature. The temperature range investigated was 200°-450°C; the gas flow rates used were 10, 30, 50, 70, and 100 cu cm/s, corresponding to the variation of residence time from 0.2 to 0.02  $\frac{\text{cu cm catalyst}}{\text{cu cm gas/s}}$ . The pressure was maintained at 1 atmosphere for all the runs. Selected runs were repeated to check reproducibility and for catalyst deactivation. All the data taken were reproducible to  $\pm 2\%$ ; no noticeable decrease in the catalytic activity was observed over the runs' durations.

Each run was obtained under steady-state conditions and consisted of an analysis of effluent gases at a given feed rate, temperature, pressure, and the quantity of the catalyst: The duration of each run was approximately 40 minutes. The quantity of the catalyst was kept constant throughout all the runs. The effects of the variables involved are discussed below.

Effect of Temperature. The number of moles of carbon dioxide converted per mole of carbon dioxide in the feed gas for all gas mixtures, and the corresponding number of moles of methane and carbon monoxide formed for selected gas mixtures at different temperatures are shown in Figures 1-5.

The production of methane per mole of CO<sub>2</sub> fed is maximum for the gas mixture containing 1150 ppm CO<sub>2</sub>: The ratio reaches 1 at temperatures around 450°C and a residence time of  $0.2 \frac{\text{cu cm catalyst}}{\text{cu cm gas/s}}$ . The conversion of carbon dioxide and the production of methane and carbon monoxide exhibited characteristic S-shaped curves, showing an increase in conversion with an increase in temperature.

The formation of carbon monoxide is favored by an increase in temperature; however, at temperatures below 350°C there is negligible formation. Above this temperature, the amount of carbon monoxide in the effluent progressively increases.

At higher temperature ranges note that all three gases exhibit asymptotic behavior regarding conversions. It is apparent that the selection of a temperature range for this experiment almost spans the entire range for carbon dioxide methanation at these concentrations.

Effect of Feed Gas Composition. The effect of feed gas composition on hydrogenation reactions is significant over the ruthenium catalyst. The carbon dioxide conversion increases with decreasing amounts of carbon dioxide in the feed gas at any temperature and for all residence times. The asymptotic values of conversion decreased from ~1 for 1150 ppm CO<sub>2</sub> to about 0.8 for 3580 ppm CO<sub>2</sub>. The amount of methane produced per mole of carbon dioxide in the feed also increases with the decrease in amount of carbon dioxide in the feed gas. It was interesting to note that the formation of carbon monoxide increases with an increase in the concentration of carbon dioxide in the feed. Consequently, the conversions may be increased by either raising the temperature to ~450°F, or by decreasing the amount of carbon dioxide in the feed gas.

Effect of Residence Time. In each case the conversion of carbon dioxide increases with an increase in residence time. At any given temperature, the production of methane also increases with an increase in the residence time. This would naturally indicate conventional reactor behavior.

However, the effect of residence time on the formation of carbon monoxide displayed a rather unconventional characteristic. Figure 5 shows an increase in the formation of carbon monoxide with a decrease in residence time over the entire range of temperatures and concentrations investigated.

## DISCUSSION

It appears possible that the following reactions are taking place:



Several investigators have shown<sup>2,3</sup> that, at higher concentrations of carbon dioxide in the feed, the methanation of carbon dioxide takes place directly by Reaction 1; carbon monoxide is formed by the side reaction, Reaction 2. It appears from our results that the methanation of ppm concentrations of carbon dioxide does not occur directly by Reaction 1, since we found that at any particular temperature carbon monoxide is produced by increasing the flow rate. This would mean that the reverse shift reaction (Reaction 2) reaches equilibrium almost instantaneously; the

methanation of carbon monoxide proceeds with time. More carbon monoxide is produced (Reaction 2) as the methanation of carbon monoxide takes place until the steady-state condition is reached. Nicolai, d'Hont and Jungers<sup>1</sup> pointed out that carbon dioxide does not react in the presence of carbon monoxide. In one of the studies at the Institute of Gas Technology<sup>10</sup> on the selective methanation of carbon monoxide using a gas mixture containing hydrogen, carbon dioxide, and carbon monoxide, it was also pointed out that ruthenium is the best selective methanation catalyst and that the reaction of carbon dioxide does not proceed in an appreciable amount until the level of carbon monoxide in the mixture reaches a certain minimum level. In the present investigation this is indeed the case. As soon as the carbon monoxide methanation reaches a steady state, leaving the concentration of carbon monoxide in the reacting mixture above this minimum, the conversion of carbon dioxide ceases completely, as indicated by Figures 1-3.

For finding the overall empirical rate expression valid for the change of conversion and corresponding rate constants at various temperatures for these reactions, an expression of the type

$$-r_{\text{CO}_2} = kC_{\text{CO}_2}^n$$

was tried for reasons given by Levenspiel,<sup>8</sup> who suggested the use of simple empirical rate expressions in chemical reactor design work. The use of such a power law rate equation is also supported by catalytic combustion studies at U.C.L.A.<sup>9</sup> Although the reaction rate should depend upon the concentration of hydrogen in addition to the concentration of carbon dioxide in the system, this term has been omitted from the rate expression used here, since hydrogen is in excess and is treated essentially as a constant.

The rate expression can also be stated in a different form

$$-r_{\text{CO}_2} = -\frac{dC_{\text{CO}_2}}{\left(\frac{V}{V_0}\right)} = kC_{\text{CO}_2}^n$$

which, when integrated, yields the expression -

$$k(n-1) \frac{V}{V_0} = C_{\text{CO}_2}^{1-n} + (C_{\text{CO}_2})_0^{1-n} \text{ for } n \neq 1$$

$C_{\text{CO}_2}^{1-n}$  was plotted against  $\frac{V}{V_0}$  for various values of  $n$ . The value of  $n$  giving the best straight line was used as the reaction order for the hydrogenation of the carbon dioxide reaction. The rate constants could then be calculated from the slopes of the lines. The best value of  $n$  was found to be 1.5. A typical plot of  $C_{\text{CO}_2}^{1-n}$  versus  $\frac{V}{V_0}$  for this value of  $n$  is shown in Figure 6 for a feed of 1150 ppm  $\text{CO}_2$ .

The reaction velocity constant is related to the reaction temperature in accordance with the Arrhenius equation

$$k = k_0 e^{-E/RT}$$

The Arrhenius plots for this reaction are given in Figure 7. The empirical frequency factor,  $k_0$ , and the activation energy for this reaction are tabulated in Table 1. All of the Arrhenius plots are linear in the temperature range considered.

Table 1. ACTIVATION ENERGIES AND SPECIFIC REACTION RATE CONSTANTS AS A FUNCTION OF THE INLET-GAS COMPOSITIONS

Concentration of CO <sub>2</sub> in Feed, ppm	E, kcal/ mole	k <sub>0</sub> , $\frac{\text{cu cm gas (ppm CO}_2\text{)}^{-0.5}}{\text{cu cm catalyst/s}}$
1150	10.8	5700
2060	11.4	4250
3580	11.5	2800

Unlike the methanation of carbon monoxide on ruthenium,<sup>7</sup> where only one Arrhenius plot was obtained for all the concentrations of carbon monoxide, three different plots are obtained for the three concentrations of carbon dioxide considered. This can be explained by the way in which the methanation of carbon dioxide takes place. Since it occurs by the reverse shift reaction, all we are dealing with is the methanation of carbon monoxide and the effect of the various amounts of carbon dioxide on such a reaction. Thus the decrease in k values, due to an increase in the concentration of carbon dioxide in the feed, can be compared to Cohen and Nobe's<sup>11</sup> work dealing with the effect of an increasing concentration of water vapor on the catalytic oxidation of carbon monoxide on nickel oxide. (This phenomenon is explained below.)

Every catalyst has a number of active sites where the reaction takes place. In the case of the hydrogenation of carbon dioxide these sites are occupied by carbon monoxide, which is reacting with hydrogen to form methane, and by carbon dioxide, which remains unreacted. As the concentration of carbon dioxide is increased, more of the sites are occupied by unreacted carbon dioxide, thus making fewer sites available for the reaction of carbon monoxide. Therefore, one would expect a decrease in the reactivity of carbon monoxide with hydrogen to form methane when carbon dioxide is present in the reacting mixture. This effect of increasing the amount of carbon dioxide is reflected in the decreasing values of the reaction constant, k.

### CONCLUSION

The hydrogenation of carbon dioxide at very low concentrations over a 0.5% ruthenium catalyst was studied. The empirical rate expression, valid for the change of conversion of CO<sub>2</sub> in the overall reaction, was found to follow the simple expression

$$-r_{\text{CO}_2} = k \text{CO}_2^{1.5}$$

where k obeyed the Arrhenius temperature dependence for each concentration at all temperatures.

The methanation of carbon dioxide took place in two steps: the formation of carbon monoxide and the subsequent hydrogenation of carbon monoxide to methane. The effect of an increasing amount of carbon dioxide in the feed was reflected in the decreasing values of the reaction constant, k.

### ACKNOWLEDGMENT

The authors wish to thank the Institute of Gas Technology which sponsored this work through its basic research program.

NOMENCLATURE

- $C_A$  = concentration of species A in effluent, ppm
- $(C_{A_0})$  = concentration of species A in feed, ppm
- E = activation energy, cal/g-mole
- k = reaction rate constant,  $\frac{(\text{cu cm gas})(\text{ppm CO}_2)^{-0.5}}{(\text{cu cm catalyst})(\text{s})}$
- $k_0$  = Arrhenius frequency factor,  $\frac{(\text{cu cm gas})(\text{ppm CO}_2)^{-0.5}}{(\text{cu cm catalyst})(\text{s})}$
- n = reaction order
- $r_A$  = rate of change of conversion of species A,  $\frac{(\text{cu cm gas})(\text{ppm CO}_2)}{(\text{cu cm catalyst})(\text{s})}$
- R = gas constant, cal/mole - °K
- T = temperature, °K
- $v_0$  = volumetric flow rate of gas, cu cm/s
- V = volume of catalyst, cu cm
- $x_A$  = moles of A converted or produced per mole of CO<sub>2</sub> in feed

REFERENCES CITED

1. Nicolai, J., d'Hont, M. and Jungers, J. C., Bull. Soc. Chem. Belges **55**, 160 (1946).
2. Binder, G. G. and White, R. R., Chem. Eng. Progr. **46**, 563 (1950).
3. Dew, J. N., White, R. R. and Sliepcevich, C. M., Ind. Eng. Chem. **47**, 140 (1955).
4. Fischer, V. and Pichler, H., Brennstoff-Chem. **14**, 306 (1933).
5. Karn, F. S., Schultz, J. F. and Anderson, R. G., Ind. Eng. Chem. Prod. Res. Develop. **4**, 265 (1965).
6. Karn, F. S., Schultz, J. F. and Anderson, R. G., Bureau of Mines Report of Investigations **6974**, 20 (1967).
7. Randhava, S. S., Rehmat, A. and Camara, E. H., "Methanation of Low-Concentration Carbon Monoxide Feeds Over Ruthenium," Ind. Eng. Chem. Proc. Design Develop., in press.
8. Levenspiel, O., Chemical Reaction Engineering, Chapter 14. New York: Wiley, 1962.
9. Accomazzo, M. A. and Nobe, K., Ind. Eng. Chem. Proc. Design Develop. **4**, 425 (1965).
10. Randhava, S. S., "Basic Kinetic Studies of Natural Gas Reformation for Low-Temperature Fuel Cell Applications and the Selective Methanation of CO and CO<sub>2</sub> of the Reformed Gas," IGT Project 7273, Chicago, September 1968.
11. Cohen, A. E. and Nobe, K., Ind. Eng. Chem. Proc. Design Develop. **5**, 214 (1966).

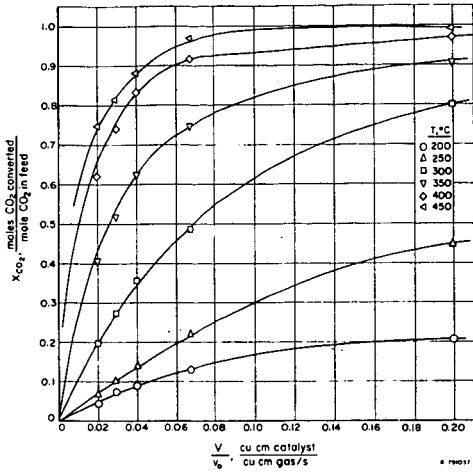


Figure 1. CONVERSION OF CO<sub>2</sub> AS A FUNCTION OF RESIDENCE TIME FOR 1150 ppm FEED GAS

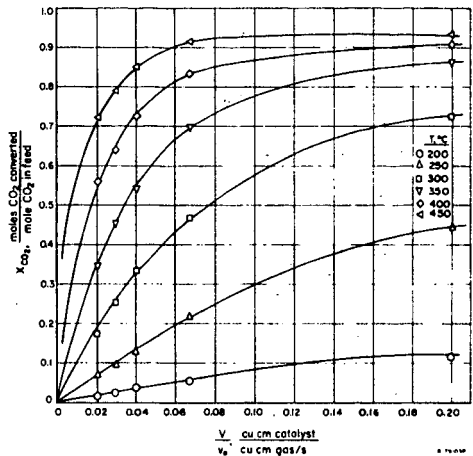


Figure 2. CONVERSION OF CO<sub>2</sub> AS A FUNCTION OF RESIDENCE TIME FOR 2060 ppm FEED GAS

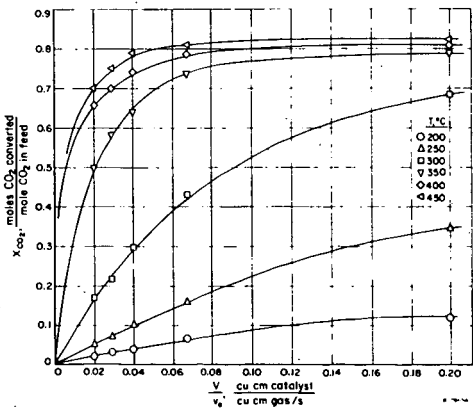


Figure 3. CONVERSION OF CO<sub>2</sub> AS A FUNCTION OF RESIDENCE TIME FOR 3580 ppm FEED GAS

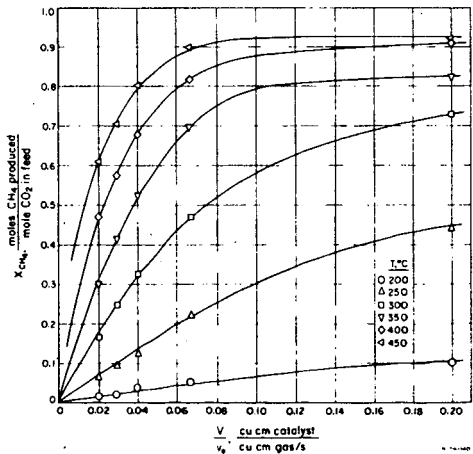


Figure 4. PRODUCTION OF CH<sub>4</sub> AS A FUNCTION OF RESIDENCE TIME FOR 2060 ppm FEED GAS

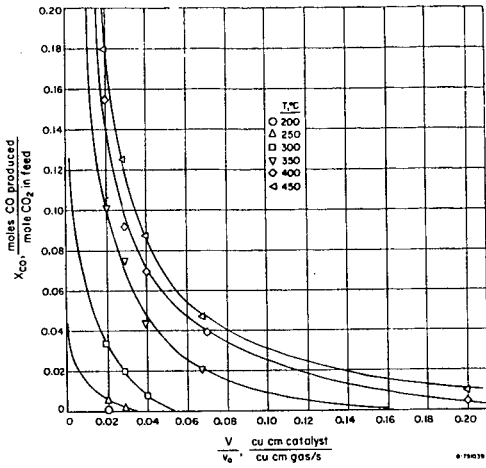


Figure 5. CO PRODUCTION AS A FUNCTION OF RESIDENCE TIME FOR 3580 ppm FEED GAS

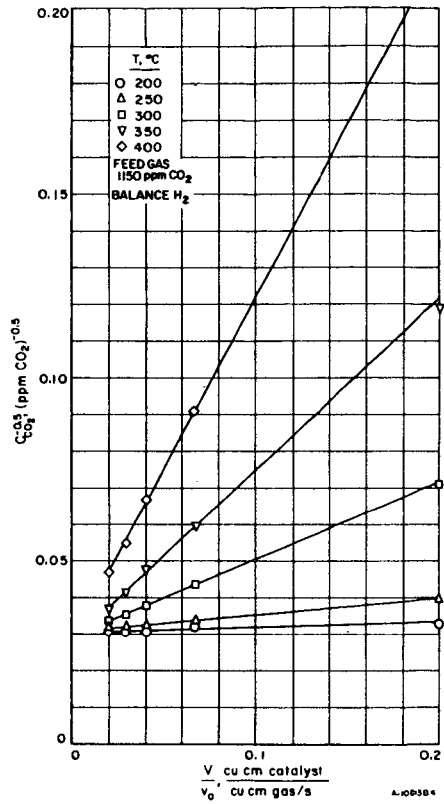


Figure 6. VARIATION IN  $C_{CO_2}^{-0.5}$  WITH RESIDENCE TIME FOR 1150 ppm FEED GAS

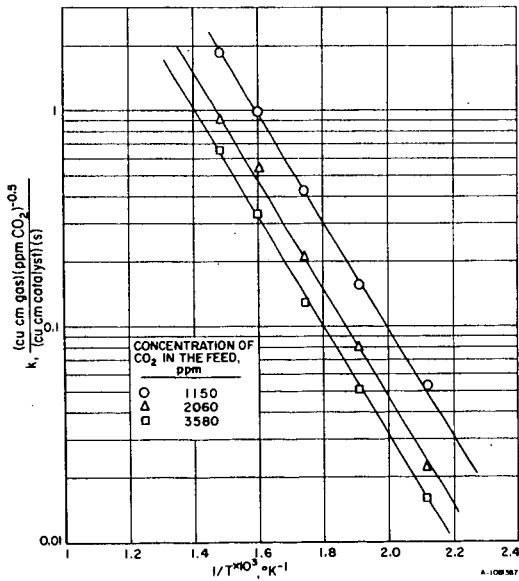


Figure 7. ARRHENIUS PLOT FOR HYDROGENATION OF  $CO_2$

METAL HYDRIDES AS A SOURCE OF HYDROGEN FUEL

J. J. Reilly, R. H. Wiswall, Jr. and K. C. Hoffman  
Brookhaven National Laboratory  
Upton, New York

Hydrogen has the potential of being a cheap and non-polluting fuel which could be used in a variety of energy converters. It is particularly attractive for use in fuel cells, where it is the preferred fuel, but it could also be used in any type of combustion engine, although in the latter case some modification of conventional designs would be required. However, a major problem involved in using hydrogen as a common fuel is the difficulty encountered in storing and transporting it. To store and transport hydrogen as a cryogenic liquid or as a compressed gas for such use does not appear practical either from an economic or a safety standpoint.

Recent studies<sup>1-3</sup> on the equilibrium relationships between hydrogen and certain metals and alloys suggest that the reversible metal hydrides formed in these systems may serve as a convenient, safe, and cheap means of storing hydrogen. In this regard the use of magnesium hydride as a source of hydrogen fuel for internal combustion engines has already been discussed.<sup>4</sup> The object of this paper is to describe how such metal hydrides may be used to supply hydrogen for use as a fuel in an electrochemical cell.

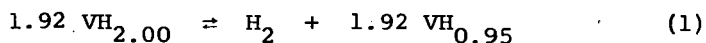
In its most simple form such a storage system consists of a vessel containing a reversible metal hydride of the type described below, a means by which heat may be added to or removed from the system, and a tap for withdrawing or adding hydrogen gas. In operation, as hydrogen is withdrawn from the system, the hydrogen pressure drops below the equilibrium dissociation pressure of the metal hydride which will then dissociate in order to re-establish equilibrium conditions. During the hydrogen evolution step heat must be added to the system since the dissociation reaction is endothermic. Dissociation will continue under these conditions as long as the designated hydride phase exists (it is possible to have more than one hydride phase present in certain systems). In order to regenerate the hydride the procedure is reversed; hydrogen is added to the

system and the hydrogen pressure is maintained above the dissociation pressure. Heat must be removed from the system during this step.

In Table 1 the pertinent properties of three candidate metal hydrides are listed and can be compared to corresponding figures for cryogenic and compressed gas storage. These compounds are vanadium dihydride ( $\text{VH}_2$ ), magnesium nickel hydride ( $\text{Mg}_2\text{NiH}_4$ ) and  $\text{MgH}_2$ . It is interesting to note that on a volume basis the hydrogen content of the solids is greater than that of liquid hydrogen and much greater than that of compressed hydrogen at 100 atm. pressure and  $25^\circ\text{C}$ . We wish to point out that a detailed discussion of the properties and synthesis of these compounds has already been given;<sup>1-3</sup> here we shall only discuss these properties briefly and in connection without particular intent.

#### Vanadium Dihydride - A Low Temperature Hydrogen Reservoir

Vanadium dihydride is capable of supplying hydrogen at a pressure of  $>1$  atm. to a fuel cell at any temperature above  $\sim 10^\circ\text{C}$ . It has a grey metallic appearance, is very brittle and can easily be ground to a fine powder. It is not pyrophoric, indeed in the presence of air its decomposition is inhibited. It can be synthesized by the direct reaction of hydrogen with the metal or with vanadium monohydride. It will decompose to form vanadium monohydride and hydrogen as follows:<sup>3</sup>



A plot showing the equilibrium dissociation pressure ( $P_d$ ) vs composition, expressed as the ratio of H atoms/total metal atoms ( $\text{H}/\text{M}$ ), is shown in Fig. 1. Reaction (1) refers to the reaction taking place in the plateau region which lies between the limits  $\text{VH}_{0.95}$ - $\text{VH}_{2.00}$ . In this region the  $P_d$  is essentially constant and not dependent on the solid composition. Above  $\text{VH}_{2.00}$  the isotherm does not rise vertically but has a slight slope to the right which is due to the nonstoichiometric character of vanadium dihydride. Below a composition corresponding to  $\text{VH}_{0.95}$  the  $P_d$  drops precipitously as only the vanadium monohydride phase is present which is quite stable.

The dissociation pressure ( $P_d$ ) of  $VH_2$  is very sensitive to the type and amount of impurities present in the starting vanadium. Thus, it has been found that the  $P_d$  of  $VH_2$  made from commercial grade vanadium (Union Carbide Corp., Materials System Division) was higher by a factor of  $>2$  than that made from high purity vanadium.<sup>3</sup> Since a higher  $P_d$  is desirable for our purposes we shall specify that the  $VH_2$  used in the systems described here be made from commercial vanadium; the data presented here has been obtained with  $VH_2$  using this as the starting material. Qualitative observation also indicated that these impurities have a catalytic effect, increasing both the rate of decomposition and formation of  $VH_2$ .

A plot of the reciprocal temperature vs the  $P_d$  for the composition range  $VH_{0.95}$  to  $VH_{2.00}$  yields a straight line (Fig. 2) which obeys the equation  $\log P_{atm} = \frac{-1989}{T_{oK}} + 7.3795$ . From these data the following thermodynamic quantities for reaction (1) can be calculated:

$$\Delta H_{298} = +9.10 \text{ Kcal}$$

$$\Delta S_{298} = +33.76 \text{ eu}$$

$$\Delta F_{298} = -0.96 \text{ Kcal}$$

Thus, the decomposition of  $VH_2$  is endothermic and heat must be supplied. However, at  $298^\circ\text{K}$  the free energy change is negative and the reaction is spontaneous. Even at a temperature as low as  $0^\circ\text{C}$  the equilibrium dissociation pressure is slightly above 1 atm. (1.25 atm.). Consequently,  $VH_2$  can supply hydrogen at a usable pressure by extracting heat from the surrounding environment if the ambient temperature is above  $0^\circ\text{C}$ . While this may be convenient in certain circumstances it is probably more efficient to utilize the waste heat of the energy converter to effect decomposition.

An idealized schematic of an integrated  $H_2$ -air fuel cell and a table of compatible metal hydride-fuel cell systems is shown in Fig. 3. As an example of a low temperature system, consider a fuel cell of the type described previously by Bartosh<sup>5</sup> but with  $H_2$  supplied by the decomposition of  $VH_2$ . The cell was a 500-watt  $H_2$ -air cell operating at  $74^\circ\text{C}$  with an aqueous KOH electrolyte. Hydrogen originally was supplied by a companion reforming-purification unit which required a low sulfur, hydrocarbon feed. The volume of the reforming unit was  $1.4 \text{ ft}^3$ .

weighed 47 lb, including fuel and water, and at maximum cell power the rate of  $H_2$  feed was 0.0632 lb/hr or 14.23 g mole/hr. We may replace the reformer with a reservoir containing  $VH_2$  and at this rate of consumption, 14.45 Kg (31.8 lb) of  $VH_2$  will last 10 hr. The volume of the fuel reservoir required for this amount, assuming a 50% void space, is 5.78 l (0.20 ft<sup>3</sup>). The amount of energy required to provide the heat of dissociation is 129.5 Kcal/hr (513 Btu/hr). The waste heat generated by the cell, at 55% efficiency, is 351 Kcal/hr (1393 Btu/hr). The only significant difference between the cell described here and that of Bartosh is that we propose to have a circulating electrolyte which is used to transfer the waste heat of the cell to the hydride bed. Considering that the waste heat is in excess by a factor of almost 3 over that required to dissociate  $VH_2$  and the large temperature difference between the hydride bed and the fuel cell, it is quite possible that simpler means of heat transfer would suffice, e.g. locating the hydride bed in an air stream previously used to cool the fuel cell. Thus, the design as shown in Fig. 3 appears quite conservative and allows a considerable degree of flexibility.

As far as start-up procedure is concerned, we would note that the dissociation pressure of  $VH_2$  is high enough to supply hydrogen at the cell operating pressure of 28 psia down to ambient temperature of 7°C. Of course, the bed will tend to cool as the hydride decomposes and the pressure will drop, but the sensible heat of the bed should be sufficient to supply the heat required until some heat is available from the cell. In addition as the bed cools below the ambient temperature some heat will be extracted from the surrounding environment.

When the  $VH_2$  content of the reservoir is exhausted it can be regenerated by supplying  $H_2$  at a pressure of >200 psia at a bed temperature of 25°C. It is necessary to conduct the regeneration reaction at a pressure substantially above the  $P_d$  since there is appreciable hysteresis in the system. Further, the rate of regeneration at any fixed temperature is pressure dependent and pressures of 200-300 psia above the  $P_d$  are recommended to attain reasonably fast reaction rates. In the latter case qualitative observation suggests that the hydride can be 90% regenerated in about 1 hr, provided sufficient cooling capacity is available to maintain the bed at 25°C.

It is possible to adapt the hydride storage concept to a more conventional scheme also shown in Fig. 3. In this case  $VH_2$  is used to provide a ballast effect in a reformer system. Hydrogen is manufactured from a hydrocarbon fuel and purified in the usual manner by passing it through palladium-silver membrane. The hydrogen may be conducted to the hydride reservoir to regenerate  $VH_2$ , or directly to the fuel cell, or both. Under peak loads the system can be designed so that some  $VH_2$  will decompose to supply the required extra hydrogen. If the fuel cell operation is intermittent, the hydride reservoir may carry most of the load during cell operation and is regenerated when the cell is down. Such an arrangement has several advantages over conventional hydrocarbon reforming-fuel cell systems which are summarized as follows:

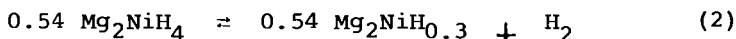
1. The reformer size is determined by the average hydrogen consumption, not peak consumption.
2. The size of the palladium silver diffuser is also determined by the average hydrogen consumption.
3. The reformer can be run continuously and hydrogen stored in the hydride bed for future use.
4. The  $VH_2$  bed can supply  $H_2$  immediately upon start-up.

The actual design of such a system will depend a great deal upon the use pattern envisioned for the fuel cell. However, it can be seen that the incorporation of a relatively small hydride reservoir should result in a practical fuel cell system having a greater degree of flexibility than any previously known.

#### High Temperature Systems

Both the  $Mg_2NiH_4$  and  $MgH_2$  may be considered in the present context as high temperature systems. They cannot abstract the heat required for decomposition from the environment; rather, such heat must come from the waste heat of the energy converter, provided its operating temperature is high enough, or from some other high temperature heat source. The most efficient arrangement is to use the waste heat of the converter and we will limit our discussion to that particular alternative.

$Mg_2NiH_4$  is a rust-colored powder having a non-metallic appearance. It is not pyrophoric and it decomposes slowly in water but rapidly in a slightly acidified solution. A pressure composition isotherm for the  $Mg_2NiH_4$  system is shown in Fig. 1. Unlike  $VH_2$  almost all the hydrogen is available except for a small amount which dissolves in the  $Mg_2Ni$  decomposition product. The decomposition reaction is as follows:



A plot of the dissociation pressure vs the reciprocal temperature is shown in Fig. 4. It is a straight line and obeys the relationship  $\log P_{atm} = -3360/T^{OK} + 6.389$ . For reaction (2) the following thermodynamic values have been determined<sup>2</sup>:

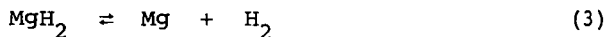
$$\Delta H_{298^{\circ}} = +15.4 \text{ Kcal}$$

$$\Delta F_{298} = +6.7 \text{ Kcal}$$

$$\Delta S_{298} = +29.2 \text{ eu}$$

The reason for including  $Mg_2NiH_4$  in this discussion is that it could be used to supply hydrogen to Bacon type fuel cells operating near  $300^{\circ}C$ . The high cell temperature would require that the electrolyte be a highly concentrated KOH solution (at least 85 wt % KOH). The advantage of  $Mg_2NiH_4$  over  $VH_2$  in this situation is that it contains 3.3 wt % available hydrogen vs 2.1 wt % for the latter. However, it is only useful in a relatively narrow temperature range from  $\sim 275^{\circ}C$  where its  $P_d$  is 1.81 atm. to  $325^{\circ}C$  at which point the  $P_d$  of  $MgH_2$  is 2.8 atm. The latter, of course, contains much more hydrogen on weight basis and for this reason would be the preferred fuel. Unfortunately Bacon type cells operate at temperatures which are too low to utilize the waste heat in order to dissociate  $MgH_2$ . Thus, making the assumption that Bacon cells were available of the same rating and  $H_2$  fuel requirement as the low temperature cell discussed above, the equivalent amount of  $Mg_2NiH_4$  necessary would be 8.56 Kg (18.8 lb) and would require a reservoir volume of 6.66 liters ( $0.23 \text{ ft}^3$ ) assuming a 50% void space. The hydride regeneration procedure is similar to that previously described for  $VH_2$  except that the regeneration temperature should be above  $250^{\circ}C$  in order to attain an acceptable reaction rate.

For high temperature fuel cells such as those using molten carbonates or solid electrolytes,  $MgH_2$  could be used as the source of hydrogen fuel. However, the preparation of pure  $MgH_2$  by direct reaction with hydrogen is difficult and requires a temperatures of  $\sim 400^\circ C$  and  $\sim 100$  atm. pressure.<sup>4</sup> In addition, the product is quite inert. However, it has been found that if a magnesium alloy containing 5-10 wt % Ni or Cu is used as the starting material the synthesis reaction is greatly accelerated and the product very active.<sup>1,2</sup> For hydrogen storage purposes, an alloy of 95% Mg and 5% Ni is recommended. Hydrogen will react with this material to form both  $MgH_2$  and  $Mg_2NiH_4$ . Decomposition will take place in two steps; first  $Mg_2NiH_4$  decomposes as shown above in reaction (2), followed by the known reaction:



A pressure composition isotherm for such a system is shown in Fig. 1. The short upper plateau is due to the presence of  $Mg_2NiH_4$ .

A plot of the  $P_d$  vs the reciprocal temperature for  $MgH_2$  is shown in Fig. 4. It is a straight line and can be represented by the equation  $\log P_{atm} = -4045/T + 7.224$ . Assuming  $Mg_2NiH_4$  (or  $Mg_2Ni$ ) acts purely as a catalyst and that there is no solubility of  $H_2$  in the Mg phase, the following thermodynamic functions have been calculated for reaction (3)<sup>2</sup>:

$$\Delta H_{298^\circ K} = +18.5 \text{ Kcal}$$

$$\Delta F_{298^\circ K} = +8.7 \text{ Kcal}$$

$$\Delta S_{298^\circ K} = +33 \text{ eu}$$

The equilibrium dissociation pressure of  $MgH_2$  at  $325^\circ C$  is 2.85 atm. and this material could be used in any system provided the waste heat could be extracted at that temperature or above. It appears to be quite suitable for high temperature cells using molten carbonate electrolytes which operate above  $400^\circ C$ . However, since the optimum  $MgH_2$  temperature is about  $350^\circ C$  ( $P_d = 5.4$  atm.), the fused salt electrolyte cannot be used as a heat transfer medium because this temperature is about  $50^\circ C$  below the melting point of the lowest melting eutectic mixture of sodium,

lithium and potassium carbonates. The operation of the metal hydride reservoir at 400°C, where the  $P_d$  is 16.4 atm., is not recommended because it is in a temperature and pressure region where the strength of materials may be a problem and leaves no safety margin as far as the molten salt is concerned. Thus a secondary heat transfer medium would have to be used, perhaps a liquid metal (e.g. mercury or sodium), or gas (i.e. air).

The great advantage of  $MgH_2$  is, of course, its high hydrogen content. In this case, in order to power a high temperature cell, similar to the 500-watt cell described above, the total weight of material (91.2%  $MgH_2$ , 8.8%  $Mg_2NiH_4$ ) required to give the same operating characteristics would be 3.950 Kg (8.69 lb), having a volume (50% void space) of about 5.4 liters (0.19 ft<sup>3</sup>). Because of the presence of the ternary hydride, the hydrogen content of the mixture is 7.3 wt % rather than 7.6 wt % as it is in pure  $MgH_2$ . In calculating the volume we made no correction for the probable increase in density resulting from the presence of  $Mg_2NiH_4$  and have assumed the density of the mixture is the same as that of pure  $MgH_2$ , i.e. 1.45 g/cc.

A hydride reservoir containing  $Mg_2NiH_4$  or  $MgH_2$  could also be used to give a ballast effect in a reformer system as described above using  $VH_2$ . The higher hydrogen content of these compounds vs  $VH_2$  is somewhat offset by the higher decomposition temperature required for the former, otherwise the same advantages would accrue as those enumerated above.

### Conclusions

We have shown how several reversible metal hydride systems may be used to supply hydrogen to several types of electrochemical fuel cells. In our judgment  $VH_2$  is the preferred material for such use because of its convenience, flexibility and the ease with which it could be integrated with the most advanced fuel cell type, i.e. aqueous, low temperature systems. However, the large hydrogen content of  $MgH_2$  could be a determining factor in certain circumstances where weight may be an over-riding consideration. The ternary hydride  $Mg_2NiH_4$  is of interest primarily because it could be used in conjunction with high temperature Bacon cells.

It is our contention that these compounds have the potential to solve a serious and long-term problem associated

with the development of a practical and economical fuel cell, i.e. the storage and generation of hydrogen. It is also apparent that they could be used in a number of alternative schemes not discussed here, where these properties would constitute an important advantage and improvement.

#### Acknowledgment

The authors wish to thank Messrs. J. B. Hughes and A. Holtz for their expert assistance in the laboratory.

#### References

1. J. J. Reilly and R. H. Wiswall, *Inorg. Chem.*, 6, 2220 (1967).
2. J. J. Reilly and R. H. Wiswall, *Inorg. Chem.*, 7, 2254 (1968).
3. J. J. Reilly and R. H. Wiswall, *Inorg. Chem.* (in press).
4. W. E. Winsche et. al., "Metal Hydrides as a Source of Fuel for Vehicular Propulsion", BNL-11754.
5. S. J. Bartosh, Proceedings of the 20th Annual Power Sources Conference, Atlantic City, N. J., May 1966.
6. K. M. McKay, "Hydrogen Compounds of the Metallic Elements", E. & F. N. Spon Ltd., London, England, 1966.

Table 1

	<u>VH<sub>2</sub></u>	<u>Mg<sub>2</sub>NiH<sub>4</sub></u>	<u>MgH<sub>2</sub></u>	<u>H<sub>2</sub> Gas</u>	<u>Liq. H<sub>2</sub></u>
Available Hydrogen Wt %	2.1	3.3	7.6	100	100
Density g/ml	~5	2.57	1.45	$7.2 \times 10^{-3}$	$7 \times 10^{-2}$
Available Hydrogen g/ml of Volume	0.105	0.085	0.110	$7.2 \times 10^{-3}$	$7 \times 10^{-2}$

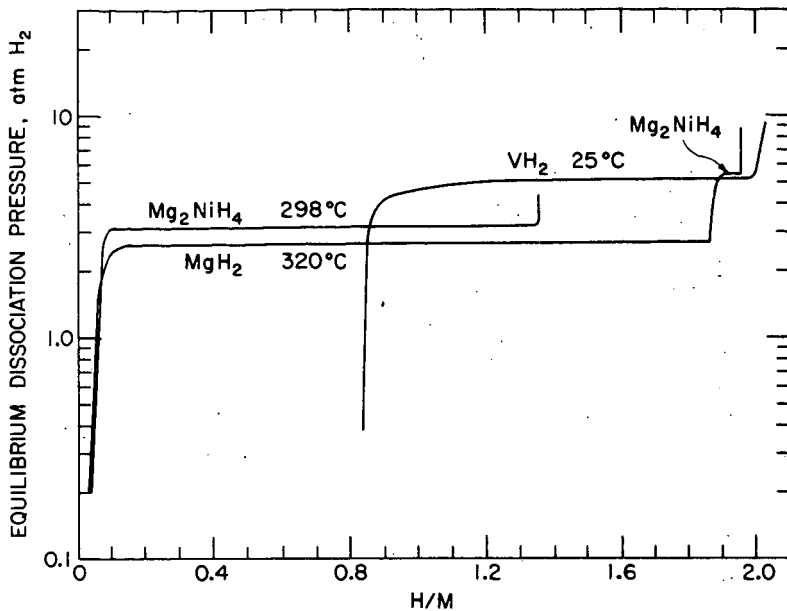


Fig. 1  
Pressure-Composition Isotherms  
for Systems Indicated.

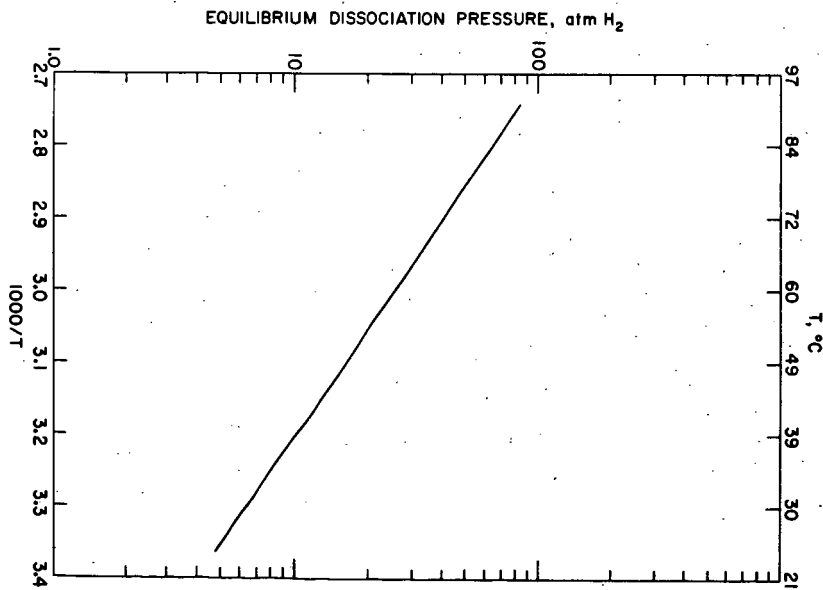
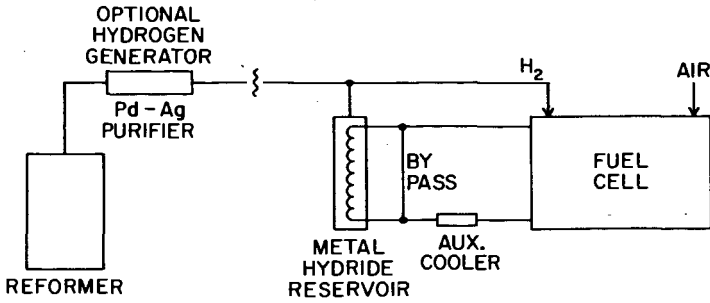


Fig. 2  
Equilibrium Dissociation Pressure  
of VH<sub>2</sub> vs 1000/T<sup>o</sup>K



METAL HYDRIDE	TEMP. °C	EQUIL. PRESS. atm	FUEL CELL	
			TEMP. °C	H <sub>2</sub> FEED PRESS. atm
VH <sub>2</sub>	25	5	75	2
Mg <sub>2</sub> NiH <sub>4</sub>	290	2.6	300	"
MgH <sub>2</sub>	340	5	>400	"

Fig. 3  
Schematic of Integrated  
Metal Hydride - Fuel Cell System

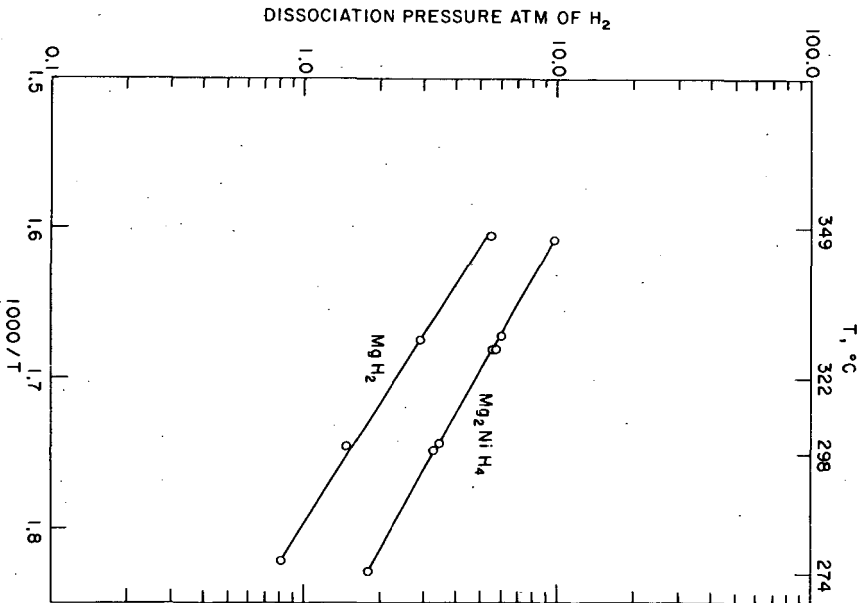


Fig. 4  
Dissociation Pressure of  
MgH<sub>2</sub> and Mg<sub>2</sub>NiH<sub>4</sub> vs 1000/T<sup>0</sup>K

## SELF-HEATING OF CARBONACEOUS MATERIALS

F. L. Shea, Jr., and H. L. Hsu  
Great Lakes Research Corporation  
Elizabethton, Tennessee

### INTRODUCTION

For quite a few years, Great Lakes Carbon Corporation has produced semi-calcined petroleum coke on a commercial scale. This coke is calcined to a maximum temperature of about 1600°F. For many years previous to this, both raw petroleum coke and fully calcined petroleum coke were handled in quantity and essentially no difficulty was encountered with spontaneous combustion. However, experience has demonstrated that semi-calcined coke is much more liable to spontaneous combustion and special precautions are necessary in handling this material. The present investigation was undertaken in connection with this phenomena.

Because of the importance of spontaneous combustion, particularly with respect to the storage of certain coals and lignites, quite a number of investigations have been conducted. There were a number of investigators who worked early in this century. Among the earliest workers to study the self-heating of coal under adiabatic conditions were Davis and Byrne<sup>(1)</sup>. In their investigation the sample was charged to a vacuum insulated container which was surrounded by an oil bath controlled to follow the temperature of the sample under test. All of their investigations

were conducted using dry coal and dry oxygen. The tests were started at approximately 70°C and usually terminated at about 140°C. They concluded that the heating tendencies of coals high in oxygen are greater in general than those of coals low in oxygen, although the heating tendency is not in all cases proportional to the oxygen content. The heating tendencies of coals of a similar rank are approximately the same. More recent work was done by Heusinger and Muenzner<sup>(2)</sup>. In their study tests were made at different starting temperatures with coal of high pyrite content. At >70°C, they found that the heat of oxidation in air gave a temperature rise which would lead to self-ignition in a few days.

In 1928, Rosin<sup>(3)</sup> published a very comprehensive article concerned with spontaneous combustion of semi-coke from brown coal. He pointed out the difference between ignition temperature and liability to spontaneous combustion which are often confused. Ignition temperature is the temperature at which ignition takes place under defined conditions, and is dependent upon the conditions. Liability to spontaneous combustion is a property possessed by a substance of heating spontaneously to the ignition temperature whereupon combustion ensues. A low ignition temperature is not the primary cause of spontaneous combustion. The quantitative work conducted by Rosin required rather large samples of coke - approximately 24 pounds which were held in insulated containers. Rosin recognized the importance of moisture and of humidity control, although it is not clear to what extent humidity was

controlled in the gases passed over the semi-coke. He concluded that moist, semi-coke absorbs more oxygen than dry semi-coke, and that it is more liable to spontaneous combustion. Also, that semi-coke is an activated carbon containing unsaturated compounds which absorb oxygen and that the absorption raises the temperature of the semi-coke to a temperature of dangerous oxidation, which finally results in combustion. Based on the work of others, he concluded the heat of wetting is sufficient to raise the temperature of semi-coke to the temperature of dangerous oxidation.

The use of D. T. A. for classifying coals on the basis of their self-heating characteristics was fully investigated by Banerjee and Chakravorty<sup>(4)</sup>.

The present paper is concerned with the measurement of the self-heating rates of carbonaceous materials when exposed to a stream of nitrogen, oxygen or CO<sub>2</sub> with controlled humidity.

#### EXPERIMENTAL WORK

##### Description of Apparatus

In designing the equipment the objective was to provide simple apparatus sufficiently well insulated so that the rather small heat of absorption or reaction could be followed by the rise in temperature of the carbonaceous material under test. It was desired to accomplish this without the necessity of having the ambient temperature closely follow the temperature rise of the sample, and without the necessity of using a very large sample.

A sketch of the apparatus is shown in Figure 1. It consists of a one-quart, wide mouth Dewar flask in an oven which may be held at constant temperature. The gases, nitrogen, oxygen or carbon dioxide, were supplied from tanks and the flow measured with a rotameter at room temperature. The gas then flowed to a flask filled with water, fitted with an electric heater in which the gas was dispersed by means of a fritted disc and allowed to rise through the water so as to saturate it.

Heat input was automatically controlled by the water temperature. The water saturated gas then flowed through a coil contained within the temperature controlled oven just ahead of the Dewar flask. The temperature of the gas was measured just prior to its entrance into the Dewar flask, using a thermocouple. A thermocouple was also mounted approximately one inch from the bottom of the sample contained in the Dewar flask. The steel tube which supplied the gas stream to the Dewar flask was fitted with a perforated platform at its base which closely fitted the inside diameter of the Dewar flask. The sample was placed on the platform which provided distribution of the gas.

In early tests some difficulty was encountered in obtaining satisfactory Dewar flasks due to insufficient insulation. Prior to placing a Dewar flask in use, its behavior was checked using a standard sample. It was found that heavy walled Pyrex Dewars were best for this particular application, as they provided maximum insulation.

The silvered Dewars used were 70 mm. I. D., 90 mm O. D., 250 mm. deep and contained no separation pads at the base. The evacuation was approximately  $1 \times 10^{-7}$  mm. of mercury.

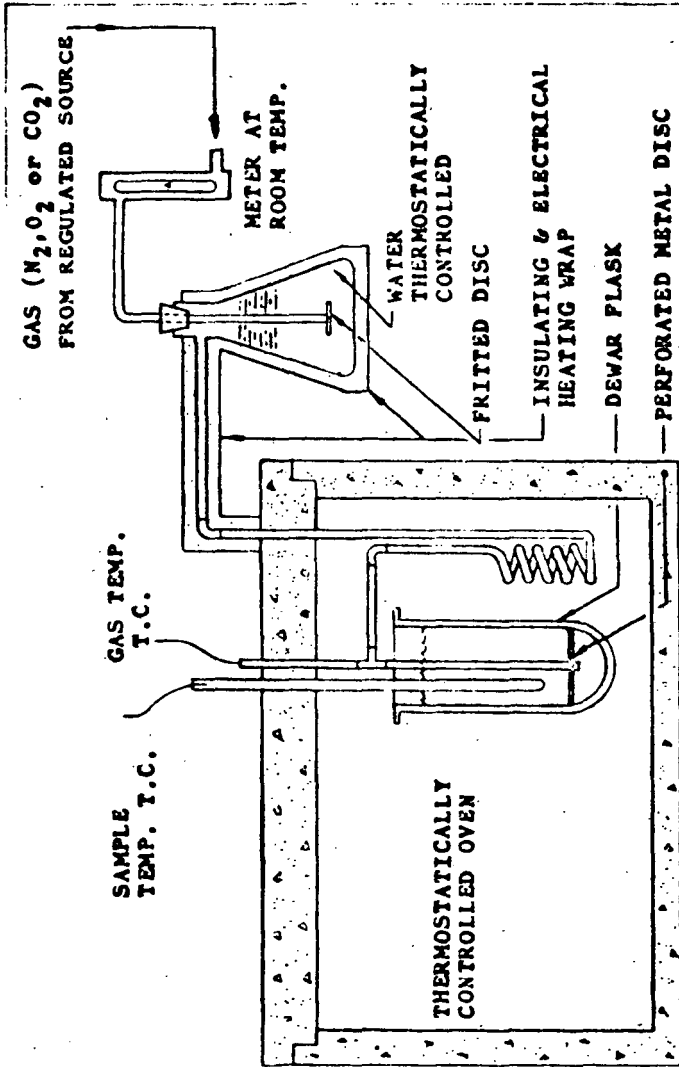


FIG. 1.  
APPARATUS FOR SELF-HEATING OF CARBONACEOUS MATERIALS

### Sample Preparation

The as-received semi-calcined petroleum coke was carefully crushed to produce a maximum of -3 on 14 mesh particles. In order to standardize test conditions, the majority of the tests were made using coke samples which were air-dried at 220°F. Vacuum drying and drying in an inert atmosphere were investigated. The temperature rise and the shape of the temperature versus time curve were within the limit of reproducibility of the test regardless of the method of drying.

The -3 on 14 mesh size fraction was also used for all other raw materials tested.

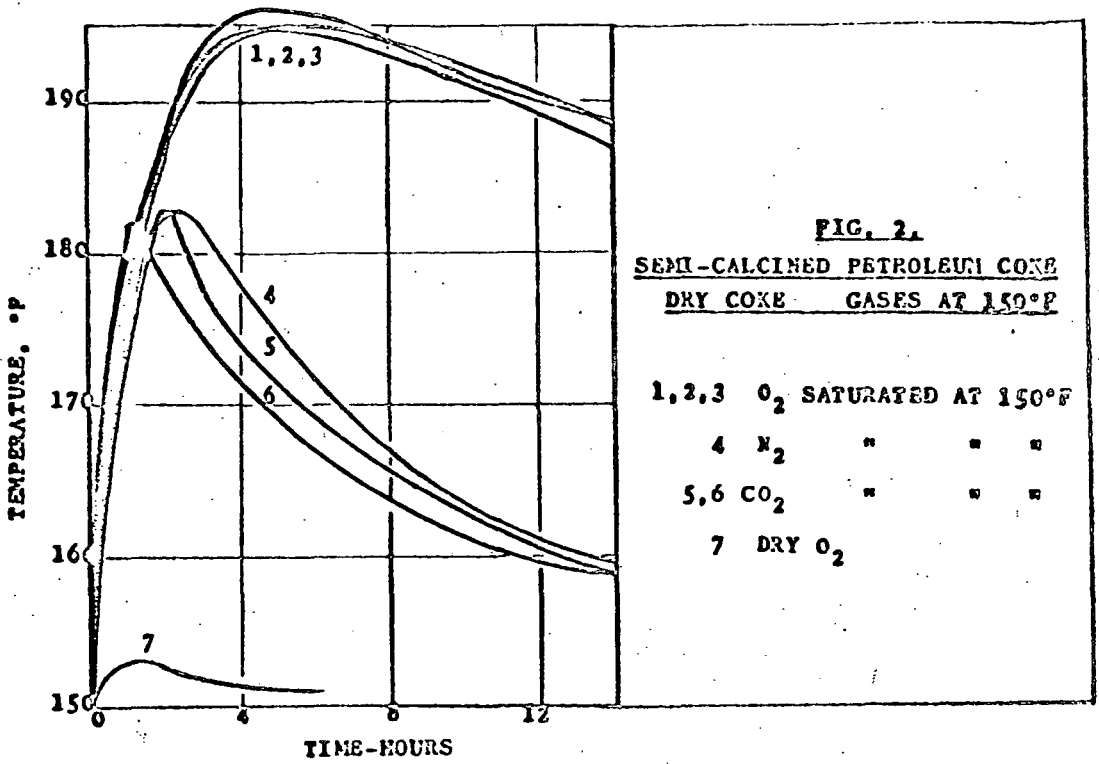
### Test Procedure

Due to the extremely low rate of heat transfer between the oven and the sample contained in the Dewar, it was necessary to charge the sample at approximately 150°F. Dried samples at 220°F were allowed to cool to approximately 150°F and then charged to the Dewar. A 600 g. sample was used. The temperature of the sample was then adjusted to 150°F by passing dry nitrogen gas through to either cool or heat the sample. To make certain the system was in equilibrium, it was held for at least ten minutes at 150°F prior to starting a run. The desired gas was then passed through the sample at a controlled flow rate, usually 0.5 cu.ft./hr. and was saturated with water at 150°F, if desired. The furnace temperature, inlet gas temperature, and temperature of the sample at a point one inch above the bottom of the sample were recorded, versus time.

## RESULTS AND DISCUSSION

In Figure 2 is shown a graph for a number of runs conducted on a sample of semi-calcined petroleum coke. All runs were made with representative portions of the same sample of coke. Curves 1, 2 and 3 were runs in triplicate made with oxygen, Curve 4 was a run made with nitrogen and Curves 5 and 6 duplicate runs made with CO<sub>2</sub>. In all runs the gases were at 150°F and saturated with water vapor. The agreement between duplicate runs is quite good and demonstrates the reproducibility of the test procedure. We may attribute the difference between the temperature versus time relationship of Curves 1, 2 and 3 versus the curves for the runs with nitrogen and CO<sub>2</sub> to the presence of oxygen versus nitrogen or CO<sub>2</sub>. There is a definite increase in the maximum temperature obtained of about 12°F when oxygen is used rather than the more inert gases. The shape of the curves after the peak temperature has occurred is of interest. With oxygen there is a tendency for the temperature to be sustained for a longer period of time indicating that the oxygen continues to be absorbed or to react, liberating heat, while with nitrogen or CO<sub>2</sub>, after the peak is reached, there is a much sharper decrease in temperature with respect to time. These data indicate that the temperature rise due to absorption of water vapor is about 33°F, while that due to O<sub>2</sub> is about 12°F.

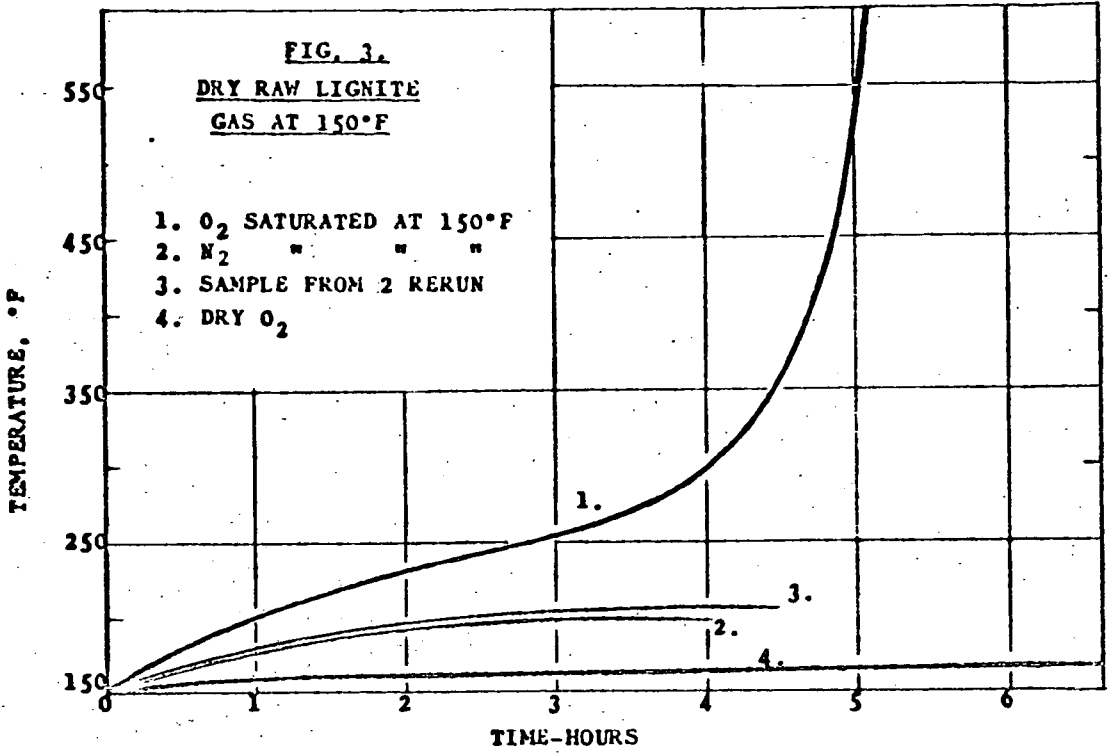
Curve 7 is for a run using dry oxygen at 150°F. The maximum temperature attained was well below that of any of the curves made with saturated gases and indicates that there is little or no reaction or absorption of oxygen in the absence of moisture.

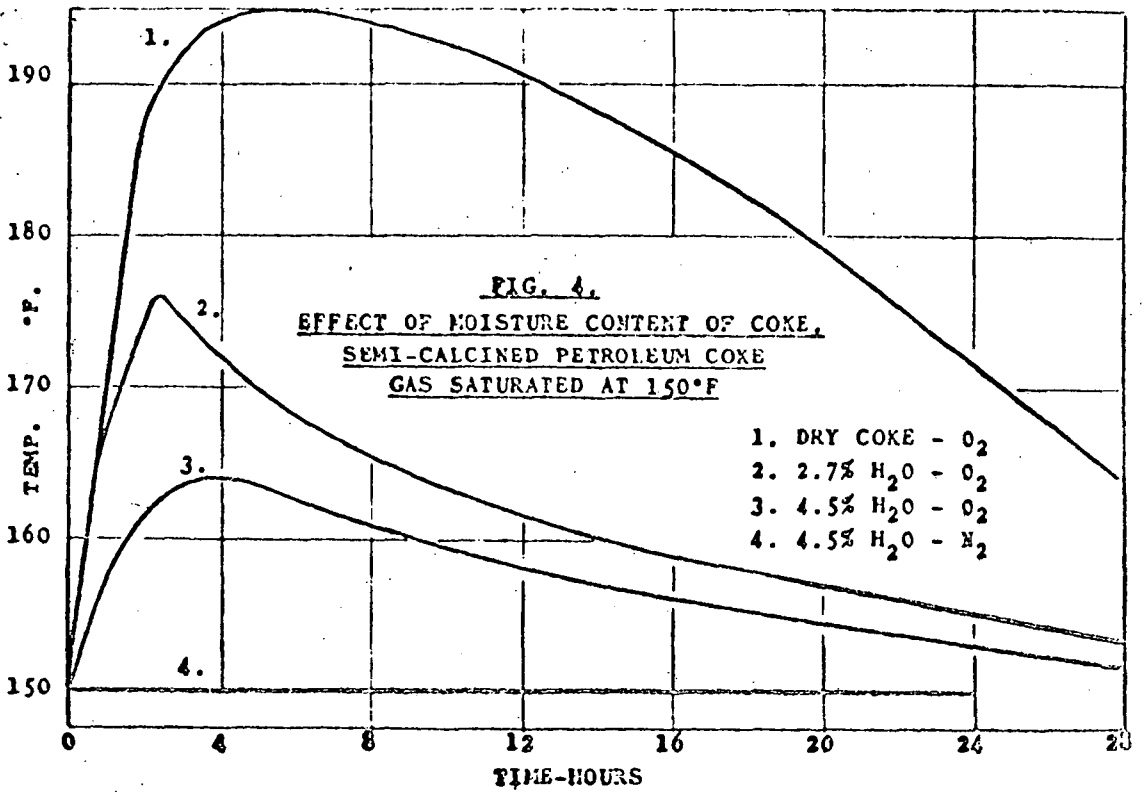


The importance of the role of water in the self-heating of carbonaceous materials is shown more strikingly in Figure 3 in which the sample was dry raw lignite. All runs were made with the gas stream at 150°F. Curve 1 was made with oxygen saturated with water vapor, Curve 2 and 3 with nitrogen saturated with water vapor and Curve 4 with dry oxygen. With dry oxygen the maximum temperature rise was 18°F, with saturated nitrogen 48°F and with saturated oxygen the sample ignited spontaneously in less than 5 hours.

All runs of Figure 4 were conducted using representative portions of a sample of semi-calcined petroleum coke. In runs 1, 2 and 3, the gas was oxygen saturated with water vapor at 150°F; in run 4, it was nitrogen saturated with water vapor. The combination of dry coke exposed to saturated oxygen gave a temperature rise of about 45°F in 5 hours, and as expected, moisture addition to the coke lowered the temperature rise in an atmosphere of saturated oxygen. In run 4 made with saturated nitrogen and coke containing 4.5% water, there was no measurable temperature rise.

From the runs of Figure 2 the contribution of O<sub>2</sub> and water vapor to the temperature rise of semi-calcined petroleum coke was estimated based on the difference between the total rise with saturated O<sub>2</sub> and that with saturated N<sub>2</sub> using dry coke. This amounted to 12°F. In the experiments presented in Figure 4, the coke was saturated with water and the temperature rise due to O<sub>2</sub> measured directly. This amounted to about 14°F,

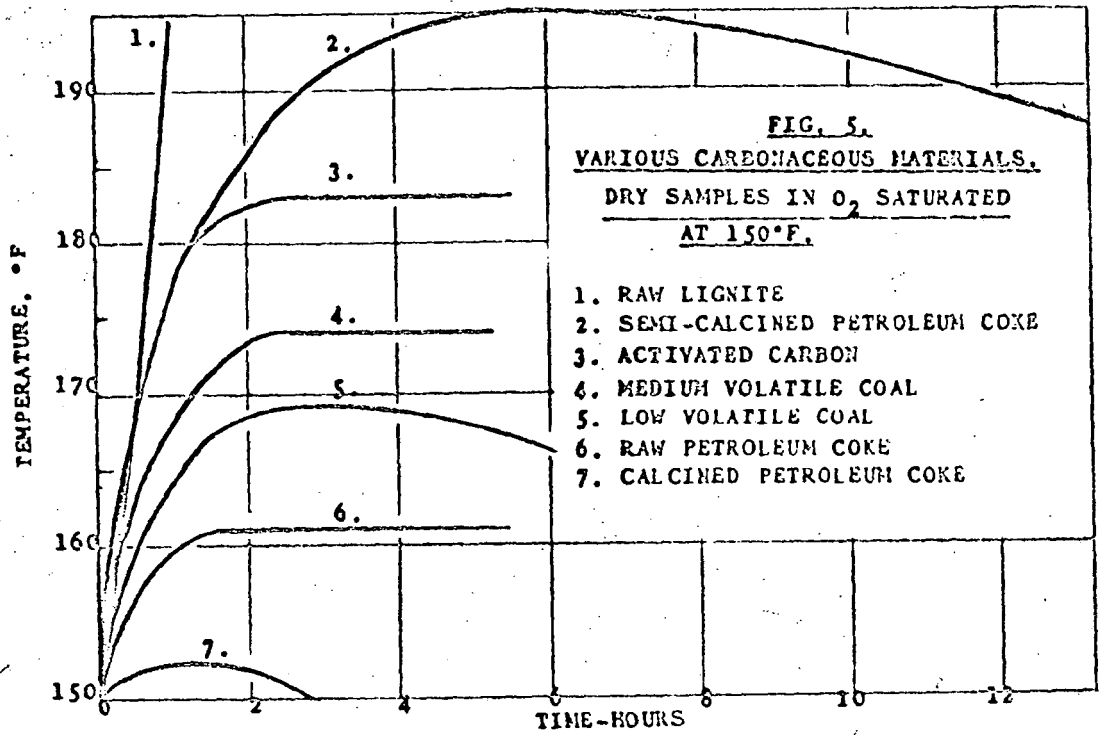




while the rise due to water vapor by difference amounted to 31°F. These are in good agreement with the estimates from Figure 2.

In Figure 5 are shown temperature versus time curves for a variety of carbonaceous materials subjected to a stream of oxygen at 150°F saturated with water vapor. From an examination of the curves it is apparent that lignite, which can be stored with safety only under water, shows the greatest tendency for self-heating in the test apparatus and actually ignites spontaneously in less than five hours. The next most active material is semi-calcined petroleum coke, which shows a maximum temperature rise of about 45°F in five hours. Surprisingly enough this material exhibits a greater temperature rise than a commercial grade of activated carbon which shows a temperature rise of about 33°F. Below this in decreasing order of temperature rise are: a medium volatile (27%) bituminous coal, a low volatile (17%) coal, raw petroleum coke with a volatile matter content of 12%, and finally calcined petroleum coke which exhibits no temperature rise under these conditions. The results of Figure 5 are in good agreement with the known behavior of the various carbonaceous materials upon storage in the field<sup>(5)</sup>.

The behavior of the activated carbon is of course an exception. Although it exhibits a rather high temperature rise in this test, it is not subject to spontaneous combustion. This is due to the fact that it is well devolatilized and does not contain an appreciable amount of hydrocarbons which are



available for combination with oxygen at temperatures in the range from about 300°F to its ignition point. Thus, it is believed that when this test with oxygen at 150°F saturated with water vapor is applied to materials which are capable of combining with oxygen in the temperature range of 300°F to their ignition temperature, it provides a good measure of the liability of the material to spontaneous ignition.

#### SUMMARY AND CONCLUSIONS

A simple procedure for the determination of the self-heating rates of various carbonaceous materials has been developed. For those materials which contain sufficient hydrocarbons to combine with oxygen at 300°F and thus ignite at relatively low temperatures, the maximum temperature rise determined in this test correlates with the liability to spontaneous ignition in the field. In a completely dry system there is no serious self-heating evident for any of the materials tested, even in pure oxygen. The absorption of water vapor by the dry carbonaceous material provides the major heating effect in the temperature range from 150°F to about 190°F. This temperature rise will occur even though the moisture be carried by an inert gas such as nitrogen or CO<sub>2</sub>. With semi-calcined petroleum coke it has been demonstrated that if oxygen is used, a higher temperature rise of approximately 14°F occurs due to absorption or reaction of the oxygen in the presence of moisture.

The importance of moisture is best illustrated by the behavior of raw lignite which in dry oxygen at 150°F shows a temperature rise of only 18°F in about 5 hours. However, if the oxygen is saturated with water vapor at 150°F, the rate of temperature rise is of the order of tenfold greater, and the lignite ignites in less than 5 hours. Of all of the carbonaceous materials investigated, raw lignite shows the greatest temperature rise in oxygen saturated with water vapor at 150°F. The next most reactive material was semi-calcined petroleum coke which is more active than any of the bituminous coals tested, and in agreement with field experience with this material where considerable difficulty is encountered with spontaneous ignition unless great care is exercised to insure proper cooling prior to storage and to exclude the access of air insofar as possible.

LITERATURE CITED

1. Spontaneous Combustion of Coal, Davis, J. D. and Byrne, J. F., INDUSTRIAL AND ENGINEERING CHEMISTRY, Vol. 17, No. 2, pp. 125-130 (1925).
2. An Adiabatic Colorimeter for Measurement of the Heat of Oxidation of Bituminous Coals at Low Temperature, Heusinger, P. and Muenzner, H., BRENNSTOFF-CHEM. 45 (12), 357-60 (1964).
3. Spontaneous Combustion of Semi-Coke from Brown Coal, Rosin, P., BRAUNKOHLE, Vol. 27, pp. 241-56, 282-292. Translation by Taylor, H. S., FUEL, Vol. 8, No. 2, pp. 66-78 (1929).
4. Use of D. T. A. in the Study of Spontaneous Combustion of Coal, Banerjee, S. C. and Chakravorty, R. N., J. Mines, METALS FUELS, 15(1), 1-5, 19 (1967).
5. Fuel by Brame and King, Fifth Edition, 1955, pp. 156, Edward Arnold Publishers, Ltd., London.

PRODUCTION AND CHARACTERIZATION OF  
CARBON DERIVED FROM COMPOUNDS OF INDENE (U)

W. E. Smith  
W. L. Harper

Union Carbide Corporation - Nuclear Division, Oak Ridge, Tennessee

The advances in structural design associated with reactor, aerospace, and related technologies increase, in turn, demands for speciality forms of structural materials. One material that is finding special and strategic application in these areas is carbon. Increased use of carbon for other, more domestic applications is projected for the future. Interest in carbon as a fabrication material is prompted by the following: (1) high temperature heat resistance, (2) resistance to chemical attack, (3) constancy of properties with time, (4) the diverse properties which carbon can exhibit and the variety of product-type into which it can be made.

Since the properties exhibited by carbon can significantly vary, use of this material necessitates control of these properties. Our efforts involve two aspects of control: (1) reproducibility, with emphasis on use of synthetic raw materials as carbon precursors, (2) manipulative control, which would allow one to make carbon with specific and preselected properties by the appropriate choice of precursor and processing conditions. It is known that chemical, mechanical, electrical, and thermal properties of carbon, or parts fabricated from carbon, are greatly influenced by the carbon type; as is well known, carbon is generally classified in terms of amorphous, graphitic, and diamond structures. Properties associated with any given classification suggest a range of values. More specifically, properties of a graphitic carbon are a function of the degree of graphitization and certain other microstructural properties.

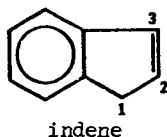
Have you considered the factors which contributed to the diverse properties exhibited by our natural deposits of carbon and carbonaceous products? Generalization will allow us to narrow the effects to two factors: (1) the nature of the organic matter from which the carbon was derived, (2) the conditions (pressure, temperature, time, etc.) under which the organic matter was converted to carbon. In our evaluation of carbon precursor materials, we have considered the same two factors. More specifically, we have attempted to correlate carbon properties with (1) the properties of the precursor material, with emphasis on effects attributed to molecular composition and structure, and (2) the processing conditions employed in converting the organic material into carbon, including the effect of temperatures up to 3000° C.

Some understanding of the relationships existing between carbon properties and precursor properties have evolved over the years. In general, organic materials which are or become infusible prior to pyrolysis do not tend to produce graphitic carbon. This type of material is characterized by thermosetting resins or highly crosslinked polymers. Thus, crystallinity seems to be dependent upon the ability of molecules to rearrange or reorient prior to pyrolysis, and such mobility necessitates an intermediate fluid or plastic state. Research efforts involving liquid crystal and mesophase studies represent attempts to correlate degree of orientation prior to pyrolysis with graphitic properties of derived carbon. Likewise, the planarity of polynuclear aromatic molecules will be a significant factor in determining the degree of graphitization of derived carbon. Molecules or molecular fragments that retain a nonplanar structure do not tend to graphitize. This seems reasonable in light of the planar, polynuclear structure that characterizes graphite. In addition to the inherent organic structure of the precursor materials, the presence of

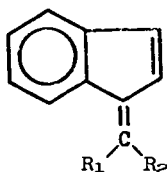
impurities such as sulfur and metallic compounds influence the graphitic properties of derived carbon.

Thus, precursor materials derived from natural sources will not be adequate for certain specialized applications since (1) they represent a complex mixture of organic structures whose composition varies with sources and refining methods, and (2) they frequently contain inorganic contaminants which vary in quantity and type with location of source.

This effort in the area of synthetic carbon precursors has included synthesis, polymerization, and carbonization studies. Much of the effort has been directed toward synthesis and evaluation of carbon precursor materials derived from indene ( $C_9H_8$ ).



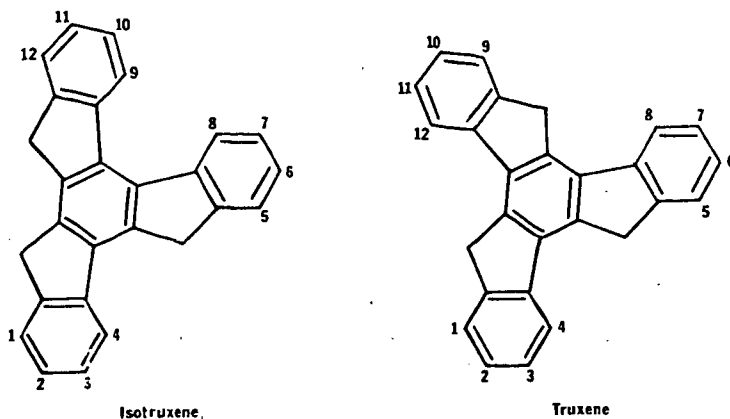
Included in the series were various indene derivatives incorporating the benzofulvene structures shown below.



	<u>R<sub>1</sub></u>	<u>R<sub>2</sub></u>	<u>Compound</u>
I	H	H	benzofulvene
II	CH <sub>3</sub>	CH <sub>3</sub>	dimethylbenzofulvene
III	H	C <sub>6</sub> H <sub>5</sub>	benzylideneindene
IV	CH <sub>3</sub>	C <sub>6</sub> H <sub>5</sub>	methylphenylbenzofulvene
V	C <sub>6</sub> H <sub>5</sub>	C <sub>6</sub> H <sub>5</sub>	diphenylbenzofulvene
VI	H	C <sub>6</sub> H <sub>5</sub> -CH=CH-	cinnamylideneindene

These compounds were synthesized by condensation reactions of indene with carbonyl compounds with the carbonyl component becoming an integral part of the benzofulvene structure.

Additional compounds that were derived from indene included  $\alpha$ -truxene (truxene) and  $\beta$ -truxene (isotruxene), both of which are trimeric derivatives of indene. As shown by the structures below, the latter compounds are structural isomers.



The preparative procedures involve reactions of indene and carbonyl compounds in the presence of amine catalysts. Heretofore, only isomeric mixtures of these two compounds could be obtained by synthetic procedures involving autoclave conditions. However, procedures used in this study will allow production of either isomer under reflux conditions, and at the exclusion of the other. The specific isomer obtained will be a function of the carbonyl compound used in the formulation.

To lend emphasis to the correlations previously suggested between carbon properties, precursor properties, and processing conditions, truxene and isotruxene shall be discussed in detail. The influence of three factors on graphitizability of carbons shall be considered. These are the effect of (1) molecular structure, (2) metallic impurities, and (3) polymerization conditions.

Initially, structural effects will be considered. Though isomeric in structure, truxene yields a nongraphitic carbon while carbon derived from isotruxene tends to be graphitic. Two factors could contribute to the disoriented structure of truxene-derived carbon: (1) the planar structure that characterizes truxene molecules is apparently disrupted prior to pyrolysis and nonplanar intermediates are formed; (2) the fluid properties before and during pyrolysis were not conducive to orientation. As observed for other nongraphitizing materials, gases evolved during pyrolysis were entrapped, resulting in a cellular or foam-like carbon. Such gases tend to be freely evolved during pyrolysis of graphitizing materials, as was observed for isotruxene. These observations are indicative of the fluid properties existing during periods in which chemical change and structural realignments will be greatest. Lack of molecular mobility during these periods would tend to inhibit orientation. Attempts to control graphitic properties of carbons by blending graphitizing and nongraphitizing materials were considered. The materials must of necessity form homogeneous solutions and must yield a homogeneous carbon. For example, mixtures of isotruxene and truxene produce homogeneous carbons with properties that are dependent on composition. Data obtained by X-ray analysis of carbons derived from isotruxene and truxene-isotruxene mixtures are shown as a function of temperature in Table 1.

Table 1

CRYSTALLOGRAPHY STUDIES ON GRAPHITIC CARBONS FROM ISOMETRIC TRUXENES

Source of Carbon	Heat Treatment Temperature (°C)	$d_{004}$ (Å)	$C_0$ (Å)	$L_c$ (Å)	$d_{110}$ (Å)	$A_0$ (Å)	$L_0$ (Å)
Isotruxene	2,800	1.6820	6.7280	314	1.2296	2.4592	259
Isotruxene	2,400	1.6845	6.7380	255	1.2299	2.4598	412
Isotruxene	2,000	1.7080	6.8320	126	1.2261	2.4522	135
Isotruxene-100	2,800	1.6317	6.7268	315	1.2294	2.4588	247
Isotruxene-truxene (75-25)	2,800	1.6914	6.7656	113	1.2300	2.4600	250
Isotruxene-truxene (75-25)	2,400	1.6946	6.7784	106	1.2290	2.4580	250

In one example of a study involving the effect of metallic impurities on graphitizability, samples of truxene-derived carbon containing induced metallic impurities were evaluated. Samples containing titanium carbide were fired to 2800° C, and were studied by X-ray analysis and photomicrography. Microstructural observation indicated large areas of graphitic carbon. As shown in Figure 1, X-ray data indicated an increased degree of graphitization as compared to the typically nongraphitic carbon derived from truxene. Other metals such as iron, nickel, chromium, or aluminum will also promote graphitization of typically nongraphitizing materials.

To show the effect that polymerization conditions can have on graphitizability, the oxidative polymerization of isotruxene will be considered. Without an oxidative cure, isotruxene yields an isotropic carbon that is not highly graphitic. After oxidative cure, X-ray analysis and microstructural examination indicate a more graphitic and a more anisotropic carbon. Changes in carbon properties with oxidative cure time are shown in Table 2.

In summary efforts to closely control properties of synthetic carbons must include close control on raw material properties and impurities, and conditions under which organic precursor materials are converted to carbon.

Table 2  
EFFECT OF HEAT TREATMENT (300° C) IN OXYGEN ON THE PROPERTIES OF ISOTRUXENE AND ISOTRUXENE DERIVED CARBON(1)

Time (hrs)	Viscosity(2) (cp)	Oxygen Content(3) (%)	Melting Range (° C)	Apparent Monomer Content(4) (%)	Coke Yield at 1,000° C (%)	Carbon Properties After 3,000° C				
						g Factor	L <sub>c</sub> (A)	d <sub>110</sub> (A)	L <sub>a</sub> (A)	
Batch 10-82-69 (O <sub>2</sub> Flow Rate, 40 cc/min)										
0	18.0	0.24	202 - 212	79.2	38.5	1.7010	0.422	120	1.2287	210
24	22.0	0.43	78 - 187	81.2	42.5	1.6906	0.656	104	1.2299	289
48	32.4	0.73	89 - 123	70.9	61.5	1.6914	0.633	112	1.2308	280*
72	56.8	1.10	93 - 142	64.5	63.5	1.6854	0.767	187	1.2307	419
96	113.2	1.28	135 - 183	58.9	75.0	1.6860	0.756	187	1.2310	319
125	427.2	1.43	182 - 196	57.6	78.0	1.6865	0.744	178	1.2304	361
Batch 10-84-69 (O <sub>2</sub> Flow Rate, 84 cc/min)										
0	17.2	0.31	201 - 209	82.7	45.0	1.7025	0.389	97	1.2292	200
24	26.4	0.89	85 - 178	78.9	63.5	1.6900	0.667	102	1.2302	377
48	61.2	1.29	123 - 163	64.4	61.5	1.6871	0.711	131	1.2303	362
72	137.6	1.17	132 - 168	59.9	73.5	1.6845	0.789	200	1.2304	447
91	627.2	1.09	184 - 222	58.5	83.5	1.6851	0.778	173	1.2303	424
Batch 10-92-69 (O <sub>2</sub> Flow Rate, 165 cc/min)										
0	18	0.24	208 - 216	69.0	26.0	1.7004	0.433	112	1.2292	206
24	32.8	0.86	92 - 122	75.0	60.5	1.6882	0.711	122	1.2304	427
48	108.0	1.45	143 - 178	56.0	77.0	1.6871	0.733	198	1.2307	591
65(5)	-	0.62	> 300	(insoluble)	89.5	1.6882	0.711	129	1.2304	367

(1) Isotruxene was heated at 300° C with constant agitation and with O<sub>2</sub> gas bubbling through molten material. Samples were removed periodically for evaluation.  
 (2) Measured with Brookfield viscometer.  
 (3) Determined by neutron activation.  
 (4) Estimated from molecular distributions shown on GPC scans.  
 (5) Material solidified after 65 hours of heating at 300° C, thus no viscosity was measured.

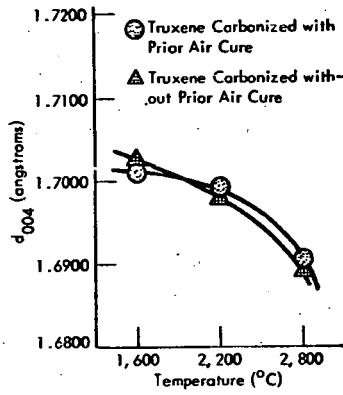


Figure 1. Correlation of Interlayer Spacing With Firing Temperature for Truxene-Derived Carbon Containing Titanium Carbide.

AN ECONOMIC COMPARISON OF PROCESSES FOR PRODUCING  
PIPELINE GAS (METHANE) FROM COAL

J. P. Henry, Jr. and B. M. Louks  
Stanford Research Institute  
Menlo Park, California 94025

An impending shortage of natural gas in the United States has led to intensive bench scale research in efforts to develop processes for preparing pipeline quality gas (methane) from coal at competitive costs. Funding of the research has been provided by the Office of Coal Research, the American Gas Association, and private organizations. Processes under development differ in the method by which steam-carbon reaction heat is added. The following list identifies the most notable processes and the method each process uses for steam-carbon reduction heat addition.

<u>Process</u>	<u>Developer</u>	<u>Heat Addition By</u>
Hot carbonate	M. W. Kellogg Co.	Sensible heat of molten salt
Super high pressure C.S.G.	Bituminous Coal Research Consolidation Coal	Combustion of pure oxygen In-situ exothermic chemical reaction
Continuous Steam-Iron	Fuel Gas Associates	In-situ exothermic chemical reaction
Hygas	Institute of Gas Technology	Electric power and in-situ exothermic chemical reaction

The processes under development are reviewed and their relative economics explained by a presentation of the thermochemistry of reactions utilized in preparing methane from coal.

## HYDROGEN: A KEY TO THE ECONOMICS OF PIPELINE GAS FROM COAL

C. L. Tsaros

Institute of Gas Technology  
Chicago, Illinois 60616

### INTRODUCTION

The objective in manufacturing supplemental pipeline gas is to produce high-heating-value gas that is completely interchangeable with natural gas — essentially methane. Large amounts of low-heating-value constituents like hydrogen or carbon monoxide or inert diluents like carbon dioxide or nitrogen cannot be tolerated.

### BASIC PROCESS CONSIDERATIONS

The basic problem in making methane from coal is to raise the  $H_2/C$  ratio. A typical bituminous coal may contain 75% carbon and 5% hydrogen, a  $H_2/C$  mole ratio of 0.4:1; the same ratio for methane is 2:1. To achieve this ratio it is necessary to either add hydrogen or reject carbon. The most efficient way is to add hydrogen. The hydrogen in the coal can supply about 25-30% of the required hydrogen, but the bulk must come by the decomposition of water, the only economical source of the huge quantities needed for supplemental gas.

There are two basic methods for adding hydrogen to coal: In the first, or indirect, method, coal reacts (by Reaction 1) with steam to form synthesis gas — mainly hydrogen and carbon monoxide.



This reaction is highly endothermic and requires combustion of carbon with oxygen, or some other heat source. The CO and  $H_2$  then react catalytically to form methane:



Prior to methanation, part of the CO is made to react with more water to increase the  $H_2/CO$  ratio.



In the second, or direct, method, methane is formed directly by the destructive hydrogenation of coal by the reaction:



The indirect method is inherently less efficient because in the process water is decomposed in Reactions 1 and 3. A portion of the hydrogen product is then converted back to water by Reaction 2. Reaction 2 is more exothermic than Reaction 4. Since Reaction 2 is carried out at a much lower temperature than Reaction 1, this heat is not available. Decomposition of an increased amount of water also consumes more energy in the indirect than in the direct method.

The major effort at IGT has been in hydrogasification, now called the HYGAS Process, because of the originally high oxygen consumption and costs of the synthesis-gas methanation route.

## PROCESS ECONOMICS

Process economic studies have been carried out in conjunction with the development program at IGT for pipeline gas from coal. A number of different process designs have been prepared in which the price of gas was reduced from the level of \$1.00 to \$0.50/million Btu. The most important effects on the cost of product gas have resulted from the way hydrogen is generated or utilized in the hydrogasifier; hydrogen has been the key factor in reducing the price of gas.

The original studies cover a period of about 10 years and have somewhat different process and cost bases. In this paper the results of seven different pipeline gas plant economic evaluations are compared. An attempt has been made to adjust these to a common and more current basis for capital and operating costs. Coal costs are assumed to be uniform at 16.1¢/million Btu. The plant size is 250 billion Btu of product-gas heating value. The seven studies are -

1. Synthesis-gas methanation
2. Hydrogasification of coal by a hydrogen/char ratio of 300% of stoichiometric
3. Partial hydrogasification with 50% of the stoichiometric hydrogen rate
4. Hydrogasification with steam-hydrogen mixtures
5. Hydrogen by the steam-iron process
6. Hydrogen from synthesis gas generated by electrothermal gasification
7. Hydrogasification with synthesis gas

The data presented in this paper have all been derived from the earlier studies to which the cited references refer. Because of the adjustments in capacity and cost index made to get a better basis for comparison, the costs differ somewhat from the originals. Sulfur by-product credit has not been included because of different sulfur contents for some of the coals used.

Several simple flow diagrams have been prepared to illustrate the different process schemes. Table 1 gives pertinent data; Figures 1 and 2 show the cost of gas in relation to different hydrogen schemes and net production rates. To permit comparison, gas prices shown are based on the same utility-type accounting procedure. The basic assumptions are 1) 20-year straight-line depreciation, 2) 7% return on rate base (end-of-year undepreciated book value plus working capital), 3) 5% interest on debt, 4) 65:35 debt/equity ratio, and 5) 48% Federal income tax. This results in an average annual return on outstanding equity for the cases shown ranging from 9.3 to 9.5%.

Return on equity is calculated as follows: Debt retirement is 5% of the initial debt. Annual depreciation exceeds annual debt retirement by a constant amount, which is called the surplus. This surplus is used to reduce the outstanding equity, which results in a linearly decreasing outstanding equity. To calculate average percent return on equity, the 20-year average net income is divided by the 20-year average outstanding equity.

Interest rates are presently high; even with some reduction in the future, they will probably be higher than 5%. To maintain attractive return on equity at higher interest, the return on rate base will also have to be raised. For a second set of gas prices, we have raised financial factors to a 7.5% interest rate and a 10.1-10.2% average annual return on equity. The income tax rate and debt/equity ratio are as before. This requires a rate of return of 9% on the rate base, from which both debt and equity return are paid.

Table 1. SUMMARY OF PIPELINE GAS FROM COAL PROCESS (250 Billion Btu/Day High-Btu Gas at 1000 psig, 90% Annual Plant Operating Factor, Gas Prices Calculated by A.G.A. Accounting Procedure, Economics of Different Processes Estimated on a Comparable Basis)

Gas Number Process	Partial Hydrogenation, Hydrogen From Spent Char						
	1	2	3	4	5	6	7
Synthesis-gas methanation	916 20,262	934 18,609	939 16,625	947 17,790	941 17,790	941 17,790	937 17,790
Product Gas, Btu/SCF							
Coal, tons/day (Equivalent to 12,400 Btu/lb)							
H <sub>2</sub> + CO Generation							
Source							
10 SCF/Day	985	470	414	295	295	308	308
Moles/hr	108,406	51,730	45,602	32,495	32,495	33,863	33,863
Oxygen, tons/day	12,500	6,020	5,440	4,109	--	--	--
Purchased Electric Power, kW	--	--	--	--	--	--	--
Overall Efficiency, %	49.9	54.3	61	66.2	72.6	61.7	65.8 <sup>c</sup>
By-products <sup>a</sup>							
Char Plus Fines, tons/day	--	--	--	1,809	468	4,161	4,557
Low-Btu Gas, 10 <sup>6</sup> Btu/day	--	--	--	--	61	--	--
Capital Investment	200	218	186	136	99	98	87
Installed Equipment Cost, \$10 <sup>6</sup>	235-241	256-262	218-223	161-165	118-121	118-121	105-108
Total Investment Cost, \$10 <sup>6</sup> <sup>b</sup>							
20-yr Avg Price of Gas	87.0	89.3	75.8	65.1	54.7	61.7	56.1
Standard Factors, #/10 <sup>6</sup> Btu	91.2	93.8	79.7	68.0	56.9	63.9	58.0
New Factors, #/10 <sup>6</sup> Btu							

<sup>a</sup> Sulfur not included because of different costs.  
<sup>b</sup> Includes working capital, which increases with higher gas price due to new financial factors.  
<sup>c</sup> In calculating efficiency, fuel to generate purchased power subtracted from by-product char.  
<sup>d</sup> 258 X 10<sup>6</sup> Btu/day.

Depending on the investment level, the effect of the higher financial factors is to raise gas price from 1.9¢ to 4.5¢/million Btu for the investment range covered.

### Indirect Methanation - Synthesis-Gas Methanation (Case 1)

The first process, methanation of synthesis gas generated by Texaco steam-oxygen suspension gasification of coal,<sup>1</sup> is shown in Figure 3. Gas made this way is expensive because of the high oxygen requirement and the low thermal efficiency. For a 250 billion Btu/day plant, 12,500 tons/day of oxygen are needed for generation of 985 million SCF/day of hydrogen equivalent (CO + H<sub>2</sub>). Investment is \$240 million; product gas costs approximately 90¢/million Btu, depending on financial factors.

### Direct Hydrogenation

The rest of the studies are based on the direct hydrogenation of coal char to methane discussed above. They represent a historical and process economic study of major steps in hydrogen usage that have occurred in the development of the HYGAS Process.

### Use of Excess Hydrogen (Case 2)

The first economic evaluation for hydrogasification was based on pilot plant data in which a large excess of hydrogen - 300% of the stoichiometric hydrogen/char ratio - is fed to the hydrogasifier<sup>2</sup> in a fluidized-bed reactor (Figure 4). Nearly complete gasification is achieved. A separate coal stream flows to the gasifier where synthesis gas for hydrogen production is generated. The coal pretreatment step, a low-temperature carbonization process, is more severe than the simpler air oxidation used in IGT's later work. More hydrogen and other volatile matter is lost in the low-temperature carbonization, requiring more net hydrogen input.

With excess hydrogen, the hydrogasifier effluent contains CH<sub>4</sub>/H<sub>2</sub> in a 0.32:1 ratio, which is upgraded to a ratio of 8.7:1 by low-temperature separation. This processing step contributes about 15¢/million Btu to the price of gas. Gas price and investment are slightly higher than for synthesis-gas methanation, even though the overall efficiency is higher, because of the higher investment. Even though the net hydrogen rate is less than half that for synthesis-gas methanation, thus cutting oxygen consumption in half, the large excess of hydrogen used in the hydrogasifier requires a compensating expense in cryogenic separation and purification.

### Partial Hydrogasification With Less Than Stoichiometric Hydrogen (Case 3)

Further development of hydrogasification showed that it is advantageous to hydrogasify only the more reactive fractions of the coal and to use the less reactive residual char for hydrogen manufacture. By the use of a moving bed, a solids down-flow-gas upflow reactor, and a hydrogen/char ratio only 50% of the stoichiometric, a high-Btu gas is produced in the hydrogasifier.<sup>3</sup> In Case 3 the hydrogasifier temperature ranged from 1350° F at the top of the bed to 1600° F at the bottom. The same char pretreatment method was used. A lower temperature and a reduced hydrogen/char feed ratio result in a high-Btu gas, eliminating the need for low-temperature separation. Partial conversion of the char reduces the net hydrogen input because more coal must pass through the reactor, yielding more volatile matter. Compared to Case 2 the investment is reduced 15% and the efficiency is raised to 60%. Savings in equipment and higher efficiency combine to lower gas price by 13¢-14¢/million Btu.

Figure 5 gives a general flow sheet for pipeline gas by partial hydrogasification with spent hydrogasifier char as the basis for hydrogen manufacture. Steam is needed in all cases, but alternative methods employ air, oxygen, or electricity as a basic input.

Figure 6 gives the basic scheme for hydrogen generation by the Texaco-type steam oxygen suspension gasification of spent char. This method is used in four (Cases 1-4) of the seven process economic studies. In all cases costs are based on the system used in Reference 5. As discussed below, electricity can also be used as a heat source. To avoid a repetitive flow sheet, both oxygen and electricity are shown as alternatives; however, the use of electricity is not a part of the Texaco Process.

#### Hydrogasification With Steam-Hydrogen Mixture (Figures 5 and 6)

An important process and economic development was the successful use of steam in the hydrogasifier. In the current concept, steam and hydrogen in approximately equal amounts are fed to a high-temperature fluidized bed where the above reactions (1, 3, and 4) occur. Since the steam-carbon reaction (1) is strongly endothermic and the hydrogen-carbon reaction (4) strongly exothermic, heat effects tend to balance, and there is not the problem of heat removal that exists when only Reaction 4 occurs. Steam acts as a moderator since, as the temperature rises because of Reaction 4, the rate of Reaction 1 increases. Steam decomposition generates hydrogen in situ, thus reducing the size of the hydrogen section and lowering the price of gas. The hydrogen feed/char ratio is reduced to about 33% of the stoichiometric value. When steam is used, the hydrogasifier effluent contains more carbon monoxide and requires more subsequent methanation than when hydrogen alone is used. About two-thirds of the total methane is made in the hydrogasifier compared to over 90% for Cases 2 and 3. However, the cost of increased methanation is more than compensated for by the other cost reductions resulting from the use of steam.

As shown in Table 1, four of the processes utilize steam with the hydrogen-rich gas. In all these cases the hydrogasifier consists of two stages: a low-temperature first stage of 1300°-1500°F to obtain a high methane yield from the volatile matter in the coal and a high-temperature fluidized-bed second stage of 1700°-1800°F to produce methane and effect the steam-coal reaction. All four of the process designs are based on the same coal rate, coal preparation, and hydrogasification steps derived from the design in Reference 6. Major differences are in the hydrogen section.

The economic effect of introducing steam into the hydrogasifier is shown by Cases 3 and 4: Investment is lowered by 25%. In both cases hydrogen is derived from synthesis gas made by Texaco-type steam-oxygen gasification of spent char. When part of the hydrogen is made in the hydrogasifier, the price of gas is shown to be reduced by 10¢-11¢/million Btu; net hydrogen is reduced by 30%. Case 4 is derived from Reference 5 with modifications, as discussed above, based on Reference 6. The 10¢ differential is confirmed by other studies.

#### Hydrogen by the Steam-Iron Process (Case 5) (Fuel Gas Associates)

The expense of using oxygen to make hydrogen has stimulated interest in alternative methods. The continuous steam-iron process, shown in Figure 7, offers potential for significant cost reduction. It involved the transfer of the oxygen in water to a stream of iron plus reduced iron oxide that flows between oxidizer and reductor. A stream of hydrogen and unreacted steam flows from the oxidizer directly to the hydrogasifier. Spent hydrogasifier char reacts with steam and air to make a producer gas that regenerates the iron oxide. Since this gas is not part of the product, air can replace oxygen. Power for air compression and other plant requirements is provided by an expansion turbine powered by spent reductor gas. Savings in investment contribute most to the 10¢ reduction in gas price from 65¢ to 55¢/million Btu. The hydrogen rate is the same, but the costs of hydrogen and onsite power generation are greatly reduced. As part of the pipeline gas from coal plant, hydrogen by the steam-iron process costs about 20¢/1000 CF compared to 29¢ for hydrogen by steam-oxygen gasification.

### Hydrogen by the Electrothermal Process (Case 6)

Another alternative to steam-oxygen gasification is the electrothermal process (Figure 6). Here resistance heating of a fluidized bed of char operating at 1800° - 1900°F supplies the heat for the steam-carbon reaction, and the steam serves both as a reactant and a fluidizing medium. Compression of high-purity oxygen is eliminated, and the reducing gas is not diluted by CO<sub>2</sub> from combustion. Power must be relatively low cost. Our economics are based on a purchased power cost of 3 mills/kWhr. There is enough spent char to supply needed electricity by either a magnetohydrodynamic or a conventional steam turbine system. Such a system would be adjacent to and integrated with the pipeline gas plant and could benefit from the use of hot char transferred directly as fuel to a fluidized boiler. Hydrogen by this method costs more than by the steam-iron process. The price of pipeline gas is very sensitive to the cost of power. A change of 1 mill/kWhr will change the gas price by 3.3¢/million Btu.

### Hydrogasification With Synthesis Gas<sup>4</sup> (Case 7)

Feeding raw, hot synthesis gas instead of hydrogen can substantially reduce the price of pipeline gas. We have shown the economic effect as applied to the electrothermal process (Figure 8). The synthesis gas is essentially CO and H<sub>2</sub>. As H<sub>2</sub> is consumed in the hydrogasifier, CO reacts with the steam present to form more H<sub>2</sub>. Because of the lower hydrogen partial pressure, a larger reactor column is needed, but its cost is largely balanced by the elimination of the hydrogen preheat system necessary when cold hydrogen is used. Major cost reductions are in the elimination of the CO shift and purification sections needed to make high-purity hydrogen and in savings in offsite equipment. Gas price is reduced by 5.5¢-6¢/million Btu.

### SUMMARY

Important process changes have occurred in the development of the HYGAS Process, resulting in much improved economics. The investment for a 250 billion Btu/day plant has been reduced from over \$250 million to \$120 million. Plant efficiency has risen from 50% to 70%. When computed on a comparable basis, these changes have resulted in reductions in the price of gas from approximately 90¢ to 55¢/million Btu. These process changes are summarized as follows:

<u>Process Change</u>	<u>Price Reduction, ¢/10<sup>6</sup> Btu</u>
Partial Hydrogasification With 50% vs. 300% of Stoichiometric H <sub>2</sub> /Char Ratio (Case 3)	14
Use of Steam in the Hydrogasifier (Case 4)	10-11
Use of Steam-Iron Process for H <sub>2</sub> (Case 5)	10-11
Hydrogasification With Electrothermally Generated Synthesis Gas	9-10

Hydrogasification with electrothermally generated synthesis gas and 0.3¢/kWhr power (Case 6) reduces pipeline-gas price by 9¢-10¢/million Btu from Case 4, with synthesis gas instead of hydrogen accounting for about 5.5¢-6¢. Gas price is then about the same as with hydrogen by the steam-iron process.

The basic IGT scheme as presently conceived consists of three stages of coal conversion as shown in Figure 8: 1) a low-temperature (1300° - 1500°F) first hydrogenation stage, either free fall or upflow, for conversion of the volatile matter; 2) a fluidized-bed second hydrogenation stage where steam and synthesis gas react at 1700° - 1850°F to produce methane, CO, and H<sub>2</sub>; and 3) a third-stage fluidized-bed

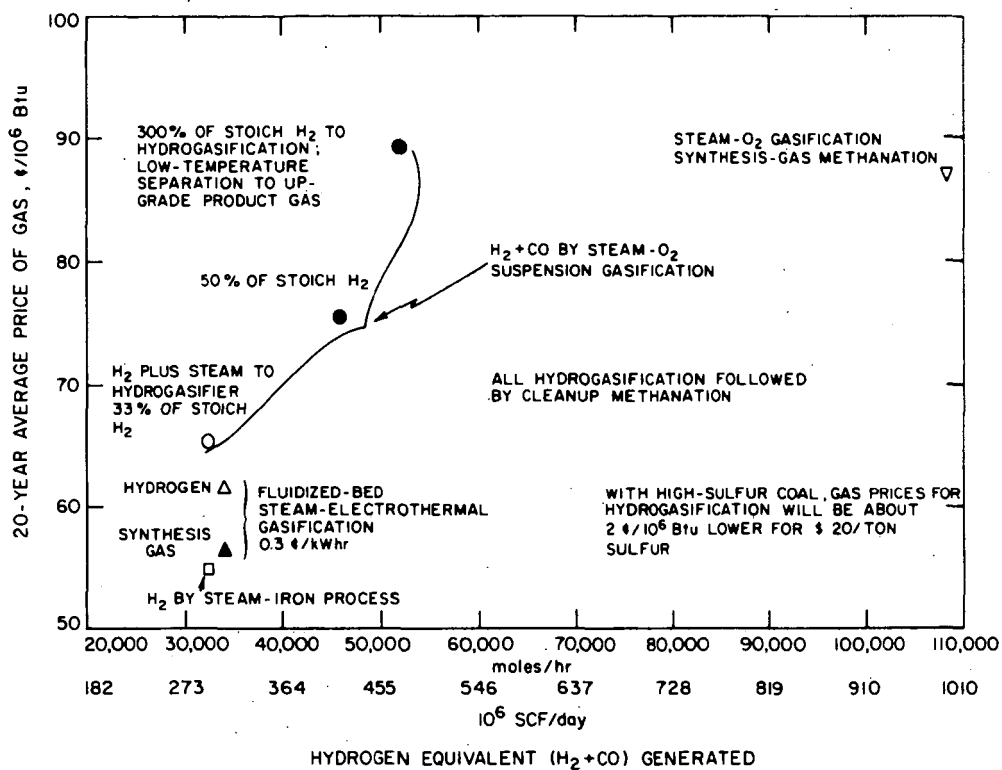
gasifier at 1800°-1900°F where spent char is converted to synthesis gas containing methane by electricity and/or oxygen.

#### ACKNOWLEDGMENT

The work reported herein is under the cosponsorship of the American Gas Association and the U.S. Department of the Interior, Office of Coal Research. Permission of the sponsors to publish this paper is greatly appreciated.

#### REFERENCES CITED

1. Heffner, W. H. et al., "Pipeline Gas From Bituminous Coal via Suspension Gasification and Catalytic Synthesis of Methane," Study CE-60-207. New York: M. W. Kellogg Co., 1960 (Unpublished report to American Gas Association).
2. Heffner, W. H. et al., "Pipeline Gas From Bituminous Coal via Hydrogasification," Study CE-61-215. New York: M. W. Kellogg Co., 1961 (Unpublished report to American Gas Association).
3. Khan, A. R., Feldkirchner, H. L. and Joyce, T. J., "Techno-Economic Evaluations of Hydrogasification of Coal and Char." Chicago: Institute of Gas Technology, 1964 (Unpublished report to American Gas Association).
4. Knabel, S. J. and Tsaros, C. L., "Process Design and Cost Estimate for a 258 Billion Btu/Day Pipeline Gas Plant - Hydrogasification Using Synthesis Gas Generated by Electrothermal Gasification of Spent Char," R&D Rept. No. 22, Interim Rept. No. 3. Washington, D.C.: Office of Coal Research, 1967.
5. Tsaros, C. L., Knabel, S. J. and Sheridan, L. A., "Process Design and Cost Estimate for Production of 265 Million SCF/Day of Pipeline Gas by the Hydrogasification of Bituminous Coal," R&D Rept. No. 22, Interim Rept. No. 1. Washington, D.C.: Office of Coal Research, 1965.
6. Tsaros, C. L., Knabel, S. J. and Sheridan, L. A., "Process Design and Cost Estimate for Production of 266 Million SCF/Day of Pipeline Gas by the Hydrogasification of Bituminous Coal - Hydrogen by the Steam-Iron Process," R&D Rept. No. 22, Interim Rept. No. 2. Washington, D.C.: Office of Coal Research, 1966.



A-70637

Figure 1. EFFECT OF H<sub>2</sub> PLUS CO GENERATION RATE AND METHOD ON PRICE OF PIPELINE GAS FROM COAL ESTIMATED ON A COMPARABLE BASIS (Initial Debt - 65%, Interest at 5%, Return on Rate Base - 7%, Federal Income Tax - 48%, Coal Cost - 16.1¢/10<sup>6</sup> Btu)

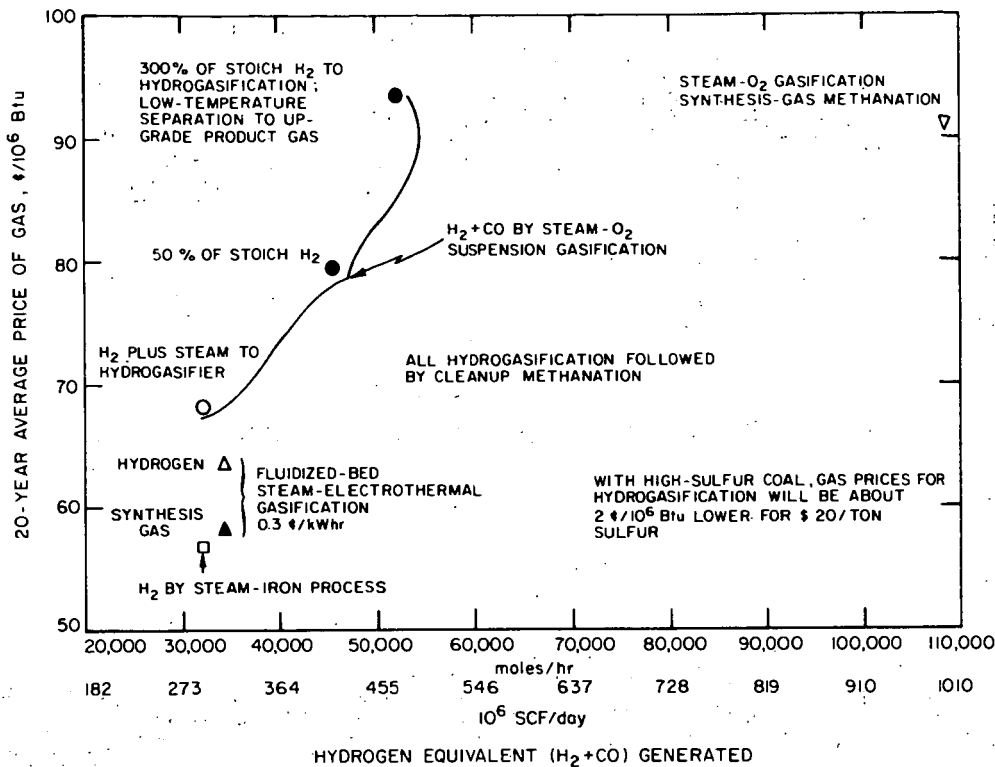


Figure 2. EFFECT OF H<sub>2</sub> PLUS CO GENERATION RATE AND METHOD ON PRICE OF PIPELINE GAS FROM COAL ON A COMPARABLE BASIS (Initial Debt - 65%, Interest at 7.5%, Return on Rate Base - 9%, Federal Income Tax - 48%, Coal Cost - 16.1¢/10<sup>6</sup> Btu)

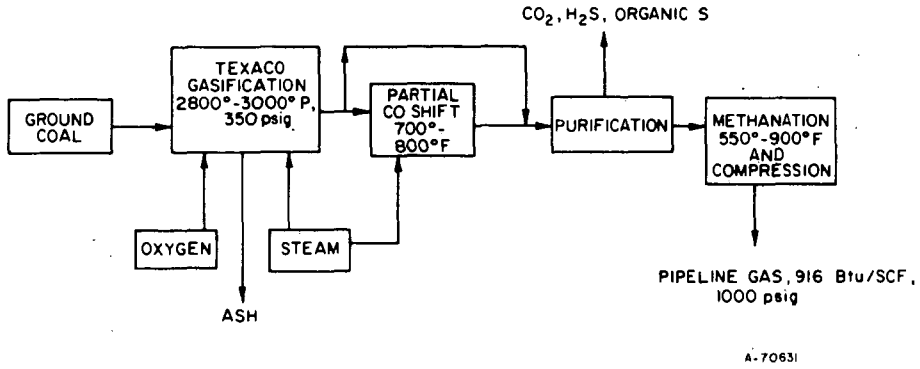


Figure 3. PIPELINE GAS FROM COAL BY METHANATION OF SYNTHESIS GAS

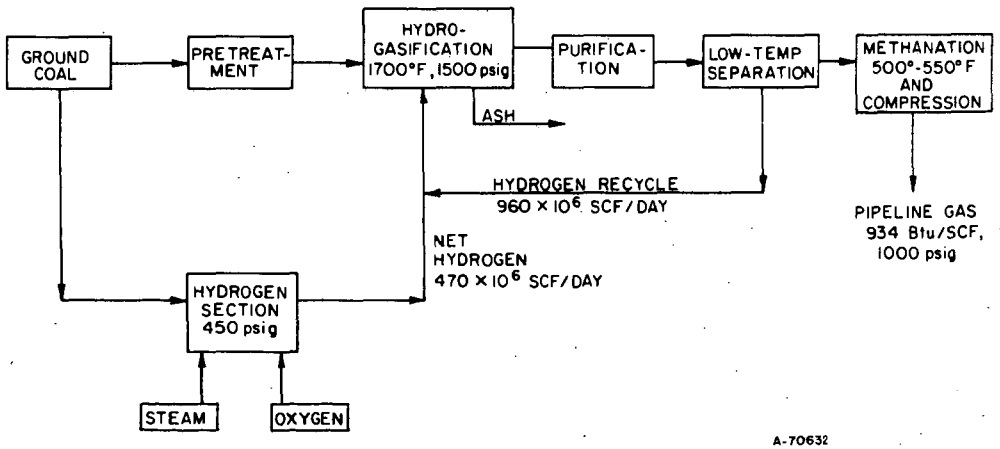
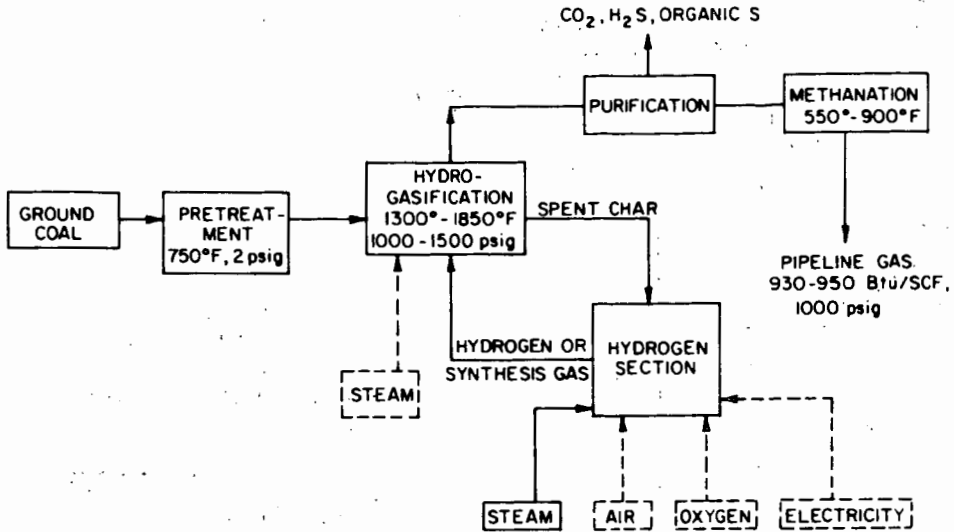
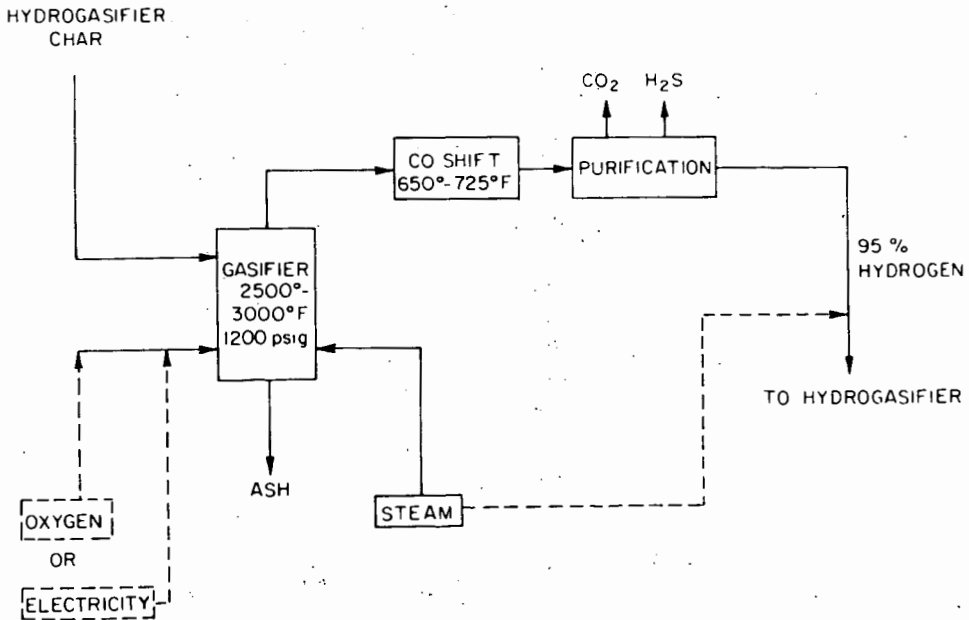


Figure 4. PIPELINE GAS FROM COAL BY HYDROGASIFICATION WITH EXCESS HYDROGEN (300% of Stoichiometric)



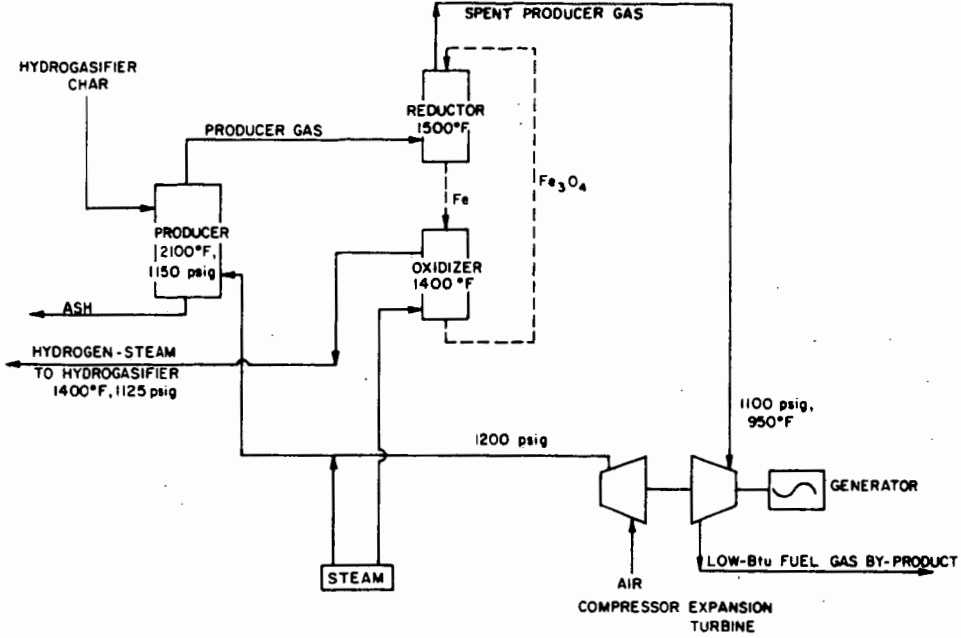
A-70633

Figure 5. PIPELINE GAS FROM COAL BY HYDROGASIFICATION WITH LESS THAN STOICHIOMETRIC HYDROGEN; HYDROGEN MANUFACTURE BASED ON SPENT CHAR WITH AIR, OXYGEN, AND ELECTRICITY AS ALTERNATIVES



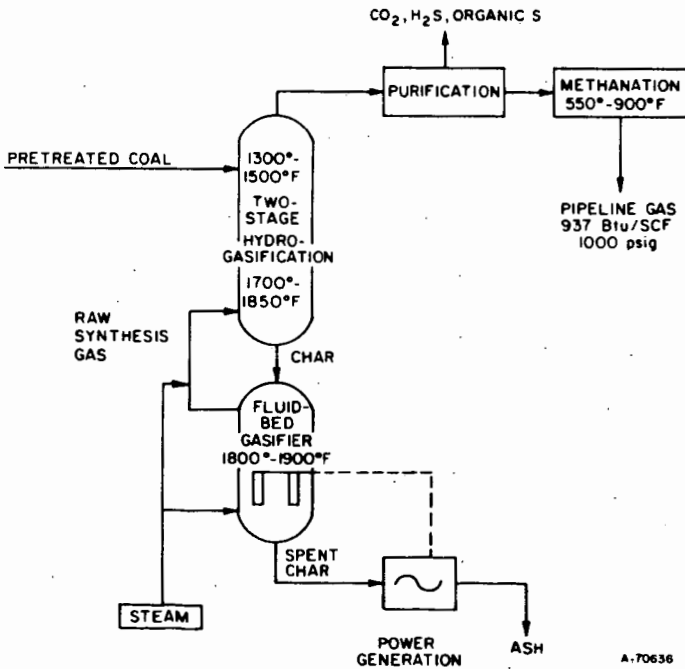
A-70634

Figure 6. HYDROGEN GENERATION BY STEAM-OXYGEN OR STEAM-ELECTROTHERMAL GASIFICATION OF HYDROGASIFIER CHAR



A-70635

Figure 7. HYDROGEN GENERATION BY THE STEAM-IRON PROCESS BASED ON HYDROGASIFIER CHAR



A-70636

Figure 8. HYDROGASIFICATION WITH SYNTHESIS GAS

OPTIMIZATION OF FIXED BED WATER-GAS  
SHIFT CONVERTER FOR PRODUCTION OF PIPELINE GAS

C. Y. Wen and H. N. Kim

Department of Chemical Engineering  
West Virginia University  
Morgantown, West Virginia

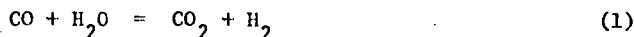
1. INTRODUCTION

With the growing shortage of natural gas, development of process for the production of high BTU gas from coal becomes more attractive, and is now under extensive investigations, most of which are sponsored by the Office of Coal Research, Department of the Interior. The overall system for production of the pipeline gas consists of several unit processes such as gasification, water-gas shift conversion, gas purification and methanation. In the present study, the water-gas shift conversion process of a large commercial scale is optimized in connection with the primary gasification and methanation processes. The objective is to search the most economical scheme for shift conversion by which the effluent gas from the gasifier can be processed to achieve a proper hydrogen-to-carbon monoxide ratio for methanation at a later stage. Conditions and compositions of raw gas vary depending on the different primary gasification processes from which it emerges. Among the various gas compositions obtainable, two cases are selected as shown in Table 1. These selections will meet the following requirements imposed on methanation: (1) production rate of pipeline gas is  $250 \times 10^9$  BTU/day; (2) heating value of pipeline gas is more than 900 BTU/SCF.

2. REACTION KINETICS

A. Rate Equations

The stoichiometric relation of water-gas shift reaction is expressed by



In addition to the above reaction, thermodynamically it is possible that several other side reactions may take place among the components of CO, H<sub>2</sub>O, H<sub>2</sub>, CO<sub>2</sub>, CH<sub>4</sub> and other hydrocarbons. These reactions involve the methane formation and the carbon deposition. Presently however the well developed commercial iron-chromium-oxide catalyst is employed under the suitable steam to gas ratio which is obtained based on equilibrium considerations, showing a satisfactory selectivity in most water-gas shift conversion processes. In this study therefore only reaction (1) will be of primary importance.

Among the different types of water-gas shift rate equations proposed so far, the first order equation of Laupichler [11], Mars [13], the second order equation of Moe [15], and the exponential form of equation of Bohlbro and others [4] are noteworthy. The recent paper of Ruthven[18] reviewed the experimental results obtained by previous investigators, and concluded that the pseudo first order rate equation is quite adequate in most cases. This equation seems to have more flexibility than others since it includes the pore diffusion effect of catalyst, which is particularly important at high temperatures.

Table 1. Flow Rates and Compositions of Feed and Product Gases

Low CO Case

	Feed		Product (dry basis)	
	lb-mole/hr	mole %	lb-mole/hr	mole %
CO	9209.0	11.78	6446.3	10.43
H <sub>2</sub> O	19155.8	24.50	--	--
H <sub>2</sub>	17817.4	22.79	20580.1	33.31
CO <sub>2</sub>	11567.3	14.79	14330.0	23.19
CH <sub>4</sub>	19721.0	25.22	19721.0	31.91
N <sub>2</sub>	716.3	0.92	716.3	1.16
Total	78186.8	100.00	61793.7	100.00

Inlet Temperature: 1000°F      Pressure: 1100 psia

High CO Case

	Feed		Product (dry basis)	
	lb-mole/hr	mole %	lb-mole/hr	mole %
CO	31850.6	35.32	12421.7	12.69
H <sub>2</sub> O	11767.5	13.04	--	--
H <sub>2</sub>	19220.3	21.30	38649.2	39.49
CO <sub>2</sub>	12002.9	13.30	31431.8	32.11
CH <sub>4</sub>	14591.7	16.17	14591.7	14.91
N <sub>2</sub>	784.5	0.87	784.5	0.80
Total	90217.5	100.00	97878.9	100.00

Inlet Temperature: 1700°F      Pressure: 1050 psia

In the present study, the pseudo first order rate equation is consistently used regardless of operating conditions. However, the result obtained from the second order equation of Girdler[7] is also presented for comparison. The two types of rate equations are summarized as follows:

(a). Pseudo first order rate equation

$$-\frac{dp}{dt} = k_o (p - p_e) \quad (2)$$

or in an integrated form

$$-\ln(1 - X/X_e) = k_o t = k_{ap}/S_v \quad (3)$$

The value of  $k_{ap}$  is obtained from intrinsic catalyst activity,  $k_s$  as follows:

$$k_s = 1079 \exp(-27300/RT) \quad (4)$$

$$k_{v1} = \frac{p_s}{p} \frac{RT}{p} k_s \quad (5)$$

$$D_{e1} = 0.069 (T/673)^{3/2} \quad (6)$$

$$\Phi_1 = 0.5 d_p (k_{v1}/D_{e1})^{1/2} \quad (7)$$

$$\eta_1 = \frac{3}{\Phi_1} \left( \frac{1}{\tanh \Phi_1} - \frac{1}{\Phi_1} \right) \quad (8)$$

$$k_{a1} = 492 k_{v1} \eta_1 (1 - \tau)/T \quad (9)$$

$$k_{ap} = k_{a1} [(P/14.7)^{0.35} - 1/\Phi_1] / (1 - 1/\Phi_1) \quad (10)$$

(b). Second order rate equation

$$r'_{CO} = k(C_{CO} C_{H_2O} - C_{H_2} C_{CO_2}/K_y) \quad (11)$$

$$k = \exp(15.95 - 17500/RT) \quad (12)$$

#### B. Mass and Heat Transfer Within Catalyst Bed

Since the water-gas shift reaction is comparatively slow and moderately exothermic, the difference in temperature and concentration between bulk phase of gas and catalyst surface is not expected to be very great. This can be shown numerically as follows. The temperature difference may be estimated by:

$$T_c - T_b = r_s \Delta H / (h_p \pi d_p^2) \quad (13)$$

where  $h_p$  is the heat transfer coefficient between the particle surface and bulk<sup>p</sup> phase, and can be calculated from [23]

$$J_H = (N_{Pr})^{2/3} h_p / (C_p G) = 0.989 (d_p G/\mu)^{-0.41} \quad (14)$$

The maximum temperature difference will result from the maximum reaction rate. The calculation based on the value,  $r_{CO} = 6$  lb-mole CO/(hr cu. ft. cat),  $G = 7000$  lb/(hr. sq. ft.) shows approximately  $(T_c - T_b) \approx 3^\circ\text{F}$ . Such a negligibly small temperature difference was also reported earlier [11], [13]. The temperature gradient within a catalyst pellet can be calculated by the following heat balance equation, assuming an uniform reaction rate in the catalyst.

$$\frac{d^2T}{dr^2} + \frac{2}{r} \frac{dT}{dr} = \frac{r_{CO}}{k_e} \Delta H \quad (15)$$

where  $k_e$ , the effective thermal conductivity may be calculated from

$$\frac{1}{k_e} = \frac{1}{(1-\xi)k_c + \xi k_g} \quad (16)$$

Solution of the above equation using proper boundary condition is

$$T = T_c + \frac{1}{6} \left( -\frac{r_{CO}}{k_e} \Delta H \right) \left[ \left( \frac{d}{2r} \right)^2 - r^2 \right] \quad (17)$$

Again  $r_{CO} = 6$  lb-mole/(hr. cu. ft. cat.) is used for the calculation of temperature difference within the pellet, yielding that  $(T - T_c)|_{r=0} < 4^\circ\text{F}$ .

In a similar manner, the concentration difference between the bulk phase and the surface of the catalyst is approximated by

$$C_c - C_b = r_s / (k_f \pi d_p^2) \quad (18)$$

where  $k_f$  is the fluid-particle mass transfer coefficient in the bed, and may be evaluated from [9].

$$\frac{J_M}{(1-\epsilon)^{0.2}} = 1.40 \left[ \frac{d_p G}{\mu(1-\epsilon)} \right]^{-0.41} \quad (19)$$

The numerical calculation indicates that the maximum difference in concentration corresponds to only 2% of bulk phase concentration.

In summary, it may be safely assumed that the differences in temperature and concentration between the bulk phase and the catalyst surface are negligibly small.

### 3. PERFORMANCE EQUATIONS

#### A. Flow Model for Fixed Bed Reactor

Flow patterns of fluid in a fixed bed reactor are describable by the dispersed-plug flow model or compartment-in-series model. The required condition may be specified as follows [12]

$$D_a/vL < 0.01 \quad (20)$$

Noting the relation  $D_a/vL = (D_a/vd)(d/L)$

and using the experimental results of Levenspiel and Bischoff [12],

$$D_a/vd \approx 0.5 \quad (21)$$

$$\text{Equation (20) is equivalent to } d/L < 0.02 \quad (22)$$

In this study the characteristic length  $d$  is the same as the unit compartment length which is selected as 1 in. Therefore, it is seen from equation (22) that if  $L$  is larger than 5 ft. the requirement is satisfied.

### B. Performance Equations for Reactor Simulation

Material balances for each component around  $n$ -th compartment are given as follows:

$$F_i^n = F_i^{n-1} + v_c^n r_{CO} \quad i = 1, 2, \dots, 6 \quad (23)$$

$r_{CO}$  is negative for  $i=1, 2$ , positive for  $i=3, 4$ , zero for  $i=5, 6$ , where  $F_1^n, F_2^n, F_3^n, F_4^n, F_5^n, F_6^n$  are the molar flow rate of  $CO, H_2O, H_2, CO_2, CH_4,$  and  $N_2$  at the exit of the  $n$ -th compartment, respectively;  $V_c^n$  is the catalyst volume per unit compartment. Energy balance around the  $n$ -th compartment under adiabatic conditions may also be expressed as:

$$-(T^{n-1} - T_o) \sum_{i=1}^6 F_i^{n-1} C_{Pim} + (T^n - T_o) \sum_{i=1}^6 F_i^n C_{Pim} = -\Delta H_{T_o} V_c^n r_{CO} \quad (24)$$

where  $C_{Pim} = \int_{T_o}^T C_{Pi} dT / (T - T_o), \quad \Delta H_{T_o} = -17698 \text{ BTU/lb-mole}$

The pressure effect on heat capacities may be considered negligible even at 1000 psig except for steam.

Pressure drop through the fixed bed reactor is calculated using Ergun's equation [8]:

$$\Delta P = \frac{150(1-\epsilon) \mu / (d_p^2 G) + 1.75}{\left(\frac{\epsilon^3}{1-\epsilon}\right) \left(\frac{d_p}{C_L}\right) \left(\frac{\rho_s}{G^2}\right)} \quad (25)$$

### C. Design Equation for Heat Exchanger

Considering the change of film coefficient and scaling problem, it is assumed that approximately 50% of water entering the tubes in heat

exchangers is evaporated to generate steam. Then the heat balance can be written as:

$$Q = W_s C_p (T_2 - T_1) \quad \text{for shell side} \quad (26)$$

$$= W_T [C_p' (t_2 - t_1) + 0.5\lambda] \quad \text{for tube side} \quad (27)$$

where  $T_1$ ,  $t_2$  are the outlet temperatures, and  $T_2$ ,  $t_1$ , are the inlet temperatures of shell side and tube side, respectively. The shell side heat transfer coefficient is calculated from:

$$(h_o D_o / k_g) = 0.36 (D_o G_s / \mu)^{0.55} (C_p \mu / k_g)^{1/3} \quad (28)$$

The pressure drop in the shell side is estimated by the following equation [10]:

$$\Delta P = f_s G_s^2 D_s L_h / (5.22 \times 10^{10} D_o S B) \quad (29)$$

where

$$f_s = 0.01185 (D_o G_s / \mu)^{-0.1876} \quad (30)$$

The tube side heat transfer coefficient for the case without phase change\* may be computed by:

$$(h_i D_i / k_w) = 0.027 (D_i G_i / \mu_w)^{0.8} (C_p \mu_w / k_w)^{1/3} (\mu_w / \mu_o)^{0.14} \quad (31)$$

Since a complete optimal design of heat exchangers is rather involved which is not called for in this study, a simplified procedure is adapted. This procedure involves the determination of an optimum heat transfer coefficient for the heat exchanger. Clearly the increasing mass velocity of gases will have a favorable effect on heat transfer coefficient but will result in a larger pressure drop. An optimum heat transfer coefficient therefore is calculated based on the highest velocity within the allowable pressure drop of 3 psi.

#### 4. ECONOMIC INFORMATION

##### A. Equipment Cost

Reactor Shell Cost: The thickness of the reactor wall,  $T_h$  is computed from [1]

$$T_h = P R' / (S_r E' - 0.6P) \quad (32)$$

and weight of reactor  $W_R$  which includes the top and bottom blank is calculated by

$$W_R = \frac{\pi}{4} e_m \left[ \left\{ (D + \frac{T_h}{6})^2 - D^2 \right\} L + \frac{F_d^2 T_h}{6} \right] \quad (33)$$

\*See appendix for the case of phase change.

Then the reactor cost becomes  $E_R = C_R I_f W_R$  (34)

Cost of catalyst supporting trays :  $E_S = 0.216 I_f N(D+5)^{3.13}$  (35)

Control Valve Cost: Average values of \$8000 per valve for a large single reactor and \$4000 for small parallel reactors are used.

Heat Exchanger Cost [17]:  $E_H = C_y I_f [850 (A_T/50)^{0.562}]$  (36)

Pump Cost: The following equations are used to estimate the cost of pumps [6] [14] associated with heat exchangers to deliver cooling water

$$E_P = 684 B_P^{0.467} \quad (37)$$

where

$$B_P = q e_w \Delta h / (246,800 E_f) \quad (38)$$

#### B. Cost of Direct Material and Utility

Catalyst Cost:  $E_c = I_c V_c$  (39)

Steam Cost: Although the cost of steam depends largely upon its source and manufacturer, a value of 60 cents per thousand pounds is primarily used.

$$\text{Thus } E_{ST} = (W_{ST}/1000) (8200) (0.6) \quad (40)$$

Cooling Water Cost: \$0.12 per thousand gallon is used for treated water.

Electricity Cost: 11 mil per kw-hr is used

#### C. Calculation of Revenue Requirement

In order to optimize the process, formulation of objective function is necessary. The objective function is developed based on the annual cost. The accounting procedure is "Utility Gas Production General Accounting Procedure" which is formulated by the American Gas Association and adopted by the Office of Coal Research. The procedure estimates the annual revenue requirement under the following conditions [21]:

Debt-equity structure	65% debt (1/20th retired annually)
Return-on-rate base	7%
Federal income tax rate	48%
Interest on debt	5%
Depreciation, 20 year straight line	5%
State and local taxes and insurance	3%

The revenue requirement is composed of three factors: operating costs, return-on-rate base; and federal income taxes. In current optimization raw material cost is not considered and one man per shift is assumed for operating labor. The steam cost is calculated separately from the revenue requirement, because of the difficulty as well as the importance of steam cost estimation in optimization.

## 5. OPTIMIZATION

### A. Process Description

The block diagram of the system for optimization is shown in Figure 1. Since the temperature of the raw gas from gasifier is usually much higher than the operating temperature for shift conversion, cooling by waste heat boiler is necessary before going into the reactor. The gas after cooled to a proper temperature is then introduced to the reactor in which the mole ratio of carbon monoxide to hydrogen is adjusted about 1/3. Therefore, for any fixed inlet gas composition, there is always a required conversion of carbon monoxide. Before the gas enters the reactor, a certain amount of steam is added to this stream. The additional steam also brings the steam to gas ratio high enough so that carbon deposition on catalyst will not take place. Determination of the proper steam to gas ratio is not a simple problem, however, because it requires the knowledge of many factors including the reaction kinetics of carbon with gases. Furthermore, the amount of steam introduced would greatly affect not only the steam cost but also reaction rate, equilibrium conversion, etc. and the optimum operating conditions.

The required conversion of carbon monoxide can be achieved in the reactor by one throughput. However, because of the cost of steam and the heavy duty required in the product gas cooler, it will be more advantageous to by-pass a portion of the feed, and mix it with the product gas that has been converted in excess in the reactor. The conversion in the reactor is adjusted to achieve the required conversion upon mixing. It is observed that in order to meet the required conversion by this scheme, the conversion in the reactor has to approach closely to the equilibrium conversion. The temperature of product gas after the shift conversion is approximately 900°F, or lower if this product is mixed with the by-passed gas. Again, it is required to cool the outlet gas before purification. The outlet temperature of product gas cooler should be decided based on the performance of purifier, but in the present study this temperature is fixed at 460°F for convenience.

### B. Adiabatic Reactor

The adiabatic operation can be represented on the conversion-temperature plot. Figure 2 shows the equilibrium curves for different values of steam to gas ratio based on the feed composition of the low CO case. On the same figure are shown the adiabatic operating lines

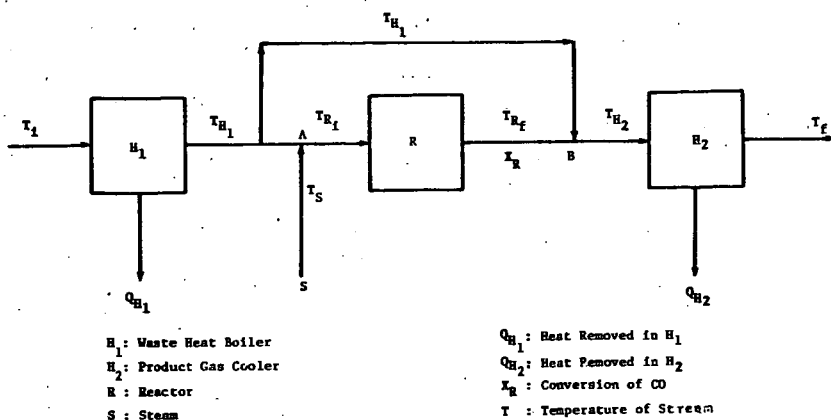


Figure 1 Block Diagram of Water-Gas Shift Conversion System Considered for Optimization

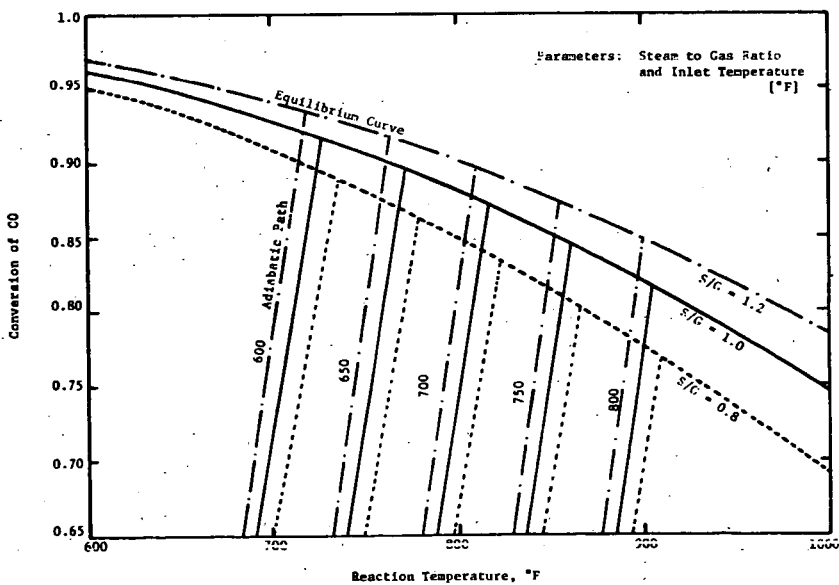


Figure 2 Reaction Paths in Adiabatic Reactor for Low CO Case

which represent the energy balance relationship starting from the given inlet temperatures. The intersection of adiabatic path with equilibrium curve is adiabatic-equilibrium point, indicating the maximum attainable conversion and temperature in an adiabatic operation. The inlet gas temperature to reactor is one of the decision variables, having an allowable range between 600°F to 800°F. The maximum allowable operating temperature is selected as 900°F, because experimentally it has been shown that undesirable phenomena such as catalyst sintering and carbon deposition could take place above this temperature.

The optimization of reactor part is to find the reaction conditions at which the total annual cost is minimized. However, since the entire system to be optimized includes heat exchangers also, the optimum conditions cannot be decided from the reactor study alone. In other words, the reactor is regarded as one stage while the entire process constitutes a multi-stage process. Therefore, at each stage the optimal decisions are obtained for every admissible value of state variables. In this study the quantities to be decided for the optimization of the reactor are: the inlet gas temperature, the conversion (or by-pass fraction), and the diameter of reactor. If we select the temperature of gas as the state variable and the remaining quantities as the decision variables, then the reactor optimization will follow the procedure of searching for the optimum conversion and optimum diameter for every admissible value of the inlet gas temperature.

It can be proven that for a given reactor volume, a smaller diameter reactor weighs less than that of a larger diameter reactor because of the thickness of the reactor wall. Therefore, once the volume of the reactor is determined from the conversion, the smallest diameter will be chosen as the optimum diameter which offers the allowable pressure drop through the reactor. This reduces the number of decision variables and simplifies the calculation.

The procedure of reactor optimization is as follows:

1. The adiabatic equilibrium conversion and temperature are determined for each of the assumed inlet temperatures with given feed composition.
2. An initial trial value of diameter is estimated approximately from the required conversion, the average temperature and the pressure of the gas stream.
3. Starting from the point near the equilibrium conversion, the annual cost for the reactor part is calculated at each point along the adiabatic line by a suitable interval of conversion. In this procedure, search methods such as Fibonacci Search or Golden Section Search may be used for higher efficiency, but in the present study a constant interval of 0.05 is taken for simplicity. Meanwhile, at each conversion the correct diameter of the reactor satisfying the pressure drop limitation is calculated by iterations. It is noted that the determination of conversion in the reactor fixes automatically the by-pass fraction of the feed gas.
4. Once the optimum conversion and the correct value of the diameter is obtained for a single reactor, the optimum number of reactors in

parallel can be decided readily, based on the optimum space velocity already determined.

After the heat exchanges and reactor are optimized individually for every admissible inlet and outlet gas temperatures, the results can be combined to locate the optimum temperatures for the overall system. To accomplish this, first it is necessary to decide the steam temperature,  $T_s$ ,

in Figure 1. Apparently, the increasing value of  $T_{H_1}$  favors the cost of  $H_1$  but affects that of  $H_2$  adversely if  $T_{Rf}$  is fixed. These two opposite tendencies can be combined to show that the highest possible  $T_{H_1}$  and consequently the lowest possible  $T_s$  should be selected for an economical operation. In this study  $T_s$  is selected as the saturation temperature of steam at the operating pressure. Once the temperature of steam is fixed, the remaining procedure is straightforward. For every value of  $T_{Rf}$  the value of  $T_{H_1}$  is calculated by material and energy balances around point A. Since the corresponding value of  $T_{Rf}$  is already obtained by an optimum  $X_R$  in the reactor, similar material and energy balances around point B yield the value of  $T_{H_2}$ . Hence, all the necessary inlet and outlet temperatures for estimating the overall costs are determined.

### C. Cold-Quenching Reactor

The adiabatic system provides a simple and economical process when the concentration of carbon monoxide in the feed gas stream is low. However, when the CO concentration is high the rate of heat evolution is so high that the removal of heat from the system becomes necessary in order to keep the reaction temperature within the desirable range. Hence, from the point of temperature control, more flexible cold-quenching system must be employed. In water-gas shift converter cold-quenching is achieved by injecting a suitable amount of cold water and vaporizing it in the quenching zone of the reactor. Since steam is a reactant and is required in excess, the water-quenching accomplishes dual effects: temperature reduction and steam supply. Figure 3(a) shows the present system of cold-quenching water-gas shift conversion process. In the first reaction zone the reaction progresses under an adiabatic condition. When the reaction has achieved a certain extent of conversion, the quenching is performed in the quenching zone by a pressurized low temperature cooling water which is completely vaporized and mixed with the reacting gas stream before entering the next reaction zone. Care must be exercised for the design and operation of quenching zone to assure complete vaporization of water in the quenching zone, otherwise the unvaporized water will drastically contaminate the catalyst in the subsequent reaction zone. After quenching, the low temperature gas continues to react in the second reaction zone. The alternate quenching and reaction continue until the desired conversion is achieved. The cooling process in the product gas cooler which follows the reactor is the same as that of the adiabatic system.

Since the cold-quenching system consists of a series of adiabatic beds, the typical optimization technique for multi-stage process, namely dynamic programming is used. In this study, a three-stage system is selected based on the results of simulation. The backward dynamic program is expressed by the well known Bellman's principle of optimality [2] as: "Whatever the initial state and decisions are, the remaining decisions must constitute an optimal policy with regard to the state resulting from the first decision." In contrast to the backward dynamic program algorithm, a forward dynamic program algorithm [3] has been proposed as: "Whatever the ensuing state and decisions are, the preceding decisions must constitute an optimal policy with regard to the state existing before the last decision." The selection of backward or forward algorithm will depend on the type of problem as well as the given boundary conditions.

In Figure 3(a) the initial state  $(X^I, T^I)$ , and final state  $(X^F, T^F)$  are fixed as described earlier, but all other values at intermediate stages must be determined by optimization. Now from the relationship between the value of  $X_3^f$  and the amount of gas by-passed, it is possible to confine the system of optimization to the region surrounded by the dotted line in Figure 3(a). Figure 3(b) shows the modified system to be optimized with  $X_1^I$  given.

Each stage except stage 1 consists of one quenching zone and one reaction zone, and has two state variables  $X, T$ , and two decision variables  $W$  and  $\Delta X$ . For example, if we use backward algorithm in stage 3, for any given value of  $(X_3^f, T_3^f)$ , we can find the optimal decision  $W_3$  and  $\Delta X_3$  such that the total cost is minimized. In stage 1 although no quenching water  $W$ , is used, the principle of computational procedure is still the same.

Generally, a backward approach has been used more frequently, and can be also applied to the present problem. However, in this study the forward concept is used because firstly, the problem is of initial condition type, and secondly, the equilibrium constraint existing at the end of each stage is helpful for taking the admissible ranges of state variables.

The general recurrence formula in N-stage process is

$$F_N(\bar{Y}_N) = \min_{\{\bar{O}_N\}} [G_N(\bar{Y}_N, \bar{O}_N) + F_N(\bar{Y}_N)] \quad (40)$$

where

$\bar{Y}_N$  and  $\bar{O}_N$  are the state and decision vectors at the N-th stage  
 $G_N$  and  $F_N$  are the objective and minimum objective function, respectively.

Then the following functional equation can be written for each stage.

$$\text{First stage, } F_1(X_1^f, T_1^f) = \text{Min}_{\{\Delta X_1\}} [G_1(X_1^f, T_1^f, \Delta X_1)] \quad (41)$$

$$\text{Second stage, } F_2(X_2^f, T_2^f) = \text{Min}_{\{\Delta X_2, W_2\}} [G_2(X_2^f, T_2^f, \Delta X_2, W_2) + F_1(X_1^f, T_1^f)] \quad (42)$$

$$\text{Third stage, } F_3(X_3^f, T_3^f) = \text{Min}_{\{\Delta X_3, W_3\}} [G_3(X_3^f, T_3^f, \Delta X_3, W_3) + F_2(X_2^f, T_2^f)] \quad (43)$$

Based on the above equations and using the material and energy balance relations, the optimization is performed starting from the first stage. Although the system is different and involves the multi-dimensionality problem, the basic principle for optimization at each stage is quite similar to that of the adiabatic system. In each case the amount of quenching water is adjusted within the capacity of quenching zone, and the intervals of variables are properly selected based on the sensitivity of objective function and on the computing time. A linear interpolation approximation is applied to connect the stages. The computational procedure is as follows:

1. At the exit of the first stage, the admissible ranges of  $X_1^f$  and  $T_1^f$  are found. In doing this, the restricted range of operating temperature,  $550^\circ\text{F} \leq T \leq 900^\circ\text{F}$ , and the equilibrium temperature-conversion relationship are considered. Then within the range the netwise two-dimensional lattice points of  $(X_1^f, T_1^f)$  are formulated.
2. The corresponding  $T_1^i$  for each of the lattice point is calculated using material and energy balance relationship in the stage. The size of reactor is evaluated, the annual cost,  $G_1$ , is then obtained and tabulated.
3. Similarly, at the exit of the second stage the admissible values of  $(X_2^f, T_2^f)$  are found.
4.  $(X_2^i, T_2^i)$ 's are calculated for different values of  $(\Delta X_2, W_2)$ , and the evaluated  $G_2$ 's are listed.
5. Interpolation is performed between  $(X_1^f, T_1^f)$  and  $(X_2^i, T_2^i)$ , and the minimum values of  $(G_1 + G_2)$  obtained are listed for every value of  $(X_2^f, T_2^f)$ .
6. By a similar computation at the third stage, all the values of  $(X_3^i, T_3^i)$  and  $G_3$  are also obtained from the admissible values of  $(X_3^f, T_3^f)$  and  $(\Delta X_3, W_3)$ .
7. Interpolation is performed between  $(X_2^f, T_2^f)$  and  $(X_3^i, T_3^i)$ . Hence, the total objective function  $(G_1 + G_2 + G_3)$  is obtained for every value of  $(X_3^f, T_3^f)$ , from which the optimum result is found.

Again the reactor part and heat exchanger part can be combined by the similar procedure shown in adiabatic system.

## 6. RESULTS

Adiabatic system: Figure 4 shows the reaction rate profiles along the reactor and Figure 5 illustrates the annual cost .vs. reactor inlet temperature for the low CO case. The optimum operating conditions and corresponding costs are listed in Tables 2 and 3 for both the low CO case and the high CO case.

Cold-quenching system: The reaction rate profile for the low CO case, and reaction paths for both cases are shown in Figures 6 to 8, respectively; the optimum operating conditions and costs are listed in Tables 4 to 6.

## 7. DISCUSSION

### A. Effect of Steam to Gas Ratio on Optimization of Adiabatic Water-Gas Shift Conversion System

As already indicated, the steam to gas ratio is one of the most important factors in the optimization of water-gas shift conversion system. However, its determination is not straightforward. To see how this factor affects the performance of the reaction and the optimization, different values of steam to gas ratio were employed for the low CO case in the adiabatic system. Figure 9 shows the reaction rate profiles along the reactor height with different steam to gas ratios of 0.8, 1.0, and 1.2. The operating conditions and costs are listed in Table 7, indicating that the major difference in cost comes from the variation in the amount of steam although there is also a considerable change in other costs.

### B. Effect of Pressure on the Reactor Performance

Since little is known about the reaction kinetics above 450 psig, the validity of rate equation used in this study is uncertain above this pressure. Besides, most of the commercial plants are operated around 400 psig or less, due to the experimental fact that the activity of iron-chromium-oxide catalyst increases rapidly with pressure in the low pressure range but above 400 psig, the effect of pressure becomes insignificant.

Two additional operating pressures of 300 psig and 600 psig are selected to study the effect of pressure on the adiabatic reactor operation. Figure 10 shows the profiles of reaction rate and Table 8 lists the operating conditions and costs. These results indicate that at high pressure although the reaction rate is increased and consequently the volume of reactor is decreased, the cost of reactor becomes higher because of the reactor wall thickness. Therefore, in general, there is no reason to operate the reaction at a high pressure unless other parts of the gasification processes are conducted under high pressures.

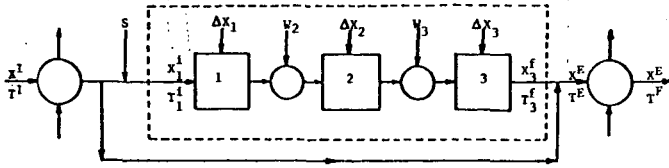


Figure 3(a)

X: Conversion of CO  
T: Temperature  
S: Steam  
W: Quenching Water

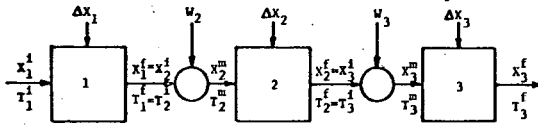


Figure 3(b)

Figure 3 Block Diagram of Cold-Quenching Water-Gas Shift Conversion System Considered for Optimization

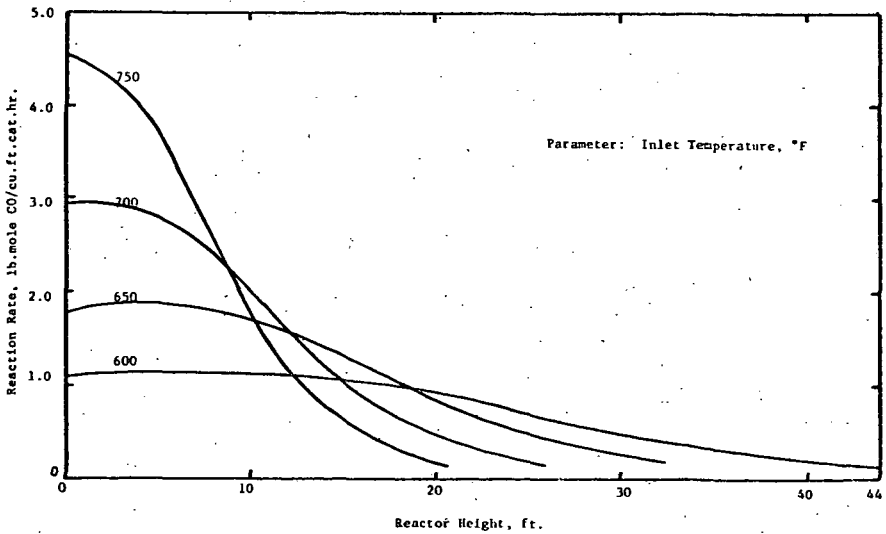


Figure 4 Reaction Rate Profiles in Adiabatic Reactor for Low CO Case

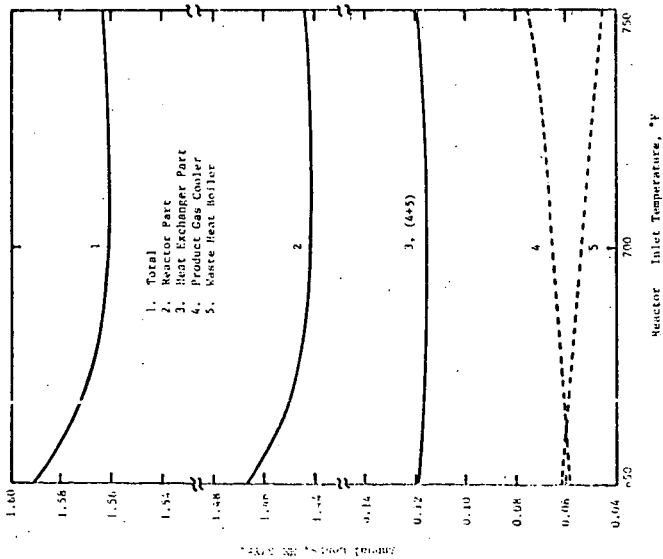


Figure 5 Total Annual Cost in Terms of Reactor Inlet Temperature Indicating 700°F is Optimum for Low CO Case

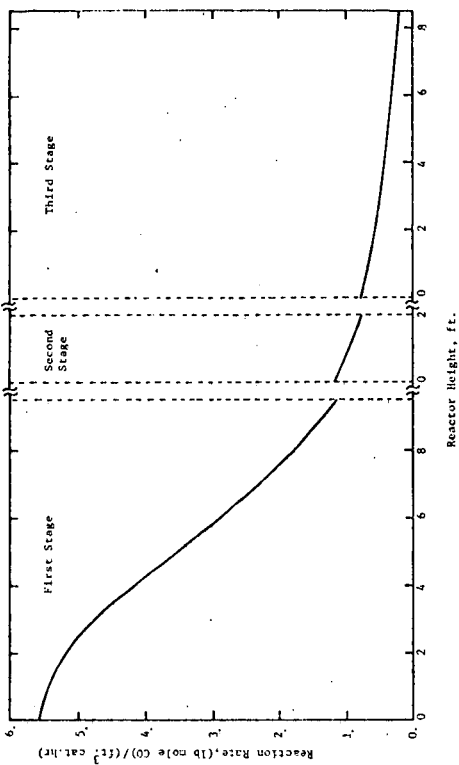


Figure 6 Reaction Rate Profile Under Optimum Condition in Cold-Quenching Reactor for Low CO Case

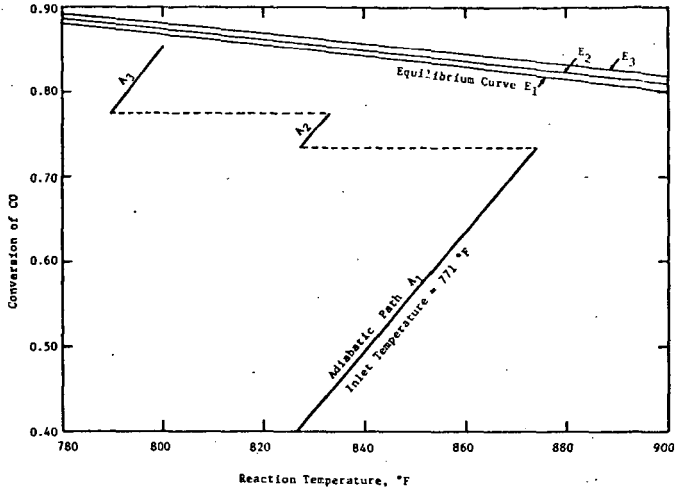


Figure 7 Reaction Path Under Optimum Condition in Cold-Quenching Reactor for Low CO Case

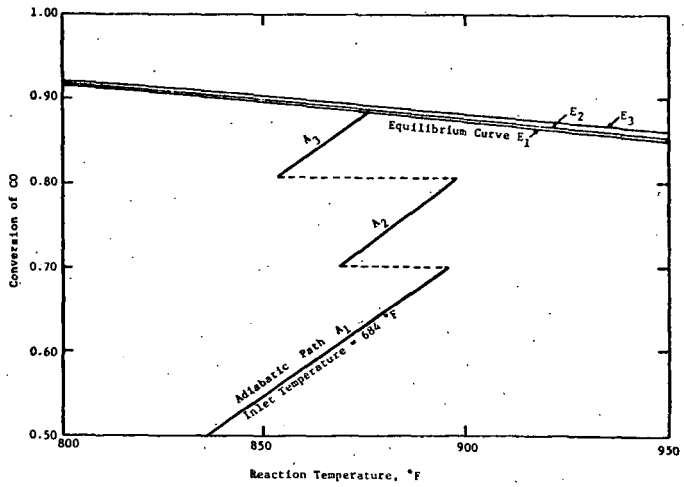


Figure 8 Reaction Path Under Optimum Condition in Cold-Quenching Reactor for High CO Case

Table 2. (Continued)

	High CO Case	Waste Heat Boiler	Product Gas Cooler 1	Product Gas Cooler 2
Inlet Temperature of Gas, °F	1700	878	570	460
Outlet Temperature of Gas, °F	771	570	10	10
Number of Heat Exchangers	10	17	333.5	33.5
Flow Rate of Water/Unit, M lb/hr	192.7	196.1	36.8	36.8
Flow Rate of Water/Unit, M lb/hr	151.9	62.2	250	250
Temperature of Steam Produced, °F	551	551	20.9	20.9
Heat Load/Unit, MM BTU/hr	84.1	34.4	739	739
Heat Transfer Area/Unit, sq.ft.	1262	1884		
Heat Transfer Coefficient, BTU/(hr.sq.ft.°F)	91.4	66.9		90.6

Table 3. Equipment and Operational Costs In Adiabatic System

	Low CO Case	Waste Heat Boiler	Reactor	Product Gas Cooler 1	Product Gas Cooler 2	Total
Reactor cost, \$			496.8			496.8
Catalyst cost, \$			36.3			36.3
Tray cost, \$			33.8			33.8
Control valve cost, \$			20.0			20.0
Heat exchanger cost, \$	41.2			34.2	49.1	124.5
Pump cost, \$	24.8			15.2	5.1	45.1
Cooling water cost, \$/yr	20.7			9.0	25.4	55.1
Operating capital, \$/yr	4.7	20.7	20.7	2.4	3.3	31.1
Return on rate, \$/yr	49.2	167.6	167.6	2.0	2.3	275.3
Federal income tax, \$/yr	1.4	22.6	22.6	1.0	1.2	15.0
Revenue requirement, \$/yr	51.4	201.8	201.8	27.4	37.4	320.0
Steam cost, \$/yr			1240.2			1240.2
Total annual cost, \$/yr	53.4	1442.0	1442.0	27.4	37.4	1560.2

Table 2. Optimum Operating Conditions In Adiabatic System

	Low CO Case*	High CO Case*
Inlet Temperature, °F	700	650
Outlet Temperature, °F	815	899
Conversion of CO	0.855	0.883
Fraction of Gas By-passed	0.649	0.309
Space Velocity, hr <sup>-1</sup> (dry gas at 60°F, 1 atm)	4380	3890
Temperature of Steam Supplied, °F	556	551
Number of Parallel Reactors	3	11
Diameter, ft.	7.0	6.7
Height, ft.	25.9	22.7
Thickness, in	3.7	3.4
Catalyst Amount/Unit, cu. ft.	600	480

\*Steam to gas ratio selected: \*1.0, †1.6

2. Heat Exchangers

	Low CO Case	Waste Heat Boiler	Product Gas Cooler 1	Product Gas Cooler 2
Inlet Temperature of Gas, °F	1000	788	704	704
Outlet Temperature of Gas, °F	765	704	5	460
Number of Heat Exchangers	6	5	6	6
Flow Rate of Gas/Unit, M lb/hr	247.4	347.4	289.5	289.5
Flow Rate of Water/Unit, M lb/hr	58.3	30.6	78.4	78.4
Temperature of Steam Produced, °F	556	556	40.3	40.3
Heat Load/Unit, MM BTU/hr	32.3	16.9	733	1162
Heat Transfer Area/Unit, sq. ft.	850			
Heat Transfer Coefficient, BTU/(hr.sq.ft.°F)	88.1	79.3		92.5

Table 3. (Continued)

High CO Case	Waste Heat Boiler	Reactor	Product Gas Cooler 1	Product Gas Cooler 2	Total
Reactor cost, \$	--	1415.8	--	--	1415.8
Catalyst cost, \$	--	106.1	--	--	106.1
Tray cost, \$	--	94.8	--	--	94.8
Control valve cost, \$	--	52.0	--	--	52.0
Heat exchanger cost, \$	68.5	--	115.6	50.7	234.8
Pump cost, \$	63.0	--	70.7	6.2	139.9
Cooling water cost, \$/yr	89.6	--	62.5	21.8	173.9
Working capital, \$	17.2	51.2	13.7	3.0	85.1
Operating cost, \$/yr	186.8	387.0	144.1	30.6	748.5
Return on rate, \$/yr	6.2	64.0	8.0	2.4	80.6
Federal income tax, \$/yr	3.3	32.1	4.1	1.2	40.7
Revenue requirement \$/yr	196.3	483.1	156.2	34.2	869.8
Steam cost, \$/yr	--	6965.5	--	--	6965.5
Total annual cost, \$/yr	196.3	7448.6	156.2	34.2	7835.3

Table 4. (Continued)

2. Heat Exchangers

	Waste Heat Boiler	Product Gas Cooler 1	Product Gas Cooler 2
Inlet temperature of gas, °F	1000	856	710
Outlet temperature of gas, °F	881	710	460
Number of heat exchangers	4	6	7
Flow rate of gas/unit, M lb/hr	371.1	290.7	249.2
Flow rate of water/unit, M lb/hr	44.9	42.7	68.8
Temperature of steam produced, °F	556	556	250
Heat load/unit, MM BTU/hr	24.8	23.5	39.0
Heat transfer area/unit, sq. ft.	517	873	1188
Heat transfer coefficient, BTU/(hr.sq.ft.°F)	98	82	87

Table 5. Optimum Operating Conditions in Cold-Quenching System for High CO Case\*

1. Reactor

	1st Stage	2nd Stage	3rd Stage
Inlet temperature, °F	684	849	853
Outlet temperature, °F	895	898	876
Conversion of CO achieved	0.701	0.803	0.883
Height of catalyst bed, ft.	8.9	2.7	8.0
Amount of quenching water, lb/hr	--	32,400	57,600
Temperature of quenching water, °F			500
Volume fraction of gas by-passed			0.309
Space velocity, hr <sup>-1</sup> (dry gas at 60°F, 1 atm)			4480
Number of parallel reactors			551
Diameter, ft			13
Height, ft			6.2
Thickness, in.			28.6
Amount of catalyst/unit, cu.ft.			3.2
Amount of packing/unit, cu. ft.			353
*Steam to gas ratio selected: 1.4			91

Table 3. (Continued)

1. Reactor

	1st Stage	2nd Stage	3rd Stage
Inlet temperature, °F	771	827	812
Outlet temperature, °F	872	833	825
Conversion of CO achieved	0.735	0.775	0.855
Height of catalyst bed, ft.	9.5	2.0	9.0
Amount of quenching water, lb/hr	--	18,000	18,000
Temperature of quenching water, °F			500
Volume fraction of gas by-passed			0.649
Space velocity, hr <sup>-1</sup> (dry gas at 60°F, 1 atm)			5690
Number of parallel reactors			556
Diameter, ft			4
Height, ft.			6.1
Thickness, in.			26.5
Amount of catalyst/unit, cu.ft.			3.3
Amount of packing/unit, cu.ft.			358
*Steam to gas ratio selected: 0.9			58

Table 4. Optimum Operating Conditions in Cold-Quenching System for Low CO Case\*

1. Reactor

	1st Stage	2nd Stage	3rd Stage
Inlet temperature, °F	771	827	812
Outlet temperature, °F	872	833	825
Conversion of CO achieved	0.735	0.775	0.855
Height of catalyst bed, ft.	9.5	2.0	9.0
Amount of quenching water, lb/hr	--	18,000	18,000
Temperature of quenching water, °F			500
Volume fraction of gas by-passed			0.649
Space velocity, hr <sup>-1</sup> (dry gas at 60°F, 1 atm)			5690
Number of parallel reactors			556
Diameter, ft			4
Height, ft.			6.1
Thickness, in.			26.5
Amount of catalyst/unit, cu.ft.			3.3
Amount of packing/unit, cu.ft.			358
*Steam to gas ratio selected: 0.9			58

Table 6 (Continued)

	Waste Heat Boiler	Reactor	Product Gas Cooler 1	Product Gas Cooler 2	Total
<b>High CO Case</b>					
Reactor cost, \$	1891.5				1891.5
Catalyst cost, \$	91.6				91.6
Tray cost, \$	64.5				64.5
Control valve cost, \$	60.0				60.0
Heat exchanger cost, \$	63.3		105.3	49.0	217.6
Pump cost, \$	58.0	4.2	61.2	5.8	129.2
Cooling water cost, \$/yr	84.6	17.7	52.9	21.2	176.4
Working capital, \$/yr		64.6	11.8	2.9	95.5
Operating cost, \$/yr		176.0	123.2	29.6	862.3
Return on rate, \$/yr		73.1	7.1	2.3	88.2
Federal income tax, \$/yr		36.8	3.7	1.2	44.8
Revenue requirement, \$/yr		184.8	134.0	33.1	995.3
Steam cost, \$/yr		6008.8			6008.8
Total annual cost, \$/yr		6648.2	134.0	33.1	7000.1

Table 5 (Continued)

	Waste Heat Boiler	Product Gas Cooler 1	Product Gas Cooler 2	Total
Inlet temperature of gas, °F	1700	867	570	570
Outlet temperature of gas, °F	823	570	460	460
Number of heat exchanger	9	15	9	9
Flow rate of gas/unit, M lb/hr	214.1	217.9	363.1	363.1
Flow rate of water/unit, M lb/hr	159.3	59.8	39.9	39.9
Temperature of steam produced, °F	551	551	250	250
Heat transfer area/unit, sq. ft.	88.3	33.1	22.6	22.6
Heat transfer coefficient, BTU/(hr.sq.ft.°F)	1218	1809	773	773
	104	68	94	94

Table 6. Equipment and Operational Costs in Cold-Quenching System

	Waste Heat Boiler	Reactor	Product Gas Cooler 1	Product Gas Cooler 2	Total
<b>Low CO Case</b>					
Reactor cost, \$	497.9				497.9
Catalyst cost, \$	28.6				28.6
Tray cost, \$	19.4				19.4
Control valve cost, \$	24.0				24.0
Heat exchanger cost, \$	26.8		41.8	54.2	120.8
Pump cost, \$	14.6	2.9	21.4	5.8	44.7
Cooling water cost, \$/yr	10.6	7.1	13.1	28.4	61.2
Working capital, \$/yr	2.5	29.2	3.7	3.6	39.0
Operating cost, \$/yr	26.0	270.0	38.0	37.8	371.8
Return on rate, \$/yr	0.7	22.6	2.6	2.5	29.4
Federal income tax, \$/yr	0.8	11.5	1.3	1.3	14.9
Revenue requirement, \$/yr	28.5	304.1	41.9	41.6	416.1
Steam cost, \$/yr		1056.6			1056.6
Total annual cost, \$/yr	28.5	1360.7	41.9	41.6	1472.7

Table 7. Effect of Steam to Gas Ratio for Low CO Case

	S/G = 0.8	1.0	1.2
Inlet temperature, °F	700	700	700
Conversion of CO-1	0.915	0.877	0.877
Space velocity/hr	4290	4380	4640
Number of reactor, ft.	6.7	7.0	7.3
Diameter of reactor, ft.	24.2	25.9	26.3
Height of reactor, ft.	3.4	3.7	3.9
Thickness of reactor, in.	429.4	496.8	544.5
Reactor cost, \$	31.1	36.3	39.7
Catalyst cost, \$	30.3	33.8	35.1
Tray cost, \$	20.9	20.0	20.0
Control valve cost, \$	479.7	550.6	599.6
Revenue requirement, \$/yr	182.4	201.7	213.3
Steam cost, \$/yr	1098.2	1240.2	1567.0
Total annual cost, \$/yr	1098.2	1441.9	1782.3

Based on dry gas at 60°F, 1 atm.

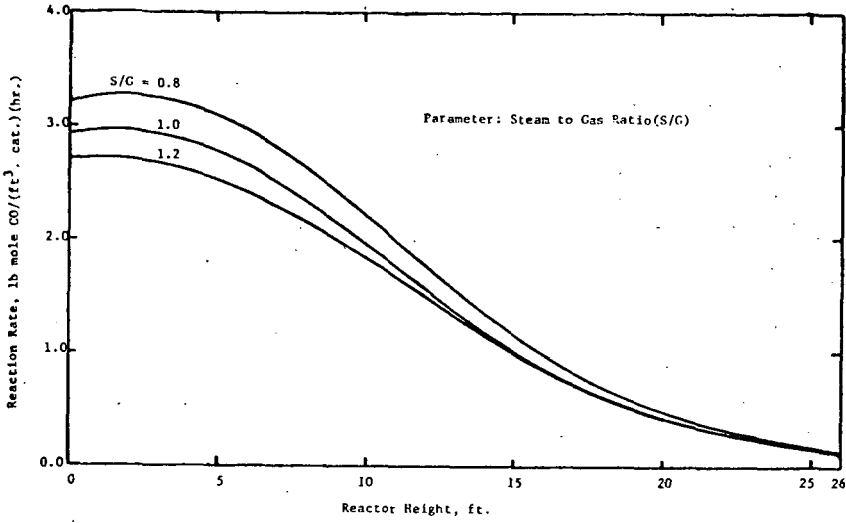


Figure 9 Effect of Steam to Gas Ratio on Reaction Rate in Adiabatic Reactor for Low CO Case

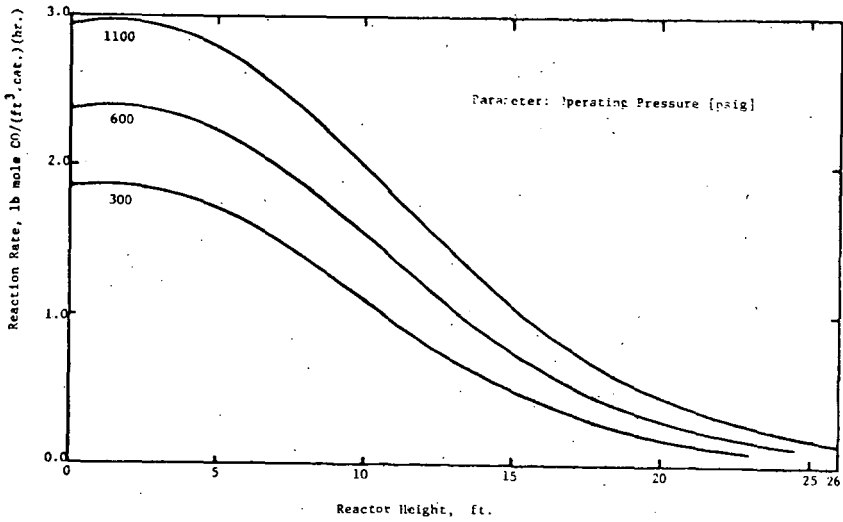


Figure 10 Effect of Operating Pressure on Reaction Rate in Adiabatic Reactor for Low CO Case

### C. Comparison of the Results Using Different Reaction Rate Expressions

In section 2, two types of rate equation, namely the pseudo-first order equation (2) and the second order equation (11) are discussed. Since the design of the reactor depends greatly upon the rate equation, it will be necessary to compare the results obtained using the two rate equations. The operating conditions and the corresponding costs based on the two equations are listed in Table 9 for the adiabatic reactor. Because the applicable range of both equations favors low pressures, 300 psig is selected as the operating pressure. As can be seen from the table only small differences exist between the two results indicating that the water-gas shift reaction can be represented by either of the two equations in this range. The second order equation however seems to provide more conservative estimate than the first order equation.

### D. Pressure Drop in Quenching Zone

Since the quenching zone is usually packed with rings and saddles, more pressure drop is expected in this region. Either of the following equations may be used for the approximation of pressure drop:

$$\Delta P/Z = 0.012 C_p G^2 / 6g_c \rho \quad (44) \quad [20]$$

or

$$\Delta P/Z = k' v^n \quad (45) \quad [1]$$

If the values,  $G = 7000 \text{ lb}/(\text{ft}^2 \text{ hr.})$  and  $\rho = 1.5 \text{ lb}/\text{ft}^3$  are used, then  $\Delta P/Z = 0.05 \text{ psi}/\text{ft}$  by equation (44) and  $0.03 \text{ psi}/\text{ft}$  by equation (45). Therefore the pressure drop through quenching zone in this study can be neglected, unless the packing height is much larger than anticipated.

### E. Effect of Sulfur Content in Gas

The sulfur content in gas is another important factor affecting greatly the performance of water-gas shift reaction. Therefore, if the amount of sulfur exceeds the allowable value, the catalyst activity deteriorates considerably requiring periodical regeneration. However, since the allowable sulfur content varies considerably depending on the type of catalyst used, the determination must be based on the experimental data obtained from the specific catalyst.

The study of Bohlbro [5] indicates that the kinetics of water-gas shift reaction may be modified by the presence of  $\text{H}_2\text{S}$  in the feed gas. According to his experimental results, if the content of  $\text{H}_2\text{S}$  is less than 100 ppm (part per million) only physical adsorption on the surface of catalyst takes place, but above 1000 ppm kinetics will be altered because

of the transformation of iron oxide into iron sulfide. On the other hand, Girdler [7] described that sulfur content above 150 ppm reduces the activity of catalyst greatly, but below 50 ppm sulfur does not have any significant effect on the activity of their catalyst. Mars [13] also discussed the effect of sulfur content on activity of catalyst showing removal of sulfur compounds from the feed gas increases the performance of reactor considerably.

The sulfur content in raw gas from the gasifier varies widely depending on the process, some of which could have as much as 0.9% of  $H_2S$ . However, this study is made based on the assumption that the sulfur content is small enough to be tolerated by the catalyst without causing substantial deactivation. In general, unless the sulfur content in the feed gas is very high, it is possible in most cases to select a proper type of catalyst that will withstand the sulfur poisoning for substantial length of time. On the other hand, if the catalyst gets deactivated it is also possible to modify the space velocity in the reactor to the corresponding reduction in catalyst activity. The recent study of Ting and Wan [19], shows another approach for handling sulfur-containing gases. Here the rate constant is modified by a sulfur correction factor, the value of which are obtained in terms of operating pressure up to 30 atm. for the gases containing  $H_2S$  as high as 0.24%.

#### F. Sensitivity Analysis

The current optimization involves a number of specific system parameters. But the information on these parameters are not necessarily accurate. Such an uncertainty of parameters is incurred by various internal and external factors and may affect the performance of optimization considerably under certain conditions. The sensitivity study here is intended to bring about a better system performance by analyzing the effect of variation in parameters on objective function. The sensitivity of a given parameter,  $S_e$  may be represented as [22]

$$S_e = [(J - \bar{J})/\bar{J}]/[(w - \bar{w})/\bar{w}] \quad (46)$$

Referring to the results listed in Table 10, it is seen that the objective function is most sensitive to the parameters involved in kinetic expression. As is also expected, the dimension and character of catalyst pellet play an important role in the reactor performance.

Table 8 Effect of Pressure on Reactor Operation for Low CO Case

	300 psia	500 psia	1100 psia
Inlet temperature, °F	700	700	700
Conversion CO	0.85	0.85	0.85
Space velocity, hr <sup>-1</sup>	2730	3500	4360
Number of reactors	3	3	3
Diameter of reactor, ft.	9.4	8.0	7.0
Height of reactor, ft.	23.0	26.5	25.9
Thickness of reactor, in.	1.5	2.4	2.7
Reactor cost, \$	249.8	338.0	496.8
Catalyst cost, \$	44.8	42.0	36.3
Tray cost, \$	49.2	31.8	31.8
Control valve cost, \$	20.0	20.0	20.0
Bare cost, \$	320.0	420.0	550.0
Revenue requirement, \$/yr	177.8	183.8	200.9
Steam cost, \$/yr	1240.2	1240.2	1240.2
Total annual cost, \$/yr	1418.0	1424.0	1441.9

Table 9 Comparison of the Results from First- and Second-Order Rate Equation at 300 psig for Low CO Case

	Eq. (2)	Eq. (1)
Inlet temperature, °F	700	700
Conversion CO	83.4	83.7
Space velocity, hr <sup>-1</sup>	0.845	0.849
Number of reactors	2730	2030
Diameter of reactor, ft.	3	3
Height of reactor, ft.	9.4	9.9
Thickness of reactor, in.	23.0	28.1
Reactor cost, \$	259.8	338.5
Catalyst cost, \$	57.4	70.3
Tray cost, \$	49.2	73.6
Control valve cost, \$	20.0	20.0
Bare cost, \$	329.0	432.1
Revenue requirement, \$/yr	177.8	219.4
Steam cost, \$/yr	1240.2	1248.9
Total annual cost, \$/yr	1418.0	1468.3

\* based on dry gas at 60°F, 1 atm.

Table 10 Parameter Sensitivity on Objective Function of Adiabatic Water-Gas Shift Conversion

Parameters	Sensitivity	
	Low CO Case	High CO Case
U <sub>h</sub>	-0.3522 x 10 <sup>-2</sup>	-0.1218 x 10 <sup>-2</sup>
U <sub>v</sub>	-0.8555 x 10 <sup>-2</sup>	-0.1977 x 10 <sup>-2</sup>
k <sub>o</sub>	-0.3540 x 10 <sup>-1</sup>	-0.1902 x 10 <sup>-1</sup>
E	0.1432 x 10 <sup>1</sup>	0.7046 x 10 <sup>0</sup>
d <sub>p</sub>	0.7971 x 10 <sup>-1</sup>	0.4330 x 10 <sup>-1</sup>
S <sub>p</sub>	-0.3340 x 10 <sup>-1</sup>	-0.1847 x 10 <sup>-1</sup>
ρ <sub>p</sub>	-0.3457 x 10 <sup>-1</sup>	-0.1892 x 10 <sup>-1</sup>
D <sub>ep</sub>	-0.3311 x 10 <sup>-1</sup>	-0.1832 x 10 <sup>-1</sup>
ρ	-0.1181 x 10 <sup>-2</sup>	-0.1305 x 10 <sup>-4</sup>
ρ	-0.7195 x 10 <sup>-3</sup>	-0.8584 x 10 <sup>-5</sup>

## 8. CONCLUSION

- A. In the operation of water-gas shift reactor, steam cost occupies the major portion of the total cost. The reduction of the amount of steam is therefore most important in making the process more economical.
- B. The total annual cost is not greatly affected by the variation in the reactor inlet temperature between 650°F to 750°F when the concentration of CO in the feed gas is low or moderate. For the gas of high CO concentration, however, the sensitivity due to the inlet temperature variation is increased.
- C. The optimum conversion is very close to the equilibrium conversion in most cases, which is mainly due to the role of steam cost in the objective function.
- D. Although the kinetics information of water-gas shift reaction may not be accurate for high pressures, the operation beyond 400 psig does not seem to have any particular advantage.
- E. In cold quenching reactor, major part of the total conversion is achieved in the first stage but both the first and the last stage of the reactor occupy the largest portion of overall reactor system.
- F. The concentration of CH<sub>4</sub> and CO in the feed gas is the primary factor affecting the process cost. Because of the steam cost, the cold-quenching system is less costly than the adiabatic system in most cases, particularly in the high CO concentration case. However, if the steam can be ignored, the adiabatic system will be suitable for low CO concentration of less than 25% on dry basis.
- G. From the sensitivity study, the objective function appeared to be somewhat sensitive to the parameters related to the kinetic expression and the character of catalyst pellet, indicating that special care must be exercised for the determination of these parameters.

## ACKNOWLEDGMENT

The authors gratefully acknowledge the support of the Office of Coal Research, Department of the Interior, Washington, D.C.

NOMENCLATURE

$A_1, A_2, A_3$	Adiabatic paths in reaction zones of the first, second and third stages, respectively
$A_h, A_v, A_T$	Heat transfer areas of the heating zone, the vaporizing zone, and the total, respectively [sq.ft.]
$B, B_p$	Baffle spacing [ft.], and Brake horse power [hp.], respectively
$C_1, C_p, C_c$	Concentration of component i [mole frac.], and concentrations of product gas in bulk of gas phase and at catalyst surface [lb mole/cu.ft.], respectively
$C_f$	A constant related to the packings and fluid flow
$C_L$	Height of a unit compartment [ft.]
$C_p, C'_p$	Heat capacities of gases and water, respectively [BTU/(lb.°F)]
$C_{pim}$	Molar temperature-mean heat capacity of component i [BTU/(lb mole, °F)]
$C_R, C_y$	Cost per pound of material used for construction of reactor shell [\$/lb], and cost year index, respectively
$d, D$	Characteristic length in reactor and inside diameter of reactor, respectively [ft.]
$D_a$	Axial dispersion coefficient [sq.ft./hr.]
$D_{e1}, D_{ep}$	Effective diffusivity of CO in catalyst pores at 1 atm and at pressure p, respectively [sq.ft./hr.]
$D_i, D_o, D_s$	Inside diameter of tube, equivalent diameter for heat transfer tube, and inside shell diameter of heat exchanger, respectively [ft.]
$d_p$	Diameter of catalyst pellet [ft.]
$E$	Activation energy in pseudo first order rate equation [BTU/lb mole]
$E^t, E_f$	Efficiency of the longitudinal joints in cylindrical shells, and mechanical efficiency, respectively
$E_c, E_{ST}$	Cost of catalyst [\$] and steam [\$/yr], respectively
$E_H, E_p, E_R, E_S$	Costs of heat exchanger, pump, reactor and catalyst supporting tray, respectively [\$]
$Fd$	flat blank diameter of top and bottom of domes of reactor [ft.]
$F_i^{n-1}, F_i^n$	Molar flow rates of component i at (n-1)-th compartment and n-th compartment, respectively [lb mole/hr.]
$f_s$	Shell side friction factor [sq.ft./sq.in.]
$g, g_c$	Gravitational acceleration [ft./sq.hr.]
$G$	Superficial gas mass velocity [lb./(sq.ft.hr.)]
$G_i, G_s$	Mass velocity in tube side and shell side, respectively [lb/(sq.ft.hr.)]
$\Delta h$	Hydraulic head [ft.]
$\Delta H, \Delta H_{T_0}$	Heat of reaction at any temperature and at temperature $T_0$ , respectively [BTU/lb mole CO]
$h_i, h_o$	Film heat transfer coefficient in inside and outside, respectively [BTU/(sq.ft.hr.°F)]
$h_p$	Fluid-particle heat transfer coefficient [BTU/(sq.ft.hr.°F)]
$I_c, I_f$	Unit cost of catalyst [\$/cu.ft.] and cost factor, respectively
$J, J$	Objective function for a given value of parameter and that at the optimum condition, respectively
$J_H, J_M$	Heat transfer factor and mass transfer factor, respectively

$K_y$	Equilibrium constant based on mole fraction
$k', n$	Constants related to the packings and fluid flow
$k$	Reaction rate constant in second order rate equation [ $\text{hr}^{-1}$ ]
$k_{a1}, k_{ap}$	Apparent catalyst activities at 1 atm and at pressure p, respectively [ $\text{hr}^{-1}$ ]
$k_c, k_e$	Thermal conductivity of catalyst and effective thermal conductivity of catalyst particle, respectively [ $\text{BTU}/(\text{ft. hr. } ^\circ\text{F})$ ]
$k_f$	Fluid-particle mass transfer coefficient [ $\text{ft}/\text{hr.}$ ]
$k_g, k_w$	Thermal conductivity of gas and water, respectively [ $\text{BTU}/(\text{ft. hr. } ^\circ\text{F})$ ]
$k_o$	Apparent first order rate constant based on the unit catalyst bed volume [ $\text{hr}^{-1}$ ]
$k_s$	Intrinsic catalyst activity based on unit surface area [ $\text{ft. lb mole}/(\text{hr. BTU})$ ]
$k_{v1}$	Intrinsic rate constant at 1 atm [ $\text{hr}^{-1}$ ]
$L, L_H$	Lengths of reactor and heat exchanger, respectively [ $\text{ft.}$ ]
$N, N_{Pr}$	Number of trays and Prandtl number, respectively
$P, \Delta P_r$	Pressure of the system and pressure drop, respectively [ $\text{lb}_f/\text{sq. in.}$ ]
$P, P_e$	Partial pressure of CO at any time and at equilibrium, respectively [ $\text{lb}_f/\text{sq. in.}$ ]
$Q$	Heat transfer rate in heat exchangers [ $\text{BTU}/\text{hr.}$ ]
$q$	Volumetric flow rate of water [ $\text{gal.}/\text{min.}$ ]
$r$	Radial distance in catalyst particle [ $\text{ft.}$ ]
$R$	Gas constant [ $\text{BTU}/(\text{lb mole, } ^\circ\text{R})$ ]
$R'$	Inside radius of cylinder [ $\text{in.}$ ]
$r_{CO}, r'_{CO}$	Reaction rate of CO [ $\text{lb mole CO}/(\text{hr. cu. ft. cat.})$ ], [ $\text{cu. ft. CO}/(\text{hr. cu. ft. cat.})$ ], respectively
$R_d$	Dirt factor in heat exchanger
$r_s$	Reaction rate per unit catalyst particle [ $\text{lb mole CO}/(\text{hr. unit cat.})$ ]
$s, S, S_e$	Specific gravity, steam flow rate [ $\text{lb}/\text{hr.}$ ] and sensitivity, respectively
$S_p, S_r, S_v$	Specific surface area of catalyst [ $\text{sq. ft.}/\text{lb}$ ], maximum allowable stress value [ $\text{lb}_f/\text{sq. in.}$ ] and space velocity at N.T.P. basis [ $\text{hr}^{-1}$ ], respectively
$t$	time [ $\text{hr.}$ ]
$T$	Temperature, The subscript denotes the stage number and the superscript represents the status [ $^\circ\text{F}$ ] [ $^\circ\text{R}$ ]
$T_1, T_2$	Temperature of shell side at outlet and inlet, respectively [ $^\circ\text{F}$ ]
$T_b, T_c$	Bulk gas temperature in reactor and surface temperature of catalyst particle, respectively [ $^\circ\text{F}$ ]
$T_h$	Thickness of reactor shell [ $\text{in.}$ ]
$T_m$	Shell side gas temperature at which vaporization of water starts to take place [ $^\circ\text{F}$ ]
$T^{n-1}, T^n$	Exit temperature of (n-1)-th compartment and n-th compartment, respectively [ $^\circ\text{F}$ ]
$T_o, T_s$	Standard temperature ( $77^\circ\text{F}$ ), and temperature of steam [ $^\circ\text{F}$ ], respectively
$U$	Overall heat transfer coefficient [ $\text{BTU}/(\text{sq. ft. hr. } ^\circ\text{F})$ ]

$U_R, U_V, U_T$	Overall heat transfer coefficients for heating zone, vaporizing zone, and whole heat exchanger, respectively [BTU/(sq.ft.hr. $^{\circ}$ F)]
$v, V$	Axial mean velocity [ft./hr.] and linear velocity of gas in empty tower [ft./sec.], respectively
$V_c^n, V_c$	Catalyst volume per unit compartment, and of total reactor, respectively [cu.ft.]
$W$	Quenching water. The subscript denotes the stage number [lb/hr]
$w, \bar{w}$	Parameter subject to variation and that at a specific value considered, respectively
$W_R, W_S$	Weight of reactor [lb.], mass flow rate of gas in shell side [lb./hr.] respectively
$W_{ST}, W_T$	Mass flow rate of steam and water in tube side, respectively [lb./hr.]
$X, X_e$	Fractional conversion of CO at anytime and at equilibrium, respectively. The subscript denotes the stage number and the superscript represents the status.
$Y_N$	State vector in N-th stage
$Z$	Height of packing [ft.]

GREEK LETTERS

$\epsilon$	Voidage of catalyst bed
$\delta_N$	Decision vector at N-th stage
$\eta_1$	Effectiveness factor at 1 atm
$\xi$	Internal porosity of catalyst
$\lambda$	Latent heat of water [BTU/lb.]
$\mu, \mu_w$	Viscosity of gas and water, respectively [lb./(ft.hr.)]
$\mu_0$	Viscosity of water at tube-wall temperature [lb./(ft.hr.)]
$\rho, \rho_m, \rho_p, \rho_w$	Density of gas reactor material, catalyst particle, and water, respectively [lb./cu.ft.]
$\phi_1$	Thiele modulus at 1 atm

APPENDIX

In case that the vaporization is taking place inside the tube, the calculation of heat transfer coefficient is difficult. However, the following simplified approach is used in this study, by separating the heat exchanger fictitiously into two zones: heating zone and vaporizing zone. Then the temperature  $T_m$  at which the vaporization starts to take place corresponding to the boundary of the two zones in the tube can be calculated by a heat balance:

$$T_m = T_1 + W_T C_p' (t_2 - t_1) / (W_S C_p) \quad (47)$$

The log-mean temperature differences in the heating zone and vaporization zone are:

$$T_{l.m.}^1 = [(T_m - t_2) - (T_1 - t_1)] / \ln [(T_m - t_2) / (T_1 - t_1)] \quad (48)$$

$$T_{l.m.}^2 = [(T_2 - t_2) - (T_m - t_2)] / \ln [(T_2 - t_2) / (T_m - t_2)] \quad (49)$$

The overall heat transfer coefficient for each zone can be obtained by

$$1/U = 1/h_i + 1/h_o + R_d \quad (50)$$

Then the heat transfer areas for heating zone and vaporization zone become

$$A_h = W_T C_p' (t_2 - t_1) / (U_h T_{l.m.}^1) \quad (51)$$

$$A_v = 0.5 \lambda W_T / (U_v T_{l.m.}^2) \quad (52)$$

Thus the total area is

$$A_T = A_h + A_v \quad (53)$$

And the average overall heat transfer coefficient  $U_T$  is obtained

$$U_T = Q / (A_T T_{l.m.}^0) \quad (54)$$

where

$$T_{l.m.}^0 = [(T_2 - t_2) - (T_1 - t_1)] / \ln [(T_2 - t_2) / (T_1 - t_1)] \quad (55)$$

REFERENCES

- [1] ASME Boiler and Pressure Vessel Code, Section VIII, Unfired Pressure Vessels, The American Society of Mechanical Engineers, New York, 1956.
- [2] Bellman, R., "Dynamic Programming," Princeton University Press, Princeton, N.J., 1957.
- [3] Bhavnani, K.H., Chen, K., "Optimization of Time-Dependent Systems by Dynamic Programming," Joint Automatic Control Conference Proceedings, 1966.
- [4] Bohlbros, H., Acta Chem. Scand., 15, 502 (1961).
- [5] Bohlbros, H., Acta Chem. Scand., 17, 7 (1963).
- [6] Chilton, C., "Cost Engineering in the Process Industries," McGraw-Hill, New York, p. 50, 1960.
- [7] Communication, Girdler Catalyst, Louisville, Ky., April, 1968.
- [8] Ergun, S., Chem. Eng. Progr. 48, 89 (1952).
- [9] Gamson, B.W., Chem. Eng. Progr. 47, 19 (1951).
- [10] Kern, D. Q., "Process Heat Transfer," McGraw-Hill, New York, 1950.
- [11] Laupichler, F. G., Ind. Eng. Chem. 30, 578 (1938).
- [12] Levenspiel, O., "Chemical Reaction Engineering," John Wiley and Sons, Inc., New York, P. 274, 1962.
- [13] Mars, P., Chem. Eng. Sci. 14, 375 (1961).
- [14] McCabe, W. L. and Smith, J.C., "Unit Operations of Chemical Engineering," McGraw-Hill, New York, 1956.
- [15] Moe, J. M., Chem. Eng. Progr. 58, 33 (1962).
- [16] Norman, W. S., "Absorption, Distillation and Cooling Towers," Longmans, England, p. 327, 1961.
- [17] Page, J. S., "Estimators' Manual of Equipment and Installation Cost," Gulf, Houston, 1963.
- [18] Ruthven, D. M., "The Activity of Commercial Water-Gas Shift Catalysts," Tripartite Conference, Montreal, Sept. 23, 1968.
- [19] Ting, A. P. and Wan, S. W., Chem. Eng., May 19, 185 (1969).
- [20] Treybal, R. E., "Mass Transfer Operations," Second ed., McGraw-Hill New York, p. 162, 1968.
- [21] Utility Gas Production General Accounting Procedure, American Gas Association, May 20, 1965.
- [22] Wen, C. Y. and Chang, T. M., Ind. Eng. Chem. Process Design Development 7, 49 (1968).
- [23] Wilke, C. R. and Hougen, O. A., Trans. A.I.Ch.E. 41, 445 (1949).

## Costs of Liquid Fuels from Oil Shale

Harry Perry <sup>1/</sup>

U.S. Department of the Interior  
18th and C Streets, N.W.  
Washington, D.C. 20240

### I. Introduction

The immense size of the oil shale deposits of Colorado, Utah, and Wyoming with their promise of riches have been a constant challenge to the scientist, the engineer, the entrepreneur and, indeed, the entire petroleum industry. The shortage of oil during World War I provided a stimulus for investors to try to bring this resource to the point of commercial utilization. By the early 1920's ownership of the land had been complicated by the terms of the Mineral Leasing Act of 1920, which changed the method by which the lands could be alienated. In addition there was no indication that the processes then under consideration were technically or economically attractive, and the establishment of an oil shale industry did not occur at that time. Subsequently, the discoveries of very large, low cost reserves of oil in East Texas delayed the possible development of the resource for many years.

Legal problems associated with title to the lands have been an integral part of the history of the oil shale deposits. Concern over the disputes about ownership led to the withdrawal of the lands in 1930 for oil shale leasing. The withdrawal has continued to the present except for three test leases which were offered in December 1968. In 1964, the Department of the Interior instituted some test cases against the pre-1920 claims which are still under consideration. Other actions were taken to test the validity of post-1920 claims and as a result, the Department of the Interior has made great strides in resolving the title clearance issues. Their resolution is indispensable to the orderly development of the resource.

### II. The Need for Synthetics

As shown in Table I, demand for energy is expected to continue to rise, as it has in the past, so that BTU consumption in the U.S. may increase about 260 percent between 1968 and the year 2000. In absolute terms this is an increase in demand of an oil equivalent of 11.0 billion to 28.7 billion barrels per year. Energy use in the form of liquid fuels is expected to increase about 190 percent over this same period or an increase of from 4.9 billion barrels in 1968 to 9.6 billion barrels in 2000. Most of the demand for petroleum will continue to be used in the transportation sector (autos, trucks, buses, airplanes); this sector is dominated by liquid fuels which supplied over 95 percent of the energy consumed in 1968.

These predictions were made during a time when, while there was an awareness that air pollution and other environmental controls could have an impact on patterns of energy consumption, the potential magnitude of the new environmental standards could not be factored into the projections. For example, recent indications that leaded gasoline may no longer be an acceptable fuel have opened up new requirements and opportunities for meeting the demands of the transportation sector. Lead-free gasoline can be produced using present technology but this requires a higher percentage of aromatics and isoparaffins if octane ratings are to be maintained. To meet any wide-spread demand for lead-free gasoline would require that the petroleum industry install an enormous amount of additional processing units, particularly for reforming and alkylation. The extra costs of lead-free gasoline have been estimated to be 2 cents per gallon or a total cost of 2 billion dollars a year in the U.S.

---

<sup>1/</sup> Mineral Resources Research Advisor, Assistant Secretary of Mineral Resources Office

The need to tool up to produce modified designs of engines and fuels could induce industry to look seriously at other automotive power plants such as gas turbines, steam engines, Wankel engines, combined gasoline-natural gas engines or electric vehicles.

Environmental considerations are rapidly creating a large new demand for a low sulfur residual oil to be used at electric generating stations and industrial plants. This fuel would replace coal which could not meet air pollution standards for sulfur oxide emissions. In PAD District I, where under present oil import regulations, unlimited amounts of residual oil imports are permitted, imported low sulfur residual has already replaced significant amounts of high sulfur coal. Recently, approval was given for importation of low sulfur residual oil into Chicago. If oil import regulations are changed (specific recommendations for change have been made to the President by a Cabinet Level Study Group) this trend could be greatly accelerated.

As previously noted, the combined effects of these two developments or others still to come, on total liquid fuel demand are still too recent to permit modification at this time of the projections shown in Table I. However, the effects of these and other changes caused by the establishment of future environmental standards will affect the patterns of demand and supply. On the other hand, all the fuel resources at our disposal will have to be used in some form if the tremendous demand for energy that has been predicted actually occurs. The fuel forms may have to be modified to meet other standards placed on them but the total energy demand could not be met if oil (or heat units derived from it) were not used in about the quantities shown in Table I.

Synthetics, whether from oil shale, tar sands or coal, will only be used when they can compete economically with other energy sources or with crude petroleum under the public policies that prevail at any given time. The ability of synthetics to enter the market will obviously depend on how much crude oil is found. This in turn is a function of the oil import program that eventually emerges, the incentive for investment in exploration, and the size of the Alaskan discovery coupled with the cost of delivering that crude oil to markets. As shown in Figure 1, the declining reserves to production ratio that started in the early 1960's is expected to continue and this should provide an incentive for the oil industry to look to other sources of supply.

### III. Oil Shale Development--Non-Technologic Factors

The development of the oil shale resource is dependent on the existence of a technically feasible process that is economic under the conditions prevailing that determine the price of crude oil. The major non-technical factors that affect the price of crude oil with which shale oil would compete are the oil import program (how much can be imported and under what conditions), the depletion allowance for oil, state prorationing practices, and Federal leasing policies both on-shore and on the Outer Continental Shelf--particularly new stringent safety regulations which may increase costs.

Other important factors that will affect the timing and the rate at which oil shale processing becomes commercial are the rate at which the clouded titles on most of the publicly owned lands can be removed; any modifications of the terms of the Mineral Leasing Act of 1920 under which the oil shale lands are leased by the Government, which of the different bidding procedures the Government elects to use, and the terms and provisions of the lease. Certain types of shale deposits are almost entirely in Government ownership. If a technology is developed for using them that is more economic than for the deposits in private hands, then the Government would control entirely by its lease offerings the rate and time when an oil shale industry would emerge.

In addition, actions taken by state and local governments could either help or deter an oil shale development, the large capital requirements to attain economies of scale will limit the number of possible participants in the industry, and the institutional practices of the oil industry will make it difficult for those not

already in the oil business to enter an oil shale industry. Moreover, the relative costs, as well as other factors, of producing synthetics from oil shale compared to coal will also be of importance in determining the onset of an oil shale industry.

#### IV. Status of Oil Shale Technology

There are basically two ways to produce a crude shale oil from oil shale. In the first, the oil shale is mined and then retorted where, by the application of heat, the crude shale oil is distilled from the oil shale. In the second, wells are drilled from the surface to the oil shale deposit, the permeability of the oil shale is increased by some method, and the shale oil distilled from the deposit by an in situ application of heat.

##### 1. Mining

Underground mining, using the room and pillar method, was extensively investigated by the Bureau of Mines and Union Oil Company during the 1950's and by the Colony Group in the 1960's. These experiments concentrated on developing methods to extract the 70-foot thick rich Mahogany ledge deposit which is found in many parts of the Piceance Basin in Colorado. Feasible methods for underground mining have been demonstrated although there are still potentials for further cost reduction.

Open pit mining of oil shale should present no problems that have not been solved in mining for other mineral resources by this method. However, there has been no experimental testing of open pit mining in the oil shale resource. The costs associated with this method of mining will depend on the thickness and grade of shale and on the geologic conditions--the thickness of the overburden and its physical characteristics. It has been suggested that appreciably lower costs than those associated with underground mining operations can be anticipated in locations where a rich deposit of shale outcrops to the surface. In such a case, there would be little investment required before commercial amounts of shale could be extracted and used and costs should be low.

##### 2. Retorting

In the retorting of mined shale a large number of processes have been proposed, but in the last decade only three have been tested extensively enough to be considered for commercial development at this time. These are the Bureau of Mines gas combustion retort, the Union Oil Company retort and Oil Shale Corp., (TOSCO) process. The Bureau of Mines and Union Oil Company retorts, both of which are internal-combustion types, are based on similar process principles with the major difference being the direction of flow of the shale and air. The TOSCO process consists of a retorting kiln in which finely crushed oil shale is heated to retorting temperature by heat exchange with hot ceramic balls heated in another vessel. It is claimed that more shale oil is recovered per ton of oil shale treated and that the shale oil is of better quality than that produced in the retorts using direct heating and a larger sized oil shale feed. However, the economics of the production of shale oil estimated in this paper are based on results obtained in the Bureau of Mines gas combustion retort since insufficient published data were available for the other two processes to make engineering estimates of costs of shale oil produced by them.

##### 3. In Situ Retorting

In situ retorting of shale using non-nuclear techniques for increasing the permeability of the oil shale has been tested by several companies and by the Bureau of Mines. Methods used in recent experiments by the Bureau of Mines to increase the permeability of the oil shale included electrolinking, hydraulic fracturing and explosive fracturing. Electrolinking followed by hydraulic fracturing did not increase permeability appreciably. Explosive fracturing following hydraulic fracturing

improved the permeability by a factor of 5. In a series of field tests, 11 new wells were drilled in an area where 4 previous wells had been drilled. The center well was ignited in an attempt to retort a 20-foot thick (22 gallons per ton) section of the oil shale located 68 to 88 feet below the surface. After six weeks of operation, the process produced 190 barrels of a medium viscosity low pour point shale oil. Later tests of the deposit indicated that only a 5-foot section of the 20-foot shale bed had been retorted. Although there remain several important unsolved problems, such as better utilization of the shale, improved control of the combustion front, and the use of wider spaced wells with reasonable pressure drop, these in situ tests have demonstrated a much higher degree of technical feasibility for the process than had previously been demonstrated.

The use of a nuclear device, exploded underground to create a chimney filled with broken oil shale which could then be retorted in place, has been under serious consideration for over 10 years in a program to be sponsored jointly by industry and Government.

Extensive preliminary engineering studies have been made to estimate (1) the size of the chimney from a given sized device detonated in oil shale, (2) the size distribution of the broken shale, and (3) the amount of shale oil that would be recovered from a single chimney.

To determine the amount of shale oil that could be recovered from a mass of broken rock containing the wide size distribution that might result in a nuclear made chimney, a 175-ton retort was constructed to simulate those conditions. The retort was filled with oil shale ranging in size from fines to one large piece weighing 7500 pounds. In a single 24-day experiment, an oil yield of approximately 60% of the Fischer assay was obtained. Operation of the retort was smooth with uniform temperature distribution across the bed and with low pressure drop. The characteristics of the shale oil were a little better than those obtained from above-ground retorting in the gas combustion retort having a somewhat lower pour point and viscosity and a lower nitrogen content.

Additional tests will be required to firm up what was learned in this single experiment but there is every indication that higher recoveries and better quality of product can be produced when the optimum operating conditions are established.

#### V. The Economics of the Oil Shale Production

In the Department of the Interior report on oil shale issued in May 1968, <sup>1/</sup> shale oil production was estimated for 5 different mining systems each using (1) a 45-foot diameter retort, (2) a 60-foot diameter retort, and (3) a second generation retort using improved technology. The capital investment, annual operating costs and cost per barrel for each of these 15 conditions are shown on Table 2.

Using a 12 percent discounted cash flow and with no value assigned to the shale resource the cost per barrel (after a 61 cents credit for by-products) is shown in Figure 2 for 6 sets of conditions. The two plants for 1972 were identical except for oil shale quality. Increasing the quality of that shale from 30 to 42 gallons per ton decreased costs 72 cents per barrel. The 1976 case, in addition to using a larger diameter retort than was used for the 1972 case, compared the effect of open pit to room and pillar mining. It also tested the effect of increasing plant size by four fold. An increase from 62,000 to 250,000 barrels per day decreased costs 27 cents per barrel.

Since these calculations were made, four important factors that significantly affect the economics have occurred. These are (1) the by-product credit of 61 cents per barrel is believed to be too high and a more realistic value is probably 41 cents per barrel for all cases except the second generation plant where 77 cents is used in these new calculations, (2) capital and operating costs of new plants have

---

<sup>1/</sup> Prospects for Oil Shale Development--Colorado, Utah, and Wyoming, Department of the Interior, May 1968

increased significantly over the 1966 costs used in the earlier report, (3) the point at which the depletion allowance is applied has been changed by law from 15 percent on the oil shale to 15 percent on the crude shale oil, and (4) the value of the semi-refined shale oil in Colorado has increased about 25 cents per barrel.

Table 3 compares the 1966 and 1969 conditions for four different types of retorts and mining systems. Capital investment costs increased about 10 percent during this period. Annual operating costs increased from a low of 13 percent for the improved first generation retort and improved room and pillar mining system (case 3) to a high of 25 percent for the first generation retort with conventional room and pillar mining (case 1).

The decreased value assigned to by-product credits of 41 cents in the 1969 study compared to 61 cents assigned in 1966 was more than balanced by the increased value of the semi-refined crude oil in Colorado. The net market value of the products resulted in an increase of 5 cents per barrel to \$3.74. On the other hand, even after the tax benefits that accrue from changing the point at which the depletion allowance may be credited, and this is approximately 10 cents per barrel, the increased capital and operating costs raised the cost of producing semi-refined crude oil from a low of 12 cents (case 3) to a high of 38 cents per barrel (case 1). As a result, the discount rate (at zero resource value) that equates cash flow to cost dropped from 13 to 9 percent for case 1 and from 22 to 20 percent for case 4 with intermediate values for cases 2 and 3.

In situ retorting costs for 1966 for both nuclear and conventional were shown in the 1968 oil shale report. For the most favorable case, i.e., nuclear in situ with a 70 percent recovery efficiency of the oil and air pressure for retorting at 50 p.s.i., costs were estimated at \$2.98 per barrel of shale oil. The 1969 costs increased 45 cents for a total cost of \$3.43 per barrel. This is a larger increase than for any of the cases shown in Table 3, and results in part from the method by which the depletion allowance was applied in the 1966 estimate. Since no oil shale is mined during in situ retorting it was not possible to take a 15 percent depletion on the oil shale. As a result, it was taken on the shale oil. Consequently, in the 1969 estimate there was no additional reduction as a result of the change in depletion allowance from oil shale to shale oil.

The 1966 estimate included costs for prevention of air and water pollution from both the retorting and refining operations. It also included costs for purchase of land and for other costs involved in storing spent shale in a manner which would prevent air pollution from the dried spent shale and water pollution from the leaching of the spent shale. However, the costs did not involve replacing as much of the spent shale as possible in either underground or open pit mines. While such costs will vary widely from lease to lease depending on other factors that determine plant location with respect to the mine (water availability, access to the property, suitable areas for the balance of waste disposal, relative elevation of the plant and mine) an average value of about 20 cents per barrel has been estimated over previous estimates for waste disposal.

Another limitation of these estimates (both the 1966 and the 1969) is that they represent average conditions and cannot reflect either the lower or higher costs that may be associated with geologic conditions that differ from the average. All new mining ventures attempt to use the highest grade deposits and the most favorable geologic conditions first in order to make the economics of the first plants more favorable. It has been suggested that if conditions particularly favorable to open pit mining could be found for the thick deposits that contain good quality shale that much lower costs than those indicated above might be attainable. Mining capital and operating costs for case 1 represent about \$1.25 per barrel of a total cost of about \$4.00. Thus, material reduction of the mining cost, for example, by 50 percent would have an important and possibly controlling impact on the economics of shale oil production. If thick beds of shale that outcropped at the surface could be located, so that very small head-end costs (requiring little overburden to be removed) before commercial production of oil shale were possible, mining cost reductions of the order mentioned may be attainable.

As mentioned above, other technology about which the Department of the Interior had insufficient information to make cost estimates similar to those made for the gas combustion retort tested by the Bureau of Mines might indicate production of shale oil at costs lower than those shown. The absence of commercial developments on privately-owned land, combined with the weak bids received on the three tracts offered by the Department in December of 1968, would appear to indicate that this other technology is probably not much more advanced than the marginal technology of the gas combustion retort.

Finally, in using these cost estimates it should be remembered that, while they are believed to be accurate within  $\pm 10$  percent, there is no certainty that they are this accurate. Even a  $\pm 10$  percent error introduces a possible  $\pm 40$  cents per barrel error which would represent a change in the D.C.F. from 9 percent to over 15 percent for case 1. Obviously, the variations of a cost engineering estimate for a non-existent technology might be even greater, and could make the difference between a very profitable or a very marginal operation.

## VI. Conclusions

In the past two years additional and promising information has been developed with respect to the in situ (nuclear and non-nuclear) retorting of oil shale. In non-nuclear in situ retorting, methods to increase appreciably the permeability of the oil shale have been demonstrated. Also proven in a retorting experiment were (1) a combustion zone can be established in fracturing oil shale, (2) this zone can be moved through shale by air injection, (3) permeability does not decrease during retorting (at the shallow depths tested), and (4) recovery of the shale oil presents no special problems.

In nuclear in situ retorting, the above-ground processing of a simulated nuclear chimney indicated that under these conditions good control of the combustion front could be achieved and that even the largest pieces of oil shale could be retorted satisfactorily. No other new experimental data have been published during the past two years to establish the feasibility of the nuclear in situ retorting process.

Earlier cost estimates of both nuclear and non-nuclear in situ retorting were based on the assumptions that the new experiments performed in the past two years would be successful. As a result, it was unnecessary to recalculate these estimates. As a result of increased capital costs the most favorable in situ case showed an increase of 45 cents per barrel between 1966 and 1969, but remained in the competitive range with above-ground retorting.

The situation with respect to above-ground retorting indicates that, for the four cases which were recalculated, although a number of changes in the assumptions must be made to reflect 1969 conditions, shale oil remains marginally competitive as it did in 1966. This, however, does not consider the availability of any greatly improved proprietary technology for either mining or retorting or the use of a lease with very favorable geologic conditions. For any of these conditions, or combinations of them, a first commercial oil shale plant may look very financially attractive.

Table 1  
Energy Consumption by Sector, 1968 and 2000  
Trillions of BTU

	<u>1968</u>	<u>2000</u>
Residential and Commercial	13,599	21,066
Industrial	19,348	32,594
Transportation	15,136	36,600
Electricity Generation	14,046	72,291
Miscellaneous and Unaccounted for	<u>295</u>	<u>-----</u>
Bureau of Mines (1969) Estimate	62,424	162,551
Estimate Made in "Energy R & D and National Progress" (1963)		135,000
Estimate Made by Batelle Northwest (1969)		170,000

Table 2 - Operating Cost of Oil-Shale Processing Alternatives 1/

	MINING OPTIONS		RETORTING OPTIONS		Second generation, 1980 7, 60-ft- diam units <sup>2/</sup>
	First generation 1972 7, 45-ft- diam units <sup>3/</sup>	Operation 10% above design	Improved first generation, 1976 7, 60-ft- diam units <sup>4/</sup>	1976 28, 60-ft- diam units	
<b>Room and pillar</b>					
Capital investment, million \$	\$138	\$142	\$197	\$724	\$204
Annual operating cost, million \$	26.8	28.1	35.7	134	36.3
Cost per barrel: <u>2/</u>					
Before by-product credit, \$	2.10	1.99	1.57	1.48	1.52
After by-product credit, \$	1.49	1.39	0.97	0.87	0.55
<b>Improved room and pillar</b>					
Capital investment, million \$	142	146	203	748	210
Annual operating cost, million \$	25.4	26.5	33.2	124	33.8
Cost per barrel: <u>2/</u>					
Before by-product credit, \$	1.99	1.88	1.46	1.36	1.41
After by-product credit, \$	1.38	1.28	0.85	0.76	0.44
<b>Open pit</b>					
Capital investment, million \$	138	141	196	721	204
Annual operating cost, million \$	26.6	27.8	35.3	133	35.9
Cost per barrel: <u>2/</u>					
Before by-product credit, \$	2.08	1.98	1.56	1.46	1.50
After by-product credit, \$	1.47	1.37	0.95	0.85	0.53
<b>Improved open pit</b>					
Capital investment, million \$	139	143	199	730	206
Annual operating cost, million \$	24.2	25.1	31.1	115	31.6
Cost per barrel: <u>2/</u>					
Before by-product credit, \$	1.89	1.79	1.37	1.27	1.32
After by-product credit, \$	1.28	1.18	0.76	0.66	0.35
<b>Advanced cut and fill</b>					
Capital investment, million \$	148	152	214	791	221
Annual operating cost, million \$	23.7	24.7	30.3	112	30.9
Cost per barrel: <u>2/</u>					
Before by-product credit, \$	1.86	1.75	1.33	1.24	1.29
After by-product credit, \$	1.25	1.15	0.72	0.63	0.32

1/ Capital investment includes working capital and operating cost includes depreciation, but no allowance is made for Federal income tax, cost of capital, or return on investment (Note difference in Table 3)

2/ Cost per barrel is in terms of semi-refined shale oil and 1966 dollars

3/ 35,020 barrels per day

4/ 62,265 barrels per day

5/ 65,540 barrels per day

Table 3 - Summary Statistics 1/

	Case 1		Case 2		Case 3		Case 4	
	1966	1969	1966	1969	1966	1969	1966	1969
Size of plant: Semi-refined oil, barrels-per-day Shale for 20 years, million tons	35,020	62,265	62,265	780	62,265	780	65,540	780
A. Capital investment, millions of dollars	138	152	203	223	199	218	221	240
B. Operating cost, millions of dollars	18.4	23.0	21.7	24.4	20.0	22.6	17.1	20.8
C. Market value of product, dollars: Semi-refined oil, per barrel By-products, per barrel Total, per barrel	3.08 .61 3.69	3.33 .41 3.74	3.08 .61 3.69	3.33 .41 3.74	3.08 .61 3.69	3.33 .41 3.74	3.08 .97 4.05	3.33 .77 4.10
D. At 12% discount rate, dollars: Cost of shale oil and by-product at zero resource value, per barrel	3.59	3.97	2.73	2.88	2.61	2.73	2.55	2.88
E. Discount rate at which resource has zero value when products have 1966 market value, percent	13	9	19	16	20	17	22	20

1/ Operating cost includes depreciation and excludes profit (Note difference in Table 2)

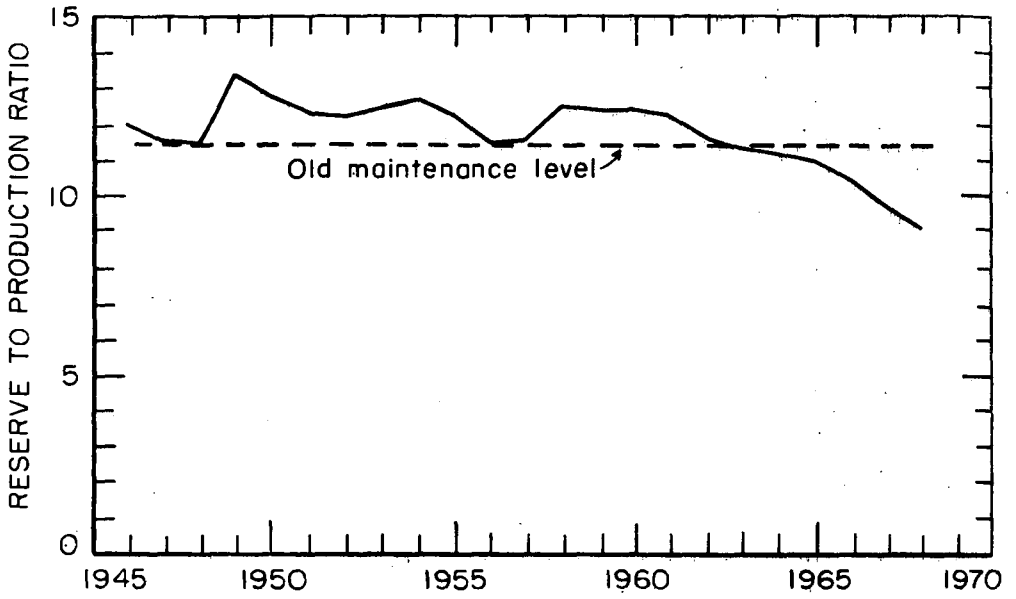


Figure 1 - Trends in the reserve to production ratio 1945-1968

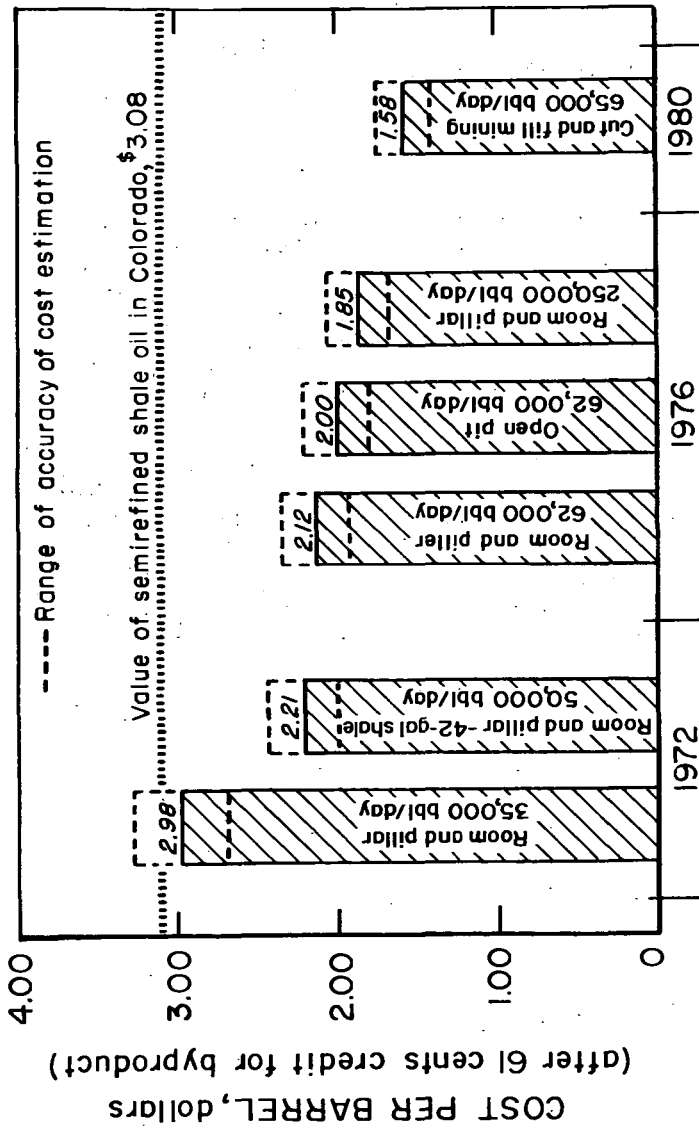


Figure 2 - Cost of shale oil at zero resource value using aboveground gas combustion retorting (12 percent discounted cash flow) 30 gallon shale (unless noted)

L-11576

COMPARATIVE ECONOMICS OF TAR SANDS CONVERSION PROCESSES

Paul V. Roberts and Russell C. Phillips  
Stanford Research Institute  
Menlo Park, California 94025

The tar sands resource is the only solid fuel resource currently being converted to liquid fuels in North America on a large scale. A 45,000 B/CD syncrude plant based on tar sands is currently in operation in the Athabasca region of Alberta. The major steps in conversion of tar sand to syncrude are (1) surface mining of tar sands, (2) hot water extraction of bitumen from mined tar sands, and (3) upgrading of bitumen by coking or hydrovisbreaking followed by hydrotreating of distillates.

The economics of a combined tar sands mining and conversion venture have been analyzed. It was found that tar sands mining costs, bitumen recovery efficiencies, choice of upgrading process, price of syncrude product, and royalty payments all significantly affect the discounted cash flow rate of return from an integrated venture. Results are presented at a level of 50,000 B/SD syncrude production and effects of the factors listed above are discussed. Effect of changing the scale of operations is also discussed.

## AN EVALUATION OF TONNAGE OXYGEN PLANTS

Sidney Katell and Paul Wellman

Bureau of Mines  
U.S. Department of the Interior  
Morgantown, West Virginia

### SUMMARY

Tonnage oxygen plants have increased in size and are available today in the 100- to 1,400-ton-per-day range. The capital investment requirements and estimated selling price are investigated in this study.

### INTRODUCTION

Interest in the production of synthetic liquid and gaseous fuels has intensified so that several systems have reached the point where prototype plants are being installed or are being considered for installation. In many of these systems high-purity oxygen is a requirement, whether it be in the direct gasification of coal, oil, or shale, or for the production of hydrogen for the hydrogasification or hydrogenation of such raw materials.

### DISCUSSION

A previous paper explored the subject of oxygen plant costs;<sup>1</sup> however, a major change has occurred since then--the size of the oxygen plant that can be built today is much larger. The present study takes into account the capital investment requirements and the production costs of these larger units and updates the data contained in the earlier study.

The parameters of the present study are as follows:

1. Location of plant: Ohio Valley.
2. Size of plant: 100 to 1,400 tons per day.
3. Purity: 99.5 percent.
4. Pressure specification: atmospheric and 450 psig.
5. Process employed: low pressure cycle.
6. Type of compressors: electric drive.
7. Cost of available power: \$0.00675 per kilowatt-hour.

Figure 1 shows the relationship between power requirements and plant capacity for the two pressures set up as a parameter. Since the production process is the same, the difference in the two curves is the power required to compress the oxygen to 450 psig discharge pressure.

Figure 2 presents the capital investment requirements for the plants ranging in size from 100 to 1,400 tons per day.

<sup>1</sup>/ Katell, Sidney, and John H. Faber. Cost of Tonnage Oxygen. BuMines Inf. Circ. 7939, 1960, 6 pp.

Table 1 presents the method used in determining the cost of operation on an annual basis for a 500-ton-per-day plant with the oxygen produced at a discharge pressure of 450 psig. The calculation is typical of the several made to establish the curves shown in figure 3. As noted direct labor costs are assumed at \$4 per hour, annual onstream time as 350 days per year, and depreciation at 15 years on a straight-line basis.

Using the discounted cash flow rate of return of 12 percent as a criterion for return on investment, the typical calculation is shown in table 2 and the values obtained are plotted in figure 4.

TABLE 1

Oxygen Plant  
500 Tons Per Day  
Oxygen Compressed to 450 PSIG

Operating Cost

	<u>Annual cost, dollars</u>
<b>Direct costs:</b>	
Power.....8,670 kwhr/hr x 8,400 hr/yr x \$0.00675/kwhr	491,600
Cooling water....135 M gal/hr x 8,400 hr/yr x \$0.020/M gal.....	22,700
Direct labor: 60 hr/day at \$4 per hour.....	87,600
Supervision @ 15 percent.....	13,100
Plant maintenance @ 2 percent of investment.....	88,000
Payroll overhead @ 25 percent of payroll.....	38,200
Operating supplies @ 20 percent of plant maintenance....	<u>17,600</u>
<b>Total direct cost.....</b>	<b>758,800</b>
<b>Indirect costs:</b>	
40 percent of labor, maintenance, and supplies.....	82,500
<b>Fixed costs:</b>	
Taxes and insurance @ 2 percent of investment.....	88,000
Depreciation @ 6.66 percent of investment.....	<u>293,300</u>
<b>Total annual operating cost.....</b>	<b>1,222,600</b>

Annual production = 500 x 350 = 175,000 tons

Cost, dollars per ton of oxygen = 1,222,600 ÷ 175,000 = \$6.99

TABLE 2

Oxygen Plant  
500 Tons Per Day  
Oxygen Compressed to 450 PSIG

Financial Analysis, DCF at 12 Percent

Discounted cash flow, n = 15 years (life of plant)  
i = 12 percent per year

$$P = R \frac{(1+i)^n - 1}{i(1+i)^n}$$

$$P/R = 4.47335/0.656826 = 6.81086$$

$$R = \$4,400,000/6.81086 = \$646,000$$

Net profit = R - Depreciation = \$352,700

With Federal Income Tax @ 50 percent,

Gross profit = 2 x \$352,700 = \$705,400

Sales = Gross profit + operating cost = \$1,928,000

Selling price, dollars per ton oxygen = \$1,928,000/175,000 = \$11.02

Capital investment = P = \$4,400,000

Sales - 175,000 tpy x \$11.02 per ton = \$1,928,000

Operating cost = 1,222,600

Gross profit = 705,400

Federal Income Tax at 50 percent = 352,700

Net profit = 352,700

Cash flow:

Depreciation = 293,300

Net profit = 352,700

Total positive cash flow = R = 646,000

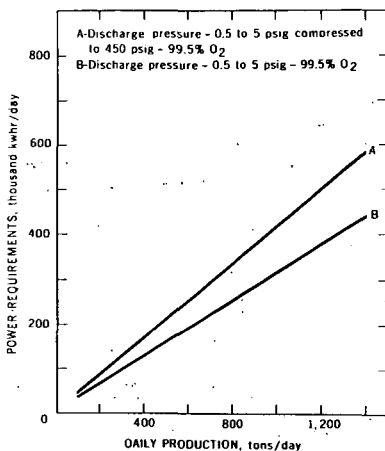


FIGURE 1. - Power Requirements for Tonnage Oxygen Plants.  
Daily Production vs. Power Requirements.

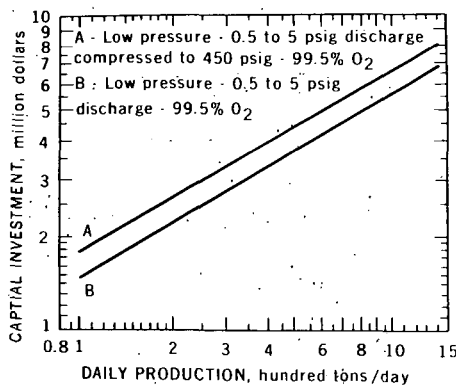


FIGURE 2. - Oxygen Plant. Capital Investment vs.  
Daily Production.

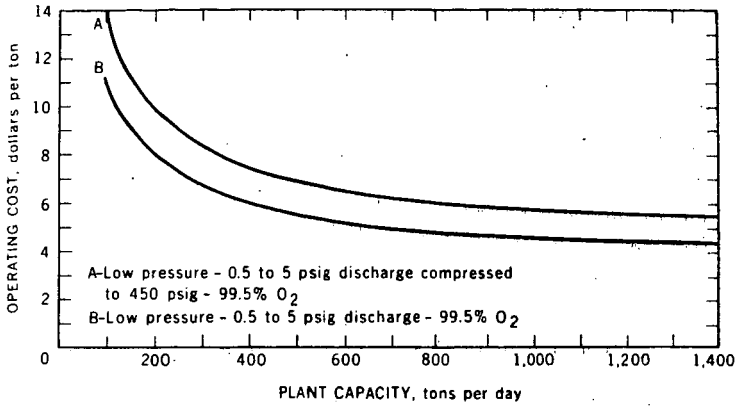


FIGURE 3. - Oxygen Plant. Operating Cost vs. Daily Production.

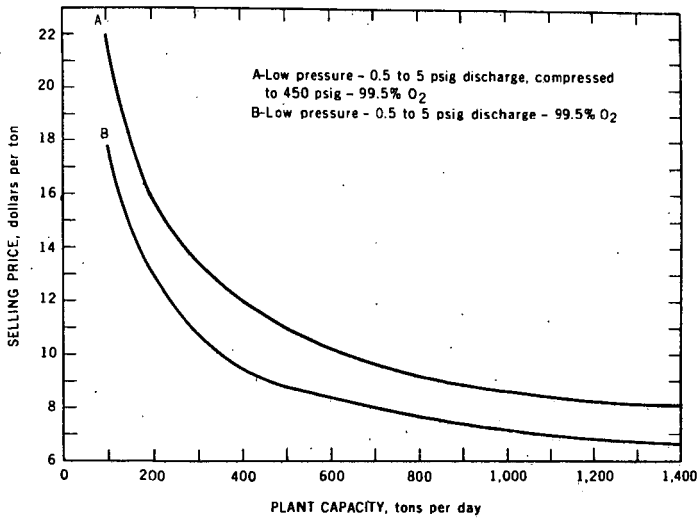


FIGURE 4. - Oxygen Plant. Selling Price vs. Daily Production.